1999

Surface plasmon enhanced interfacial electron transfer and resonance Raman, surface-enhanced resonance Raman studies of cytochrome c mutants

Junwei Zheng
Iowa State University

INFORMATION TO USERS

This manuscript has been reproduced from the microfilm master. UMI films the text directly from the original or copy submitted. Thus, some thesis and dissertation copies are in typewriter face, while others may be from any type of computer printer.

The quality of this reproduction is dependent upon the quality of the copy submitted. Broken or indistinct print, colored or poor quality illustrations and photographs, print bleedthrough, substandard margins, and improper alignment can adversely affect reproduction.

In the unlikely event that the author did not send UMI a complete manuscript and there are missing pages, these will be noted. Also, if unauthorized copyright material had to be removed, a note will indicate the deletion.

Oversize materials (e.g., maps, drawings, charts) are reproduced by sectioning the original, beginning at the upper left-hand corner and continuing from left to right in equal sections with small overlaps. Each original is also photographed in one exposure and is included in reduced form at the back of the book.

Photographs included in the original manuscript have been reproduced xerographically in this copy. Higher quality 6" x 9" black and white photographic prints are available for any photographs or illustrations appearing in this copy for an additional charge. Contact UMI directly to order.

UMI®

Bell & Howell Information and Learning
300 North Zeeb Road, Ann Arbor, MI 48106-1346 USA
800-521-0600

Surface plasmon enhanced interfacial electron transfer and resonance Raman, surface-enhanced resonance Raman studies of cytochrome c mutants

by

Junwei Zheng

A dissertation submitted to the graduate faculty

in partial fulfillment of the requirements of the degree of

DOCTOR OF PHILOSOPHY

Major: Analytical Chemistry

Major Professor: Edward S. Yeung

Iowa State University

Ames, Iowa

1999

Graduate College
Iowa State University

This is to certify that the Doctoral dissertation of

Junwei Zheng

has met the dissertation requirements of Iowa State University

Signature was redacted for privacy.

Major Professor

Signature was redacted for privacy.

For the Major Program

Signature was redacted for privacy.

For the Graduate College

TABLE OF CONTENTS

CHAPTER 1

GENERAL INTRODUCTION

Surface plasmon of nanostructured metal particles has received increasing attention and been extensively studied in recent years. A number of optical phenomena, including Surface-enhanced Raman Scattering (SERS)[1-8], surface-enhanced absorption and luminescence[9], second Harmonic generation (SHG)[10], can be strongly enhanced when molecules adsorbed on roughened metal surfaces or on surfaces of nanostructured metal particles. Those enhancements have been attributed to the excitation of the collective electron oscillations or surface plasmon oscillations that engender huge electromagnetic field both inside and out side of small metal particles. The fields inside result in strong absorption of radiant energy. The fields outside, on other hand, stimulate enhanced optical emissions, which are then further enhanced by resonant interaction with particle at the shifted frequency. Beyond the surface enhanced optical phenomena, the enhancement due to surface plasmon resonance has also recently been observed in photochemistry[11]. One of the specific objectives of this dissertation was fourfold on utilization of surface plasmon resonance to enhance the electron transfer at silver/solution interfaces. The photoinduced electrochemical reductions of nitrite, CO_2, microperoxidase-11 as a model compound for heme proteins were exclusively studied on the surfaces of electrochemically roughened silver electrodes.

Raman spectroscopy is an important analytical technique for chemical and biological analysis due to the wealth of the information on molecular structure, surface processes, and interfacial reactions. In particular, Resonance Raman and Surface-enhanced Resonance Raman scattering spectroscopy can directly provide the specifically structural information

about the heme group in cytochromes[12-15]. The correlation between RR of heme group in cytochrome c and the local and global conformation of the protein was specifically interested in this dissertation. The water mutants from rat cytochrome c were investigated particularly in the low-wavenumber region of RR spectrum. The effects of ligand switching process caused by the mutation of phenylalanine-82 with histidine in yeast iso-1-cytochrome c on the conformation, stability, electron transfer spectroscopic properties of the protein were studied.

Dissertation Organization

The background and literature reviews for two important areas related to the dissertation research are included in the remainder of this chapter. First, the mechanisms of SERS are summarized, photoinduced charge transfer in SERS as well as enhanced photochemistry on rough surfaces are described. Second, the principle and applications of Resonance Raman and Surface-enhanced Resonance Raman (SERRS) spectroscopies in the study of cytochrome c is briefly described.

Chapters 2 through 8 of this dissertation include papers that have been published or written for peer-reviewed journals. Chapter 2, a paper accepted by *Journal of Physical Chemistry* (JP990928H), was on the utilization of surface plasmon resonance for the photoinduced electrochemical reduction of nitrite at roughened silver electrode surface. Chapter 3, a paper submitted to *Journal of Electroanalytical Chemistry*, was a continued study of photoinduced electron transfer at silver/solution interface. The electrochemical reduction of CO_2 mediated with methylviologen both in the solution and adsorbed on the electrode surface was investigated.

Chapter 4, a short paper submitted to *Journal of Physical Chemistry*, was about the application of EPR method in the study of photoinduced electron transfer at nanostructured silver metal surface. Chapter 5 was on the study of electrochemistry and SERS of microperoxidase-11, which is used as a model compound for heme protein. Part of this chapter was published in "*Spectroscopy of Biological Molecules: Modern Trends*" (Ed. P. Carmona, R. Navarro, and A. Hernanz, Kluwer Academic Publishers: Dordrecht, Netherlands, 1997). The rest of the work was included in a paper to be submitted to *Journal of Photochemistry and Photobiochemistry*.

Chapter 6, a paper published in *Journal of Raman Spectroscopy*, described the application of Resonance Raman spectroscopy in correlating the conformation and optical properties of cytochrome c water mutants. The unique information obtained in low frequency region of Resonance Raman spectrum is particularly emphasized. Chapter 7, a paper submitted to the *Biospectroscopy* in memory of Dr. Therese M. Cotton, was a detailed spectroscopic study on yeast-iso-1-cytochrome c mutant, F82H. UV/Vis absorption, Circle Dischroism and Resonance Raman spectroscopies were employed to study the ligand switching effect in the mutant. Chapter 8, a paper submitted to *Bioelectrochemistry and Bioenergy*, was a further study on the stability and electrochemical properties of F82H.

The dissertation concludes with a general summary of the research achievement and possible direction for future work.

The Mechanisms for Surface-enhanced Raman Scattering

The surface-enhanced Raman effect was first discovered from pyridine adsorbed on roughened silver electrode in 1974[16]. Immediately after its discovery, most research was

concerned with understanding the SERS phenomenon itself. Although extensively fundamental studies have been devoted to obtaining a better understanding of the sources of enhancement[1-8], a complete theory of this effect has not yet been achieved. It is generally agreed that in any given adsorbate-substrate system several enhancement mechanisms may be operating. The relative importance of various mechanisms is somewhat controversial.

The SERS phenomenon can be qualitatively understood in the classical theory of light scattering[17]. Consider an incident light beam inducing an oscillation dipole in a particle, which emits light at the frequency of the dipole oscillation. If the magnitude of the incident electric field, E(t), is not too large, the induced dipole moment can be approximated as:

$$P = \alpha \bullet E(t) \qquad (1)$$

where α is the polarizability of the molecule.

The Raman intensity is proportional to the square of the induced dipole, P, which can be enhanced through two possible ways: (1) the molecular polarizability (i.e., molecular effect) and/or (2) the electric field experienced by the molecule (i.e., field effect). As a result, theoretical models generally involve two types of enhancement mechanisms: electromagnetic enhancement and chemical effect.

Electromagnetic Enhancement Model

Many visions of electromagnetic theory have been developed at different levels of completeness over the years. Model systems which have been treated include isolated spheres, isolated ellipsoids, interacting spheres, interacting ellipsoids, randomly roughened surfaces treated as collections of hemispherical bumps or gratings[1-8]. A qualitative understanding of the mechanism of surface plasmon resonance can be obtained for nanosystems where the dimensions of the particles are much smaller than the laser

wavelength. According to Rayleigh approximation, the 'induced' electric field at the surface of the particle E_c is give by:

$$E_c = \frac{1}{1+[(\varepsilon(\omega)/\varepsilon_0)-1]A} E_{inc}$$

where A is the depolarization factor, E_{inc} is the incident field outside the particle, $\varepsilon(\omega)$ and ε_0 are the dielectric constants of the bulk metal and the surrounding medium, respectively. The dielectric constants, $\varepsilon(\omega)$, can be further expressed as a complex value $\varepsilon(\omega) = \varepsilon_1(\omega) + i\varepsilon_2(\omega)$. Then E_c can be approximated by:

$$E_c = \frac{\varepsilon(\omega)-\varepsilon_0}{\varepsilon(\omega)+2\varepsilon_0} E_{inc}$$

Surface plasmon resonance occurs when the real part of the denominator approaches to zero (i.e., $\varepsilon(\omega) \rightarrow 2\varepsilon_0$). At this resonance condition, E_c is large if the associated imaginary part of $\varepsilon(\omega)$ is also small. Thus, excitation of surface plasmon greatly increases the local field experienced by the molecules adsorbed on the surface of the particles. The requirement for substrates is fulfilled simply by selecting an excitation frequency for which the real part of $\varepsilon(\omega)$ satisfies a resonance condition and the imaginary part of $\varepsilon(\omega)$ is as close to zero as possible. Metals such as Ag, Au and Cu are often used in SERS studies because both of the above conditions occur in the visible region. For metals such as Pt and Pd, the imaginary part is too large to produce efficient enhancement, although their real part of $\varepsilon(\omega)$ is small.

The electromagnetic enhancement model well explains many experimental observations. For instance, the range dependence of the enhancement can be explained by

dipole decay law. The enhancement falls off as $G = [r/(r+d)]^{12}$ (G, enhancement factor) for a single molecule located at distance d from the surface of a sphere of radius r; or $G = [r/(r+d)]^{10}$ for a monolayer of molecules[18,19].

Electromagnetic enhancement should be nonselective for all molecules adsorbed on a particular surface, however, the molecules such as CO and N_2 differ by a factor of 200 in their SERS intensities under the same experimental conditions[20]. Other several lines of evidence also suggest that there is a second enhancement mechanism, which operates independently of the electromagnetic mechanism[21,22].

Chemical Effect Model

An important process that produces an increase in the molecule polarizability, α, involves a charge transfer mechanism, which is associated with the formation a chemical bond between the metal and the adsorbate. This chemical effect is associated with the overlap of the metal and adsorbate electronic wavefunctions. The electronic states of adsorbate are shifted and broadened by the interaction with the surface of metal, or new electronic states are generated and act as the resonant intermediate state in Raman scattering due to the chemisorption of the adsorbate. As a result, the electron in the Feimi level of the metal can be excited by the incident light, and tunneled into a charge transfer state of the adsorbed molecule. The charge transfer process induces a nuclear relaxation in the adsorbate molecule which, after the return of the electron to the metal, leads to a vibrationally excited neutral molecule and to emission of a Raman-shifted photon.

A major difference between the electromagnetic and chemical models is the fact that the chemical effect contribution to SERS is necessarily short-ranged, usually in monolayer.

This mechanism depends on the adsorption site, the geometry of bonding, and the energy level of the adsorbate.

New Trends in Application of SERS

The analytical applications of SERS in biomedical and basic biological science still remain as the most attractive area. Considerable attention has been focused on the structure, topology and composition of biomedical species. The interesting studies include living cells and cell-cell and cell-virus interactions[23-25], drug pharmacokinetics and the distribution of drugs within the cells[26,27], cell membrane components and transport processes in membranes[28-30], immunoassays[31,32], as well as DNA gene probes, gene diagnosis[33,34]. The major advantages of SERS for its biomedical application are the high surface enhancement and selectivity, only molecules or groups in a molecule very close to the metal surface can contribute to the signal in SERS spectra. Another advantage of the SERS is the remarkable reduction in fluorescence background, which often is a serious obstacle in Raman studies of biomedical material.

The combination of SERS with other analytical techniques such as gas chromatography, thin-layer chromatography, flow injection analysis have appeared recently. Carron and coworkers[35] reported a new gas chromatography detector composed of SERS substrates coated with 1-propanethiol, which functions to concentrate organic analytes on the surface. Horvath et al.[36] developed a method for drug analysis by separating a mixture via TLC, followed by SERS detection from chromatography plate. The analysis of organic pollutants in water using flow injection analysis coupled with SERS has also proposed[37]. Sensors based on SERS detection have also been developed for a wide range of analytes,

including organic molecules in aqueous solution, nerve agents, molecules of environmental importance[38-41].

Single molecule detection or the SERS on single silver particle has received tremendously attention in recent years. The initial works in this area were done by Kneipp et al.[42], who used fiber-optic probe for the surface-enhanced resonance Raman measurement of rhodamine 6G, a linear concentration range between 10^{-11} and 10^{-14} was achieved. Later, the authors extended their work to single molecule detection of Rhodamine 6G, crystal violet and cyanine dye as well as a single DNA base molecule[43-47]. On other hand, using near-field cofocal technique, Nie et al.[48-50] achieved approximately 10^{14} to 10^{15} of the intrinsic Raman enhancement factors for single rhodamine 6G molecule on silver colloid. Recently, an elegant work on size-dependent optical enhancement in single metal particles was also reported by these authors[51]. Obviously, the capability of SERS for single molecule detection opens many opportunities for scientist to address current problems in SERS and to explore new frontiers in various disciples such as analytical chemistry, molecular biology, and nanostructured materials.

Cytochrome c and Its Raman Scattering Spectroscopy

Cytochrome c

Cytochrome c is an electron carrier between cytochrome reductase and cytochrome oxidase and plays an important role in energy transduction in the mitochondrial respiratory chain[52,53]. One of the most extensively studied c-type cytochromes is yeast iso-1-cytochrome c. The structures of both oxidized and reduced forms of this protein have recently been determined with high resolution[54,55]. The yeast iso-1-cytochrome c molecule has the typical

cytochrome c fold with the polypeptide chain organized into a series of α-helices and fairly extended loop structure[56]. The protein fold envelops the heme prosthetic group within a hydrophobic pocket formed by a shell of polypeptide chain one or two residues thick. The polypeptide chain backbone, heme group, and heme ligand of yeast cytochrome c from different species are illustrated in Figure 1. The two vinyl groups of the heme become saturated by the formation of two thioether linkages with two cysteine residues, Cys-14 and cys-17. The iron atom is bonded to the four pyrrole nitrogens in the porphyrin plane and axially coordinated with the sulfur atom and imidazole group from Met-80 and His-18, respectively, which form additional two points for the attachment of heme to the polypeptide. Because heme prosthetic group is buried within a hydrophobic pocket formed by the polypeptide chain, only ca. 9.5% of the total surface area of the heme are exposed to external solvent. An important amino acid residue, phenylalanine-82, is suggested to play the role in regulation of the solvent exposure of heme group and, in turn the electron transfer properties of the protein. The heme group itself is not absolutely planar but is distorted into a saddle shape. The distortion of the porphyrin plane originates the rich features in RR spectrum that will be described below. Two propionic side-chains of the heme group are buried within the protein matrix and form a number of hydrogen bonds with nearby polar groups. Thus, any conformational changes in the protein immediate next to heme group may affect the interaction between propionic acid side-chains and protein matrix. As expected, the conformational changes of the protein surrounded heme group may be reflected in the spectroscopic properties associated with these side-chains as that discussed in detailed later in the dissertation.

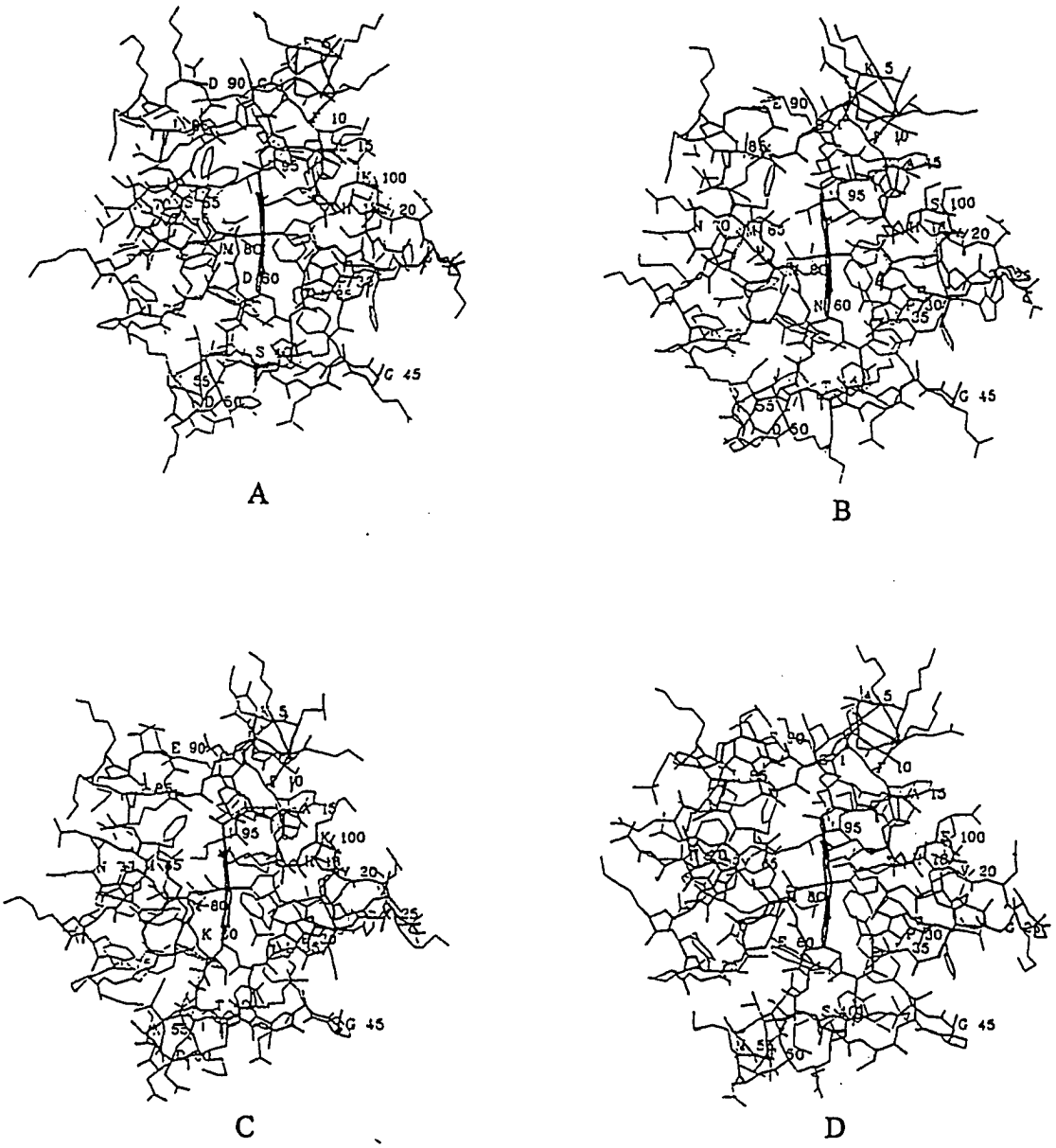

Figure 1. Stereo-drawing illustrating side chain placement in (A) yeast iso-1, (B) Tuna, (C) horse, and (D) rice cytochrome c. Side chain groups are drawn with thin bonds, while the polypeptide chain backbone is drawn in thick lines. The heme group and ligand bonds are also drawn in thick lines.[52]

The conformation of cytochrome c can be influenced by many factors, such as pH of the media, interaction with its redox partner, temperature and presence of the denaturants. Among the factors that affect cytochrome c conformation, the oxidation state effects is most interested for gaining the insight into the nature of oxidation state-dependent conformational changes occurring during cytochrome c--mediated electron transfer events has proven surprisingly elusive. An abundance of experimental evidence indicates that the structural differences do exist between oxidized and reduced forms of cytochrome c. Recently, high-resolution three-dimensional structure analyses of yeast iso-1-cytochrome c have been completed in both oxidation states using isomorphous crystalline material and similar determination methodologies. Although comparable values were observed for the overall average thermal factor for all atoms in the polypeptide chain of cytochrome c in both oxidation states, four regions of the polypeptide chain have significantly high thermal factors in the oxidized form, as shown in Table 1. Particularly, the side chains of three amino acid residues, Asn-52, Tyr-67 and Phe-82 show higher mobility in the oxidized form. Those residues will be involved in the studies in this dissertation. The significant changes in heme group upon oxidation are those: more pronounced distortion of heme group, the substantive increases in thermal factors of the side chain of Met-80 and a minor change in the orientation of His-18. It is worth being noted that oxidation also results in the position change of pyrrole ring A propionate group; its hydrogen bonds to Asn-52 and Typ-59 are much weaker in oxidized form.

The conserved internal water molecule, Wat-166, which is expected to provide a significant contribution toward stabilizing the positive charge on the heme iron group, also undergoes a large shift in position in response to oxidation state, as indicated in Figure 2. The

Table 1. Structural changes observed upon oxidation of yeast iso-1-cytochrome c.[52]

A. *Positional displacements of polypeptide chain*
   1. Movement of Arg13 and Gly84 to form a hydrogen bond.
   2. Lengthening of the interaction between Trp59 and the heme pyrrole ring A propionate group, with an associated change in Asp60.

B. *Thermal factor parameters of main chain atoms*
   1. Lower values observed for residues 37–39, focussed at Arg38
      —side chain of Arg38 also has reduced values.
   2. Higher values found for three polypeptide chain segments
      (a) residues 47–59, focused at Asn52
      (b) residues 65–72, focused at Tyr67
      (c) residues 81–85, focused at Phe82
      —All three side chains of Asn52, Tyr67 and Phe82 show higher mobility.

C. *Heme structure and ligands.*
   1. Increased distortion of heme planarity
   2. Readjustment of the pyrrole ring A propionate group with a realignment of hydrogen bonding interactions
   3. Movement (CB and CE atoms) and higher thermal parameters for the Met80 side chain.
   4. Rotation of the imidazole ring plane of His18.

D. *Internal water structure.*
   1. Large displacement of Wat166 towards the heme iron atom, coupled with a change in hydrogen bonded interactions
   2. Wat166 movement is facilitated by shifts in the protein matrix to enlarge the available internal cavity space
   3. Reorientation of the dipole of Wat166 to favor stabilization of the charged heme iron atom

E. *Hydrogen bond interactions*

1. Stronger:	Gly41 N–Heme O2A
2. Weaker:	Trp59 NE1–Heme O2A
3. Lost:	Asn52 ND2–Heme O2A
	Asn52 ND2–Wat166
	Met80 SD–Tyr67 OH
4. New:	Wat121–Heme O2A
	Gly84 O–Arg13 NH1
	Asp60 OD1–Wat124

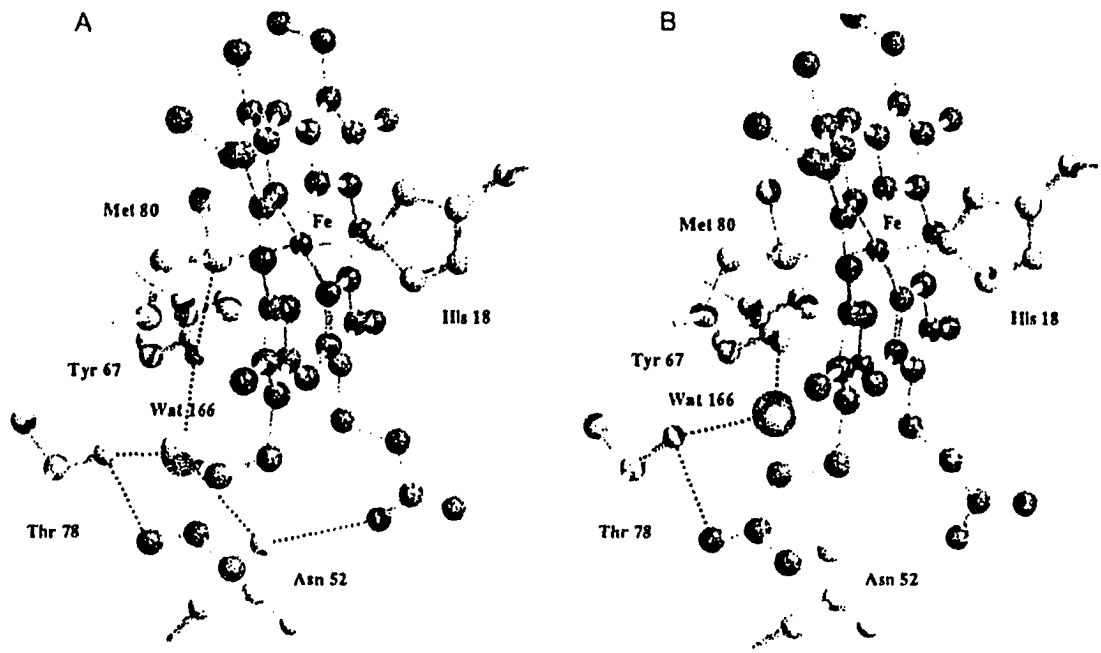

Figure 2. Heme and polypeptide chain structure about the internally water molecule Wat166 in (a) reduced and (b) oxidized yeast iso-1-cytochrome c. Heme ligand interactions are indicated by thin white bonds, whereas hydrogen bonds are drawn by thin black dashed lines. In reduced protein, Wat166 interacts with three highly conserved residues (Asn52, Tyr67, and Thy78). In oxidized protein the hydrogen bond to Asn52 is broken.[52]

most affected is Asn-52, to which Wat-166 no longer forms a hydrogen bond. The hydrogen bond between Asn-52 and the pyrrole ring A propionate group is also lost. Another related change is the loss of the Tyr-67 to Met-80 hydrogen bond in oxidized state. This change is expected to be an additional factor for stabilizing the oxidized state of the protein through making the Met-80 less electron-withdrawing and assisting proper orientation of the dipole moment of Wat-166 adjacent to the heme group. In addition, the positioning of Wat-166 may also result in the modification of the strength of the Met-80-heme iron ligand interaction and in this way play an integral role in the electron transfer process. More details of this feature will be described in Chapter 6.

Since the biological function of cytochrome c is to carry out oxidation-reduction reactions, homogeneous and heterogeneous electron transfer processes associated with cytochrome c have been widely studied for gaining the insight into the electron transfer mechanism of the protein. The electron transfer properties of cytochrome c can be affected by many factors, such as polarity of the heme environment, the charges on the protein, the spin and coordination states of the heme iron atom. A detailed understanding of the electron transfer mechanism so far is not yet available. In particular, the role of the protein or specific amino acid pathways in intraprotein or interprotein electron transfer is under intense scrutiny. At this point, site-directed mutagenesis provides a powerful method for studying the role of a specific amino acid residue in the structure and function of cytochrome c. Based on the achievement of Hall and Smith[57,58] for cloning and sequencing iso-cytochrome c from bakers yeast, *saccharomyces cerevisiae*, and the development of oligonucleotide-directed site specific mutagenesis[59,60], Pielak et al.[61] were the first to apply the site-directed mutagenesis technique in cytochrome c for preparing and expressing three mutants of yeast iso-1-

cytochrome c in which Tyr, Ser and Gly were substituted for Phe-82. The advantages of the site-directed mutagenesis include (1) achieving specific structural modifications in a controlled manner; (2) specifically modifying the kinetics and thermodynamics of the electron transfer properties of cytochrome c; (3) offering the versatility of spectroscopic properties on the structural basis. Up to now, a number of cytochrome c mutants has been prepared, selected examples are cited here.

Mutations that affect electron transfer properties of the protein have been of considerable interest to a number of investigators. As mentioned above, Phe-82 is proposed to have the role on regulation the electron transfer properties of cytochrome c. Mutations at this position have been designed as a means of evaluating the proposed role of this residue. Various amino acids, such as Ser, Tyr, Leu, Ile, Ala, Gly and His have been substituted for Phe-82. The stability of the interaction between Met-80 and the heme iron atom, the midpoint reduction potential and the kinetics of its reduction by $Fe(EDTA)^{2-}$ are significantly affected by the substitutions[62, 63]. In addition to the effect on the electron transfer properties, the profound effects of the substitution on the negative Soret Cotton effect in the circular dichroism spectrum of ferricytochrome c was also observed, particularly of the substitution of non-aromatic amino acid residues[64,65]. The intensity of the negative Soret Cotton effect varies with the identity of the residue in the order Phe>Tyr>Gly>Ser=Ala>Leu>Ile. Luntz et al.[66] reported that the substitution of Phe for Tyr-67 results in the reduction potential of the protein 35 mV lower than that of the wild type protein, due to the loss of internally bonded water molecule and the strengthening of the interaction between Met-80 and heme iron.

Cytochrome c possesses three physilogenetically-conserved proline residues that are presumably involved in the correct folding of the protein to form the native structure.

Mutations at those positions may directly affect protein stability and folding. The effects of substitution of Pro-71 with Thr on the equilibrium and kinetics of yeast cytochrome c unfolding have been studied by Nall and co-workers[67]. The mutation leads to an increase in the rate of formation of alkaline form of the protein. The substitution of Pro-30 by Ala, on other hand, results in the increases of the flip rates of Tyr-48 and Phe-46 as well as the dynamic attributes of the protein[68].

The regulation of the electrostatic properties of the protein by mutations can also influence the electron transfer properties. Arginine-38, of which the guanidino side chain occupies an internal location to form a hydrogen bond with heme propionate-6[69], has been modified with Lys, His, Glu, Asn, Leu and Ala to decrease the electron-withdraw ability of the residue at this position[70]. The reduction potential of cytochrome c decreased, with the greatest decrease (50 mV) observed for Ala mutant. In the case of mutation for Lysine-72, a surface residue having critical role in the electrostatic recognition of cytochrome c[71], surprisingly minimal changes in the properties of cytochrome c were observed for the Arg and Asp mutants relative to the wild type[72,73]. With the replacement of Lys-72 by Asp, however, the rate of electron transfer from the ferrocytochrome to cytochrome c peroxidase compound I within the electrostatically stabilized complex formed between the two proteins was increased from 245 s^{-1} to 440 s^{-1}.

Relatively little attention has been directed at perturbation of the heme iron ligands in cytochrome c through site-directed mutagenesis. Only Sorrell et al.[74] attempted to replace His-18 with Arg residue in yeast iso-2-cytochrome c. Interestingly, the reduction potential of the mutant was the same as that of wild type protein, except that mutant showed less efficient

reacting with the electrode. This behavior was presumed to be the result of greater reorganization energy of the mutant.

Resonance Raman

Resonance Raman spectroscopy is a well-established and powerful tool for elucidating structure-function relationships in biomolecules[13,14]. The underlying principle of this technique is that the excitation falls close to or within an electronic absorption band of a chromophoric group in a molecule. In this way, vibronic coupling with the electronically excited state greatly increases the probability of Raman scattering from vibrational transitions in the electronic ground state. This, in turn, provides high selectivity because only vibrational modes associated with the chromopheric group are subjected to intensity enhancement. The basic theory of RR scattering is briefly outlined below.

The intensity of Raman band can be expressed as:

$$I_s = \frac{8\pi \upsilon_s^4}{9c^4} I_0 \Sigma \left| (\alpha_{\rho\sigma})_{gf} \right|$$

where I_0 is the intensity of the incident laser beam of frequency ν_0, ν_s is the scattering frequency, c is the velocity of light, $(\alpha_{\rho\sigma})_{gf}$ is the transition polarizability tensor, or the change in polarizability α caused by the g→e→f transition, g and f denote the initial and final states, respectively, of the electronic ground state, e represents the excited electronic state. Second-order perturbation theory gives the Kramers-Heisenberg equation for the polarizability:

$$(\alpha_{\rho\sigma})_{gf} = \frac{1}{\hbar}\sum_{e}\frac{< f|\mu_\rho|e >< e|\mu_\sigma|g >}{\upsilon_{eg} - \upsilon_0 + i\Gamma_e} + \frac{< f|\mu_\sigma|e >< e|\mu_\rho|g >}{\upsilon_{ef} + \upsilon_0 + i\Gamma_e}$$

where μ_σ and μ_ρ are dipole moment operators, |g>, |f> and |e> are wavefuction of initial, final and electronic excited states, respectively, Γ_e is the band width of the eth state ($i\Gamma_e$ term is called the damping constant), ν_{eg} and ν_{ef} are the frequencies corresponding the energy differences between the state described. In normal Raman scattering, $\nu 0$ is chosed so that $\nu_0 << \nu_{eg}$, Raman intensity is proportional to $(\nu_0 - \nu_{eg})^4$. As ν_0 approaches ν_{eg}, the denominator of the first term in $(\alpha_{\rho\sigma})_{gf}$ becomes very small, hence this term (resonance term) becomes so large that the intensity of the Raman band becomes enormously. This phenomenon is called Resonance Raman scattering.

More specific information can be obtained by expressing the total wavefunction as the product of the electronic and vibrational wavefunctions via the Born-Oppenheimer approximation. Then $(\alpha_{\rho\sigma})_{gf}$ can be approximately expressed as:

$$(\alpha_{\rho\sigma})_{gf} \cong A + B$$

A-term is the leading term, it is ordinarily the dominant contribution to the RR intensity. Only totally symmetric modes can be enhanced via A-term. B-term involves two electronic excited states and provides a mechanism for resonance-enhancement of non-totally symmetric vibrations. The B-term becomes important in the case where a forbidden or weakly allowed transition gains intensity from vibronic mixing with a strongly allowed transition. The mixing modes are then prominent in the RR spectrum when excited at the weak transition.

Both of A-term and B-term resonance are typically found in the RR spectra of heme proteins and their model compounds. As shown in Figure 3, heme proteins and metalloporphyrins such as cytochrome c and Ni(OEP)[75,76], exhibit two electronic transitions; Q_0(or α) and B (Soret) bands together with a vibronic sideband Q_1 (or β) in the 600-350 nm region. The RR spectra in Figure 4 were obtained by B, Q_1 and Q_0 excitation. The former is dominated by totally symmetric vibrations, whereas the later two are dominated by non-symmetric vibrational modes.

The RR spectroscopy is particular useful to gain deep insight into the structure of the active sites in heme proteins and their immediate protein environments down to molecular level, which may be beyond the resolution of X-ray crystallography or NMR spectroscopy. In particular, the complete assignment of the bands in RR spectrum of cytochrome c has been well established[77]. The important spectral regions include marker band region (1300-1700 cm^{-1}) and fingerprint region (below 500 cm^{-1}). The bands in marker band region originate from modes, which include predominantly C-C and C-N stretching vibrations of the porphyrin. Two important marker bands fall in the region[13]: oxidation sensitive band, ν_4, and coordination and spin state sensitive band, ν_3. The typical bands for different oxidation, coordination and spin states of porphyrin iron are shown in Figure 5. The bands in fingerprint region originate from modes, which include considerable contributions from vibrations involving the peripheral substituents of the porphyrin. Hence, these modes should sensitively reflect the specific structure of the heme pocket in cytochrome c and can be regard as a fingerprint for heme-protein interactions.

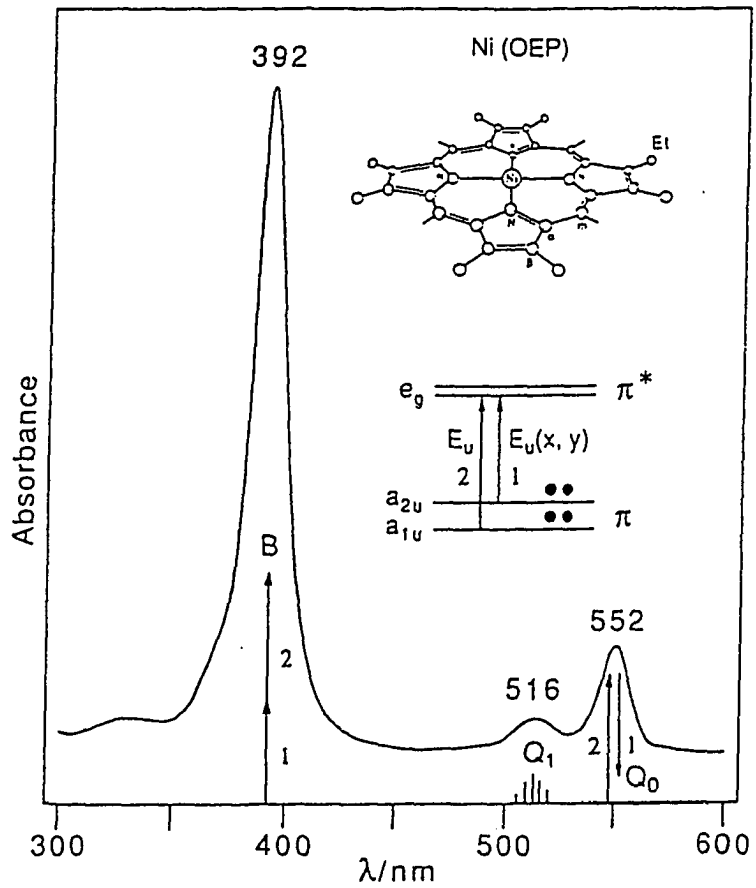

Figure 3. Absorption spectrum and energy level diagram of Ni(OEP).[75]

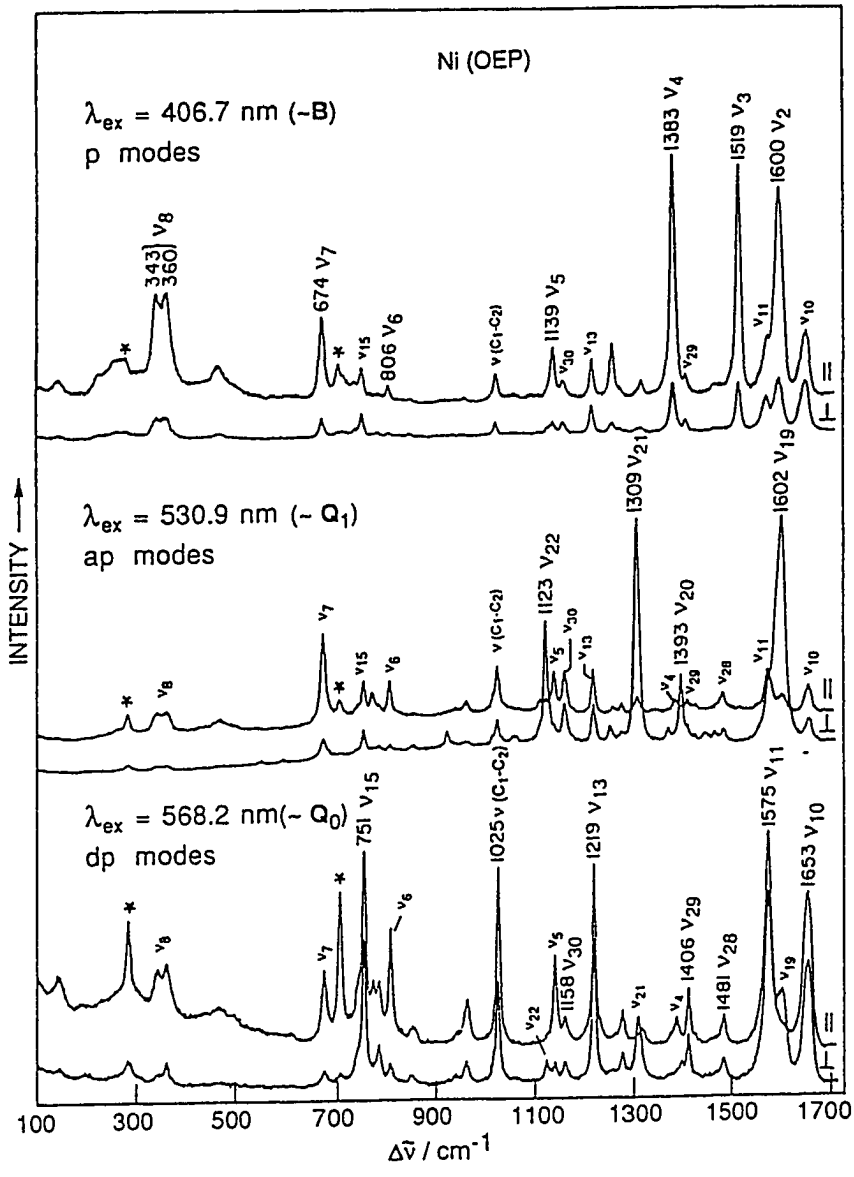

Figure 4. Resonance Raman spectra of Ni(OEP) obtained by three different excitations.[76]

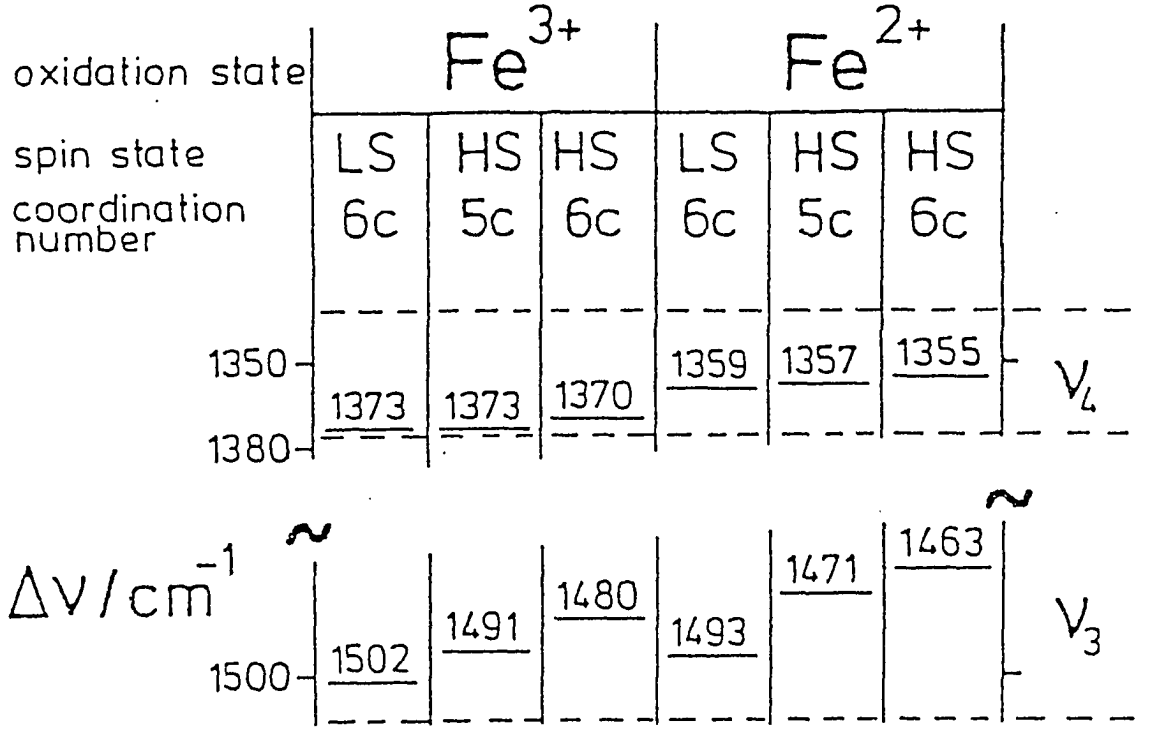

Figure 5. Structure correlations of porphyrin modes.

Surface-enhanced Resonance Raman Scattering (SERRS)

The intensity of Raman scattering in SERRS can be further enhanced as the excitation wavelength is in resonance with the electronic transition of the adsorbate on roughened metal surfaces, due to the surface enhancement effect as described above. SERRS combines the merits of both RR and SERS and enable one to characterize in-situ interfacial behaviors of cytochrome c[5,78-80]. It has been successfully applied to investigate electrochemical and conformational properties of cytochrome c adsorbed on the silver electrode and silver sols.

References

1. M. Moskkovits; *Rev. Mod. Phys.* **1985**, 57, 783.
2. M. Merker; *SPIE Milestone Series*; ed. B.J. Thompson, SPIE Optical Enginerring Press: Bellingham, WA, 1990.
3. R.L. Birke, T. Lu, J.R. Lombardi, *Techn. Charact. Electrodes Electrochem. Processes*; ed. R. Vaema, J.R. Selman, Wiley, New York, **1991**.
4. T.M. Cotton, J.H. Kim, R.E. Holt; *Adv. Biophys. Chem.* **1992**, 2, 115.
5. T.M. Cotton, J.H. Kim, G. Chumanov; *J. Raman Spectrosc.* **1991**, 22, 729.
6. T. Vo-dinh; *Trends Anal. Chem.* **1998**, 17, 557.
7. A. Otta; *J. Raman Spectrosc.* **1991**, 22, 743.
8. A. Campion, P. Kambhampati; *Chem. Soc. Rev.* **1998**, 27, 241.
9. A. Harstein, J.R. Kirtly, J.C. Tsang; *Phys. Rew. Lett.* **1980**, 45, 201.
10. C.K. Chen, A.R.B. de Castro, and Y.P. Shen; *Phys. Rev. Lett.* **1981**, 46, 551.
11. A. Nitzan, L.E. Brus; *J. Chem. Phys.* **1981**, 75, 2205.

12. B. Cartling; in *Biological Applications of Raman Spectroscopy*; T.G. Spiro, Eds.; John Willy & Sons: New York, **1988**.

13. R.H. Felton, N.-T. Yu; in *The Porphyrins*; D. Dolphin, Eds.; Academic Press: New York, **1978**.

14. K. Niki, O. Vrana, V. Brabee; in *Experimental Techniques in Bioelectrochemistry*; V. Brabec, D. Walz, G. Milazzo, Eds.; Birkhauser Verlag: Basel, Swizerland, **1996**.

15. J. Twardowski, P. Anzenbacher; in *Raman and IR Spectroscopy in biology and Biochemistry*; Ellis Horwood, Ltd.: Chichester, U.K., **1995**.

16. M. Fleischmann, P.J. Hendra, A.J. McQuillan; *Chem. Phys. Lett.* **1974**, 26, 163.

17. C.L. Stevenson and T. Vo-dinh; in *Modern Techniques in Raman Spectroscopy*; J.J. Laserna (ed.); Wiley, New York, **1996**.

18. A. Otta; *J. Raman Spectrosc.* **1991**, 22, 743.

19. A. Otta; *Surf. Sci.* **1985**, 162, 891.

20. M. Moskovits, D.P. Dillela; in *Surface Enhanced Raman Scattering*; R.K. Chang, T.E. Furtak, Eds.; Plenum: New York, **1982**, p243.

21. Y.-S. Choi, J.-J. Kim, S. Miyajima; *Chem .Phys. Lett.* **1996**, 255, 45.

22. P. Kambhampati, C.M. Child, A. Campion; *J. Chem. Soc., Faraday Trans.* **1996**, 92, 4775.

23. K. Sokolov, N.E. Byramova, L.V. Mochalova, A.B. Tuzikov, S.D. Shiyan, N.V. Bovin, I. Nabiev; *Appl. Spectrosc.* **1993**, 47, 535.

24. H. Morjani, J.F. Rjou, I.R. Nabiev, F. Lavelle, M. Manfait; *Cancer Res.* **1993**, 53, 4784.

25. I.R. Naviev, H. Morjani, M. Manfait; *Eur. Biophys. J.* **1991**, 19, 311.

26. K. Sokolov, P. Hodorchenko, A. Ptukhov, I. Naviev, G. Chumanov, T.M. Cotton; *Appl. Spectrosc.* **1993**, 47, 515.

27. W.S. Sutherland, J.D. Winefordner; *J. Raman Spectrosc.* **1991**, 22, 541.

28. E. Wood, C. Sutton, A.E. Beezer, J.A. Creighton, A.F. Davis, J.C. Mitchell; *Int. Pharm.* **1997**, 28, 73.

29. R. Picorel, T. Lu, R.E. Hold, T.M. Cotton, M. Seibert; *Biochemistry* **1993**, 29, 707.

30. B.N. Rospendowski, J.M. Campell, J. Reglinski, W.E. Smith; *Eur. Biophys. J.* **1992**, 21, 257.

31. X. Dou, T. Takama, Y. Yamaguchi, H. Yamamoto; *Anal. Chem.* **1997**, 69, 1492.

32. T.E. Rohr, T.M. Cotton, F. Ni, P. Tarcha; *J. Anal. Biochem.* **1989**, 182, 388.

33. V. Decket, D. Zeisel, R. Zenobi; *Anal. Chem.* **1998**, 70, 2646.

34. N.R. Isola, D.L. Stokes, T. Vo-Dinh; *Anal. Chem.* **1998**, 70, 1352.

35. K.T. Carron, B.J. Kennedy; *Anal. Chem.* **1995**, 67, 3353.

36. E. Horvath, J. Mink, J. Kristof; Mikrochim. *Acta, Suppl.* **1997**, 14, 745.

37. N. Weissenbacher, B. Lendle, J. Frank, H.D. Wanzenbock, B. Mizaikoff, R. Kellner; *J. Mol. Struct.* **1997**, 410-411, 539.

38. R. Kellner, B. Mizaikoff, M. Jakusch, H.D. Wanzenbock, N. Weissenbacher; *Appl. Spectrosc.* **1997**, 51, 495.

39. N. Taraneko, J.P. Alarie, D.L. Stokes, T. Vo-Dinh; *J. Raman Spectrosc.* **1996**, 27, 379.

40. T. Murphy, H. Schmidt, H.-D. Kronfeldt; *Proc. SPIE-Int. Soc. Opt. Eng.* **1997**, 3107, 281.

41. E. Koglin, B.J. Kip, R.J. Meier; *J. Phys. Chem.* **1996**, 100, 5078.

42. K. Kneipp, Y. Wang, R.R. Dasari, M.S. Feld; *Appl. Spectrosc.* **1995**, 49, 780.

43. K. Kneipp, Y. Wang, H. Kneipp, R.R. Dasari, M.S. Feld; *Exp. Tech. Phys.(Lemgo, Ger.)* **1995**, 41, 225-234.

44. K. Kneipp, Y. Wang, H. Kneipp, L.T. Perelman, I. Itzkan, R.R. Dasari, M.S. Feld; *Phys. Rev. Lett.* **1997**, 78, 1667-1670.

45. K. Kneipp, H. Kneipp, R. Manoharan, I. Itzkan, R.R. Dasari, M.S. Feld; *J. Raman Spectrosc.* **1998**, 29, 743-747.

46. K. Kneipp, H. Kneipp, V.B. Kartha, R. Manoharan, G. Deinum, I Itzkan, R.R. Dasari, M.S. Feld; *Phys. Rev. E: Stat. Phys., Plasmas, Fluids, Relat. Interdiscip. Top.* **1998**, 57, R6281-R6284.

47. K. Kneipp, H. Kneipp, G. Deinum, I. Itzkan, R.R. Dasari, M.S. Feld; *Appl. Spectrosc.* **1998**, 52, 175-178, 1493-1497.

48. S. Nie, S.R. Emory; *Science*, **1997**, 275, 1102-1106.

49. S.R. Emory, S. Nie; *J. Phys. Chem. B* **1998**, 102, 493-497.

50. S.R. Emory, S. Nie; *Anal. Chem.* **1997**, 69, 2631-2635.

51. S.R. Emory, W.E. Haskins, S. Nie; *J. Am. Chem. Soc.* **1998**, 120, 8009-8010.

52. R.A. Scott, A.G. Mauk; *Cytochrome c: A multidisciplinary Approach*; Sausalito, Calif. University Science Books, 1996.

53. S. Papa, B. Chance, L. Ernster; *Cytochrome systems: Molecular Biology and Bioenergentics*; Plenum press, New York, 1987.

54. G.V. Louie, G.D. Brayer; *J. Mol. Biol.* **1990**, 214, 527.

55. A.M. Berghuis, .D. Brayer; *J. Mol. Biol.* **1992**, 223, 259.

56. T. Takano and R.E. Dickerson, *J. Mol. Biol.* **1981**,153, 79.

57. M. Smith, D.W. Leung, S. Gillam, Cr. Astell, D.L. Montgomery, B.D. Hall; *Cell* **1979**, 16, 753.

58. D.L. Montgomery, D.W. Leung, M. Smith, P. Shalit, G. Fay, B.D. Hall; *Proc. Natl. Acad. Sci., USA* **1980**, 77, 541.

59. M. Smith; *Ann. Rev. Genet.* **1985**, 19, 423.

60. M. Smith; *Phil. Trans. R. Soc. Lond* **1986**, A317, 295.

61. G.J. Pielak, A.G. Mauk, M. Smith; *Nature* **1985**, 313, 152.

62. L.L. Pearce, A.L. Gartner, M. Smith, A.G. Mauk; *Biochemistry* **1988**, 28, 3152.

63. S. P. Rafferty, L. L. Pearce, P. D. Barker, J. G. Guillemette, C. M. Kay, M. Smith and A. G. Mauk; *Biochemistry* **1990**, 29, 9365.

64. G.L. Pielak, K. Oikawa, A.G. Mauk, M. Smith, C.M. Kay; *J. Am. Chem. Soc.* **1986**, 108, 2724.

65. Rafferty, S. P.; Pearce, L. L.; Barker, P. D.; Guillemette, J. G.; Kay, C. M.; Smith, M.; Mauk, A. G. *Biochemistry* **1990**, *29*, 9365.

66. T.L. Luntz, A. Schejter, A.E.A. Garber, E. Margoliash; *Proc. Natl. Acad. Sci., USA* **1989**, 86, 3524.

67. T.B. White, P.B. Berget, B.T. Nall; *Biochemistry* **1987**, 26, 4358.

68. P.R. Gooley, N.E. Mackennzie; *FEBS Lett.* **1990**, 260, 225.

69. G.R. Moore, D.E. Harris, F. Leitch, G.A. Pettigrew; *Biochim. Biophys. Acta* **1984**, 764, 331.

70. R.L. Cutler, A.M. Davis, S. Creighton, A. Warshel, G.R. Moore, M. Smith, A.G. Mauk; *Biochemistry* **1989**, 28, 3188.

71. F. Gonzalez; *Parmacol. Rev.* **1989**, 40, 243.

72. D. Holzschu, L. Principio, K.T. Conklin, Dr. Hickey, J. Short, R. Rao, G. McLendon, F. Sherman; *J. Biol. Chem.* **1987**, 262, 7125.

73. J.T. Hazzard, G.L. McLendon, M.A. Cusannovich, G. Das, F. Sherman, G. Tollin, *Biochemistry* **1988**, 27, 4445.

74. T.N. Sorrell, P.K. Martin, E.F. Bowden; *J. Am. Chem. Soc.* **1989**, 111, 766.

75. T.G. Spiro, X.Y. Li; "Resonance Raman Spectroscopy of Metalloporphyrins," in *Biological Applications of Raman Spectroscopy*; T.G. Spiro, Eds., Vol.3 John Willy, New York, 1988.

76. X.-Y. Li, R. S. Czernuszewicz, J.R. Kincaid, P. Stein, and T.G. Spiro; J. Phys. Chem. **1990**, 94, 47.

77. P. Hildebrandt, and M. Stockburger; in *Raman Spectroscopy: Sixty years on Vibrational Spectra and Sturcture*; H.D. Bist, Eds., Elsevier Science, Netherlands, Vol. 17A, 1989.

78. T.M. Cotton, S.G. Schultz, and R.P. van Duyne; J. Am. Chem. Soc. **1980**, 102, 7960.

79. T.M. Cotton; in *Spectroscopy of Surfaces*; R.J.H. Clark and R.E. Hester, Eds., Wily, New York, 1988.

80. P. Hildebrandt, and M. Stockburger; Biochemistry **1989**, 28, 6710.

CHAPTER 2

PHOTOINDUCED ELECTROCHEMICAL REDUCTION OF NITRITE AT ELECTROCHEMICALLY ROUGHENED SILVER SURFACE

A paper accepted by the *Journal of Physical Chemistry*(JP990928H)

Junwei Zheng, Tianhong Lu, Therese M. Cotton and George Chumanov

Abstract

Photoelectrochemical reduction of nitrite and nitrate was studied on the surface of an electrochemically roughened silver electrode. The dependence of the photocurrent on photon energy, applied potential and concentration of nitrite was determined. It was concluded that the photoelectrochemical reduction proceeds via photoemission process followed by the capture of hydrated electrons by electron acceptors. The excitation of plasmon resonances in nanosize metal structures produced during the roughening procedure resulted in the enhancement of the photoemission process. Ammonia was detected as one of the final products in this reaction. Mechanisms for the photoelectrochemical reduction of nitrite and nitrate are proposed.

Introduction

The reduction of nitrite is of significant importance for many reasons including remediation of environmental pollutants and chemical technology. Nitrites are present in high concentration in caustic radioactive waste from nuclear plants and the reduction to gaseous products would greatly lessen the volume of such waste [1,2]. The reduction of nitrite to various compounds (for example, hydroxylamine) would provide industrially useful

intermediates for the production of many chemicals [3]. Methods based on electrochemical reduction can also be potentially used for the detection of nitrite in different analytical applications [4,5].

In spite of considerable effort, efficient electrochemical reduction of nitrite could not be achieved because of the large overpotential that is required at neutral and alkaline pH's (ca. -1.4 V in 1 M NaOH at a Ag cathode [6]). The reduction can occur at less negative potentials in acidic media; however, under these conditions nitrite is unstable and decomposes to form different species, thereby complicating the process [7]. Various approaches that have yielded some measure of success in lowering the high overpotential include the use of catalytic electrode materials, such as Ni [6], Zn [6], Cd [8] and Cu [6], the addition of catalysts such as metal cyclams to the electrolytic solution [9], and the adsorption of the catalyst on the electrode, as in the case of copper-phenanthroline complexes on graphite [10]. Highly promising photoassisted reduction of nitrate has been also studied at mercury electrodes immersed in suspensions of semiconductor particles [11-13].

The first observation of the photoelectric effect at a metal-electrolyte interface is attributed to Becquerel, who in 1839 noted an electric current between two electrodes immersed in dilute acid solution when one of the electrodes was illuminated with light [14]. Following his observation, this effect was extensively studied and finally demonstrated to result from photoemission process (reviewed in [15]). The concept was postulated as early as 1965 by Barker et al. who proved that at certain electrode potentials and photon energies the observed photocurrent arises from photoelectron emission from the metal into the electrolyte solution [16]. Prior to his work, Berg attributed experimentally observed photocurrent at a mercury electrode to the absorption of light by the metal and production of

"hot electrons" causing an increase of the electron transfer rate to the solute in the solution [17]. Heyrovsky invoked the concept of photodecomposition of surface charge transfer complexes formed between a metal and a solvent or solute [18]. The absorption of light by these complexes resulted in bond rupture and electron transfer either to the metal or to the adsorbate, depending upon whether the latter functions as an electron donor or an electron acceptor, respectively. Both of these mechanisms are feasible and, at different experimental conditions, can contribute to varying extents to the observed photocurrent. However, the fundamental photoemission process is the direct ejection of an electron into the solution and does not depend upon the presence of photoactive species. Ejected electrons undergo rapid thermalization and hydration in solution. The hydrated electron may then react with species in solution (scavengers) or, if none are present, return to the electrode thereby reducing the net photocurrent to zero.

From the dependence of the photocurrent on photon energy and electrode potential, Barker noted that the experimental results did not fit the model developed for photoemission into vacuum [16]. The presence of the electrical double layer in a condensed medium has a strong influence on the photoemission process. A new quantum mechanical theory was required to describe the photoemission phenomena at metal/electrolyte interfaces. Based on the method of threshold approximation, a so-called "2/5-law" was developed by Brodsky and Gurevich [19]. The "2/5 law" has been widely accepted for determining the relationship between the applied potential and the photoemission current.

The effects of the surface roughness on the photoemission have been addressed in several studies. In 1974 Sass et al. demonstrated that the photocurrent for proton reduction at roughened silver electrodes increased by approximately 100 fold over that at smooth Ag

surface [20]. The dependence of the photoemission upon photon energy was found to correlate with the surface plasmon absorption in silver. Corrigan and Weaver studied laser-induced electron transfer at metal surfaces for Co(III) and Cr(II) amine complexes [21]. A substantial enhancement of the photocurrent was obtained after electrochemical roughening of silver and gold surfaces. More recently, Kostecki and Augustynski have observed strong cathodic photocurrents for silver electrodes immersed in saturated CO_2 solutions [22]. The maximum of the photocurrent also corresponded to the peak of the plasmon resonance in silver.

In the present study, the excitation of surface-plasmon resonances on the surface of electrochemically roughened silver electrode was used to enhance electroreduction of nitrite. It is demonstrated that the photoinduced electroreduction occurred via photoemission of electrons from the metal with subsequent capturing by the electron acceptor. Ammonia was identified as one of the final products in this reaction.

Experimental Methods

Electrochemical measurements were carried out in a conventional three-electrode cell. A platinum wire served as the auxiliary electrode. A saturated calomel electrode (SCE) was used as the reference electrode. All potentials are reported with respect to the SCE. Working electrodes were constructed from a polycrystalline silver wire that was sealed into glass tubing with Torr Seal (Varian Associates, Palo Alto, CA) epoxy resin. The surface area of the electrodes was ca. 0.09 cm^2. Before each experiment, the electrode surface was polished in sequence with aqueous suspensions of 5, 0.3, and 0.05-micron alumina until a

shiny, mirrorlike finish was obtained. The electrodes were cleaned by sonication three times (total 30 min) in Milli-Q water.

The silver surface was electrochemically roughened using double-potential step oxidation-reduction cycles performed with a custom-built potentiostat/integrator. The supporting electrolyte was 0.1 M Na_2SO_4. All solutions were purged with nitrogen gas for 15 min prior to each experiment. Three cycles of the following sequence were performed: the potential was initially stepped to +0.55 V at which 25 mC/cm^2 of charge was allowed to pass, and then the potential was stepped to -0.60 V until the current reached a minimum. The electrochemical roughening increased the surface area of the electrode from 0.09 to 0.15 cm^2 as determined by underpotential lead deposition.

Cyclic voltammetric measurements were performed at room temperature with a Model 173 potentiostat/galvanostat connected to a Model 175 universal programmer (Princeton Applied Research). The cyclic voltammograms (CVs) were plotted on an X-Y recorder. The scan rate was 10 mV/s in all of the experiments.

The working electrode was irradiated with 362, 413, 647 457, 476, 488, 496, 514 nm light using Kr^+ (Coherent, Innova 100) and an Ar^+ (Coherent, Innova 200) lasers. The light was focused to a 2 mm spot on the electrode surface. The power was measured with Model 210 (Coherent) power meter. Unless otherwise stated, the laser power was 100 mW in all of the experiments.

In the bulk electrolysis experiments the electrode potential was maintained at –1.0 V. The surface was irradiated continuously and the solution was stirred. The concentration of NH_3 formed during the photoelectrolysis was determined by the Nesslor method [23].

Results and Discussion

Effect of electrode material and surface treatment. The effect of irradiation on the electrochemical reduction of the nitrite (1 mM $NaNO_2$ in the 0.1 M Na_2SO_4 solution, pH=7) at different electrodes is shown in Figure 1. Cathodic currents measured in the dark and under irradiation were compared for different electrodes. The comparison was performed at -1.0 V where there was almost no electrochemical nor photoelectrochemical evolution of hydrogen. In the case of the mercury electrode, very little difference (less than -0.1 μA) can be noted between CVs measured in the dark and in the light (Figure 1, A). A somewhat greater photocurrent (ca. -0.4 μA) was observed at the polished silver surface (Figure 1, B). The roughened silver electrode, in contrast, exhibited a large increase (approximately 26 fold, from ca. -0.4 μA to -10.7 μA) in cathodic current during the illumination (Figure 1C). This increase can not be simply attributed to the small (ca. 1.5 fold) increase in the surface area resulted from the roughening. Moreover, the onset potential of the current was also shifted positively by approximately 400 mV from –1.0 V to –0.6 V under illumination (Figure 1, C). These facts indicate that the photocurrent at the roughened electrode is enhanced due to the excitation of plasmon resonances in nanoscale metal structures generated during the roughening procedure.

Effect of excitation wavelength on photoelectrochemical response. Cyclic voltammograms measured in 1 mM $NaNO_2$ and 0.1 M Na_2SO_4 solution in the dark and under irradiation with a series of excitation wavelengths are shown in Figure 2. Curve (a)

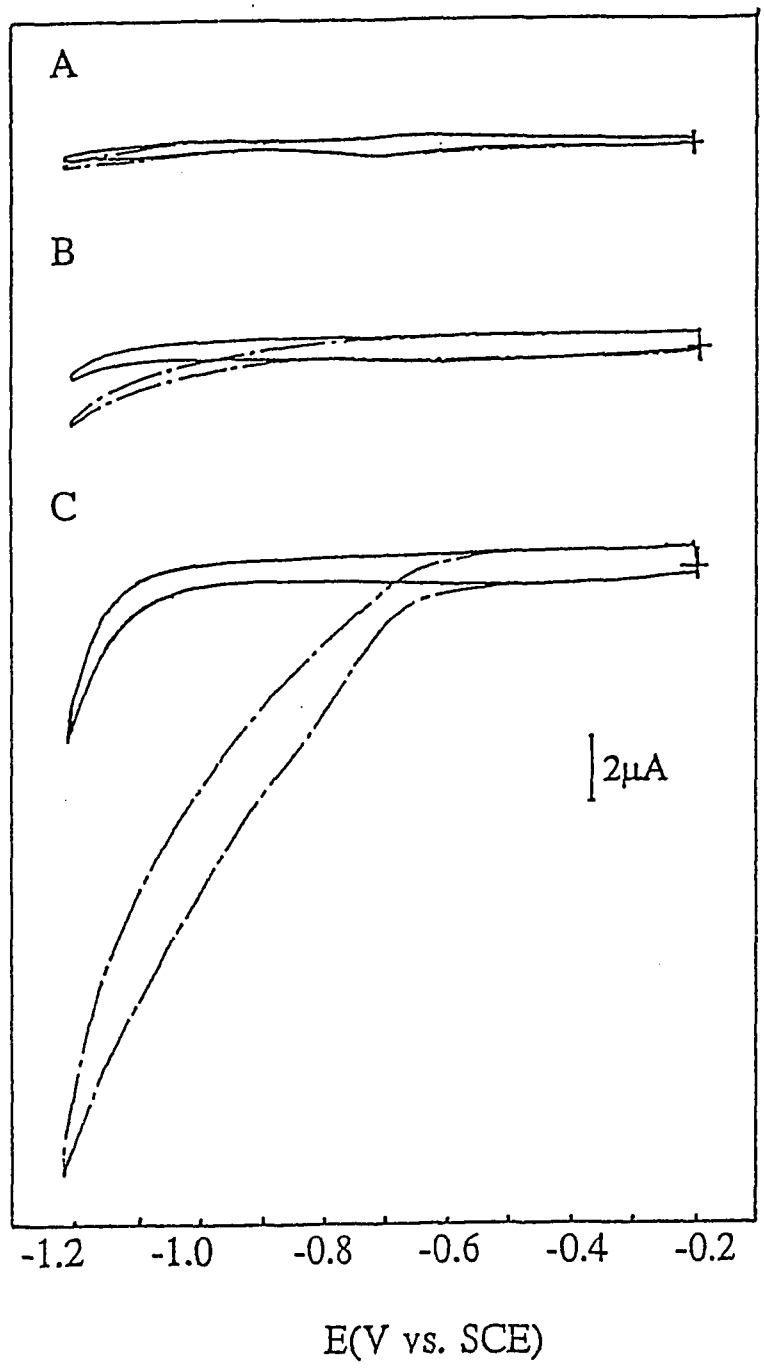

Figure 1. Cyclic voltammograms of 1 mM $NaNO_2$ in 0.1 M Na_2SO_4 solution at the (A) Hg, (B) polished Ag, (C) roughened Ag electrodes. Solid curve: in dark, Dashed curve: with 413 nm irradiation.

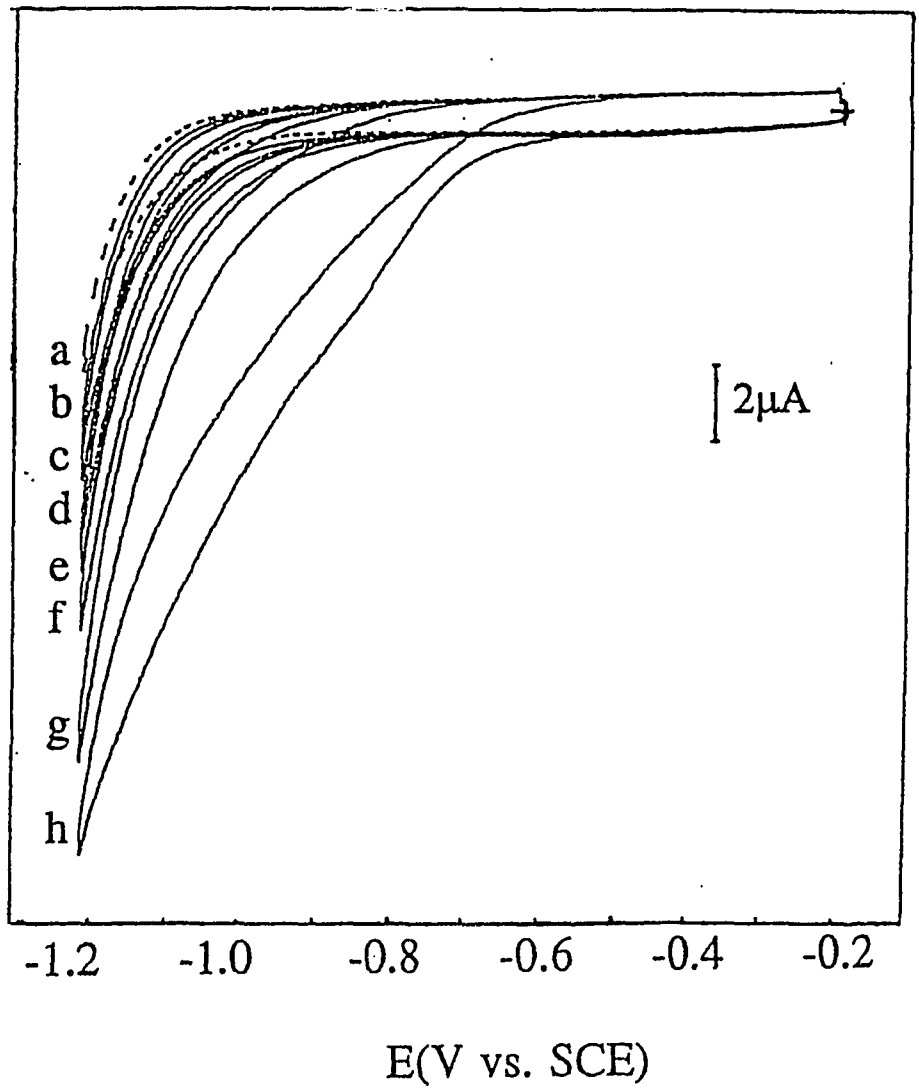

Figure 2. Excitation wavelength dependence of cyclic voltammograms of 1 mM $NaNO_2$ in 0.1 M Na_2SO_4 solution at the roughened Ag electrode. (a) dark (b) 647 (c) 514 (d) 496 (e) 488 (f) 476 (g) 457 (h) 413 nm.

depicts the dark current for the potential scan from –0.2 V to –1.2 V. The successive curves b – h were obtained during laser irradiation with wavelengths from 647 to 413 nm. Two important features should be noted: the photocurrent increases with photon energy and the onset potential for the reduction of nitrite shifts positively as the photon energy is increased. The overall shape of curves (a-g) are very similar, but curve (h) (413 nm excitation) has a distinct shoulder near -0.85 V and relatively larger photocurrent in the potential region between -0.8 and -1.0 V. The shoulder is even more pronounced at higher excitation energy (363.8 nm) and appears shifted to more positive potentials (Figure 3). Two peaks in the potential scan under irradiation suggest the presence of two photoinduced electrochemical processes that are "hidden" in inaccessibly negative region without irradiation.

The dependence of the photocurrent at -1.0 V on the excitation wavelength is plotted in Figure 4. Although, this "action spectrum" is not of sufficiently high resolution to determine accurately the maximum in the curve, it is clear that the photocurrent increases rapidly in the spectral region from 500 to 400 nm and decreases below ca. 400 nm. The data, therefore, indicate a resonance behavior of the photocurrent, corresponding to the plasmon resonance absorption in silver.

The possibility that the photocurrent at a roughened silver electrode may result from a photoemission process in which nitrite functions as a scavenger of hydrated electrons, is considered next. The dependence of the photocurrent on photon energy and applied potential is well-characterized for the photoemission process from metals into vacuum [24]. However, this is not an appropriate model for metals in contact with electrolytes, as shown in the study of Barker et al [16]. In the case of the photoemission into vacuum, the

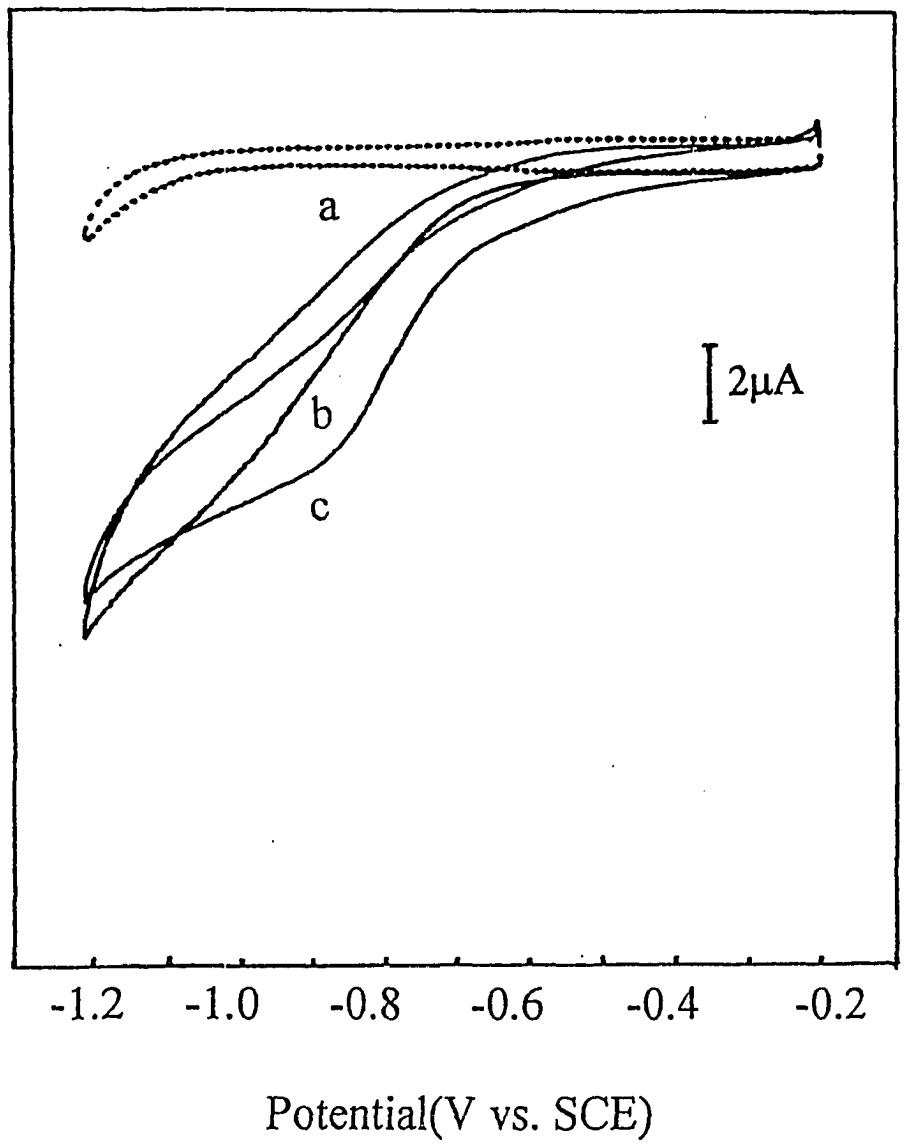

Figure 3. Excitation wavelength dependence of cyclic voltammograms of 1 mM $NaNO_2$ in 0.1 M Na_2SO_4 solution at the roughened Ag electrode. (a) dark (b) 413 nm (c) 363.8 nm.

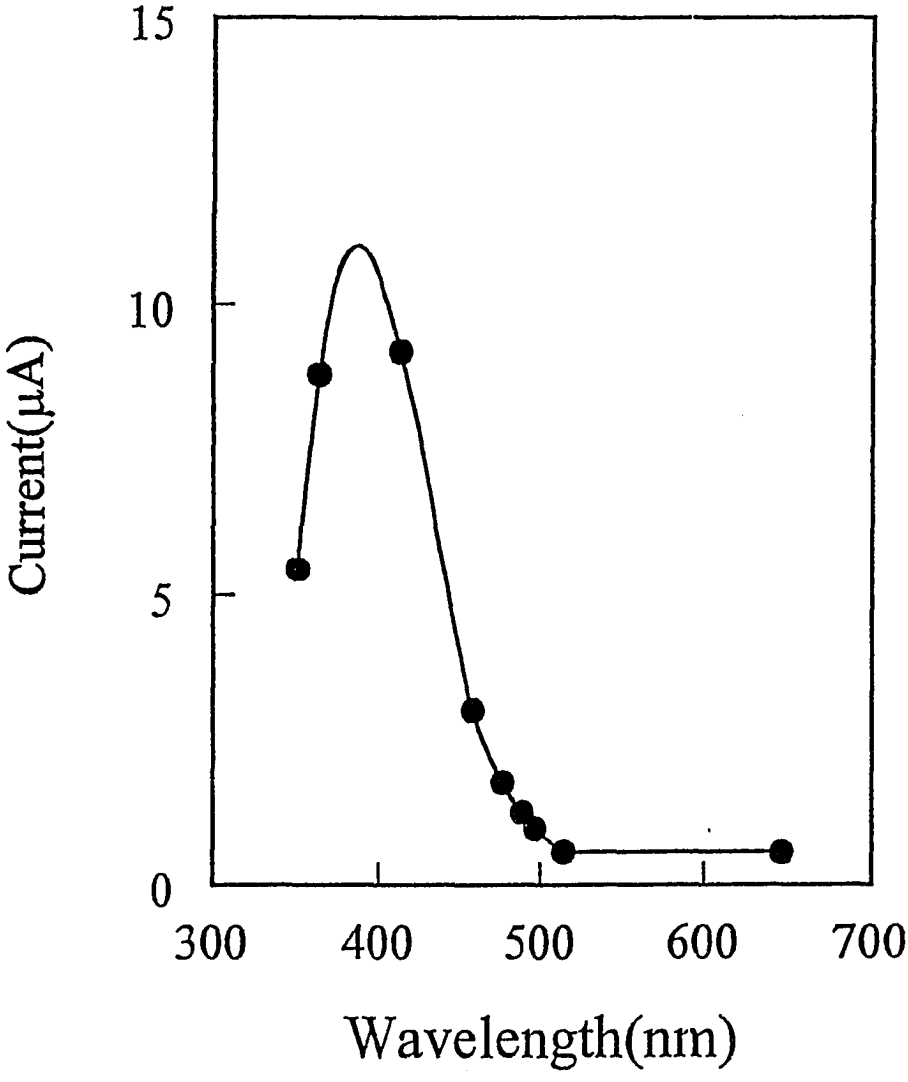

Figure 4. Excitation wavelength dependence of photocurrent at -1.0 V for nitrite reduction at the roughened Ag electrode. Data obtained from Figure 2 and 3.

photocurrent is known to depend quadratically on the difference between the energy of the excitation photon ($\hbar\omega$) and the threshold photon energy ($\hbar\omega_o$):

$$I \sim (\hbar\omega - \hbar\omega_o)^2 \qquad (1)$$

This is known as Fowler's parabolic law for the photocurrent where the threshold photon energy is equal to the work function of the metal. In the case of the photoemission into an electrolyte solution, the theoretical description by Brodsky and Gurevich [19] predicts the "5/2 law":

$$I \sim (\hbar\omega - \hbar\omega_o(E))^{5/2} \qquad (2)$$

where the threshold photon energy is now dependent upon the electrode potential E. Thus, the two distinct features of photoemission into an electrolyte solution include the 5/2 power dependence and the shift in the threshold photon energy with the electrode potential:

$$\hbar\omega_o = \hbar\omega_o(E_o) + e\,(E - E_o) \qquad (3)$$

where E_o is the potential of zero charge. Data obtained for the photoreduction of nitrite ion will next be analyzed in terms of the above two predictions.

The plot of the photocurrent raised to the 0.4 power versus potential measured at -1.0 V is shown in Figure 5. In the case of 1 mM $NaNO_2$ in a 0.1 M Na_2SO_4 solution, a nonlinear behavior can be observed near the onset potential (Figure 5, curve a). A similar phenomenon was also reported by Pleskov et al., who claimed that the nonlinearity is related to the low concentration of electrolyte or electron acceptor in the double layer [25]. The "5/2 law" which is based on the threshold approximation is only valid for concentrated electrolytes, where the potential drop between metal and solution is confined to the dense

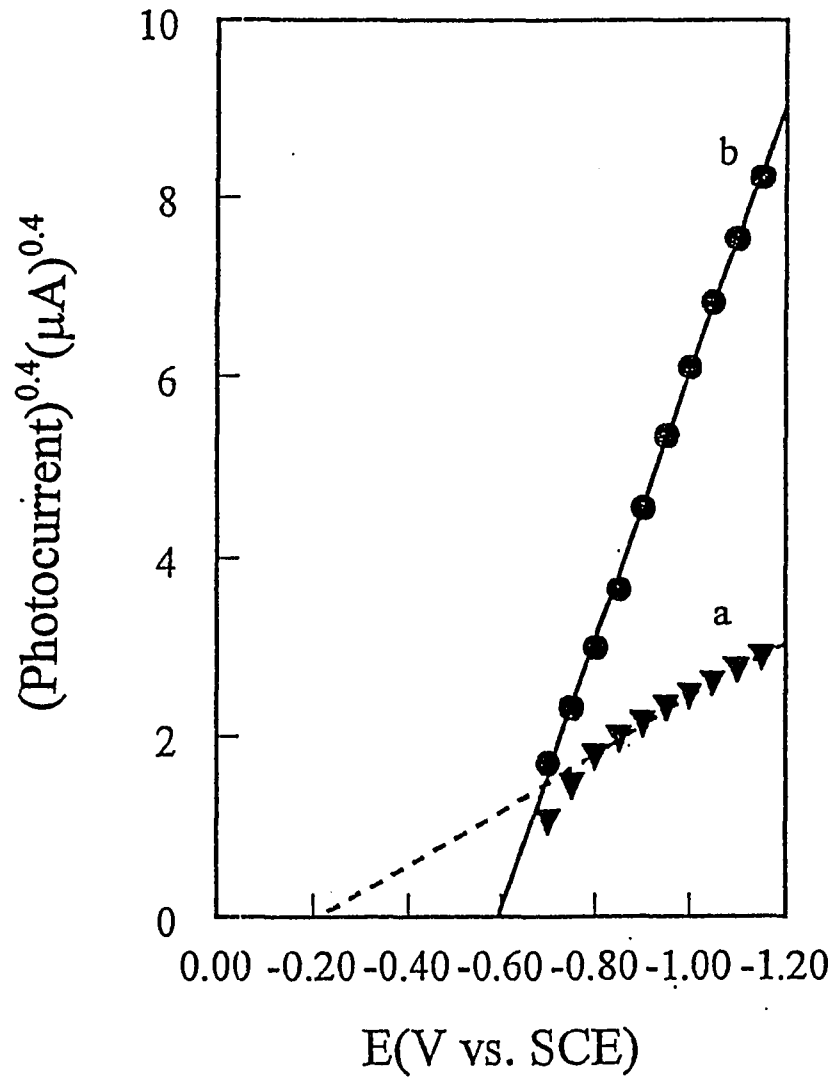

Figure 5. Potential dependence of photocurrent for nitrite reduction at roughened Ag electrodes in (a) 1 mM $NaNO_2$ + 0.1 M Na Na_2SO_4 solution.

part of the double layer. As can be seen in the case of 0.5 M $NaNO_2$ in the 1 M Na_2SO_4 solution, the data fit the expected linear relationship quite well (Figure 5, curve b).

The plot of the onset potential versus photon energy is shown in Figure 6. The onset potential was determined from Figure 2 as the potential at which the current started to flow in the cathodic scan. The relationship is linear, in agreement with Equation (3), however the slope is ca. -2.0 instead of -1.0 expected for concentrated acceptor solutions [26]. The larger slope could result from low acceptor concentration [15].

The photoelectrochemical response as a function of nitrite concentration in the range between 0.5 and 10 mM exhibits nonlinear behavior (Figure 7, insert). According to the model in which hydrated electrons are captured by electron scavengers, it is expected that this response should follow square root dependence at low concentrations and reach saturation at high concentrations [19]. Indeed, the corresponding plot in Figure 8 confirms this model for the photoreduction of nitrite at electrochemically roughened silver surface. The square root dependence reflects the fact that not all photoemitted electrons were captured by nitrite ions; some electrons returned to the electrode. This back current is affected by nitrite concentration. The dependence of the photocurrent on the incident laser power follows linear behavior which is characteristic of a one-photon process [27] and is expected for the power used in these experiments (Figure 9).

The time evolution of the photocurrent in a quiescent solution of 1m M nitrite ion is shown in Figure 10. The initial current of approximately 24 μA decayed exponentially in 40 seconds to a steady state value of 12 μA corresponding to the diffusion controlled photoelectrochemical reduction process. It is important to mention, that this current remained nearly constant as long as the concentration of nitrite ions remained unchanged,

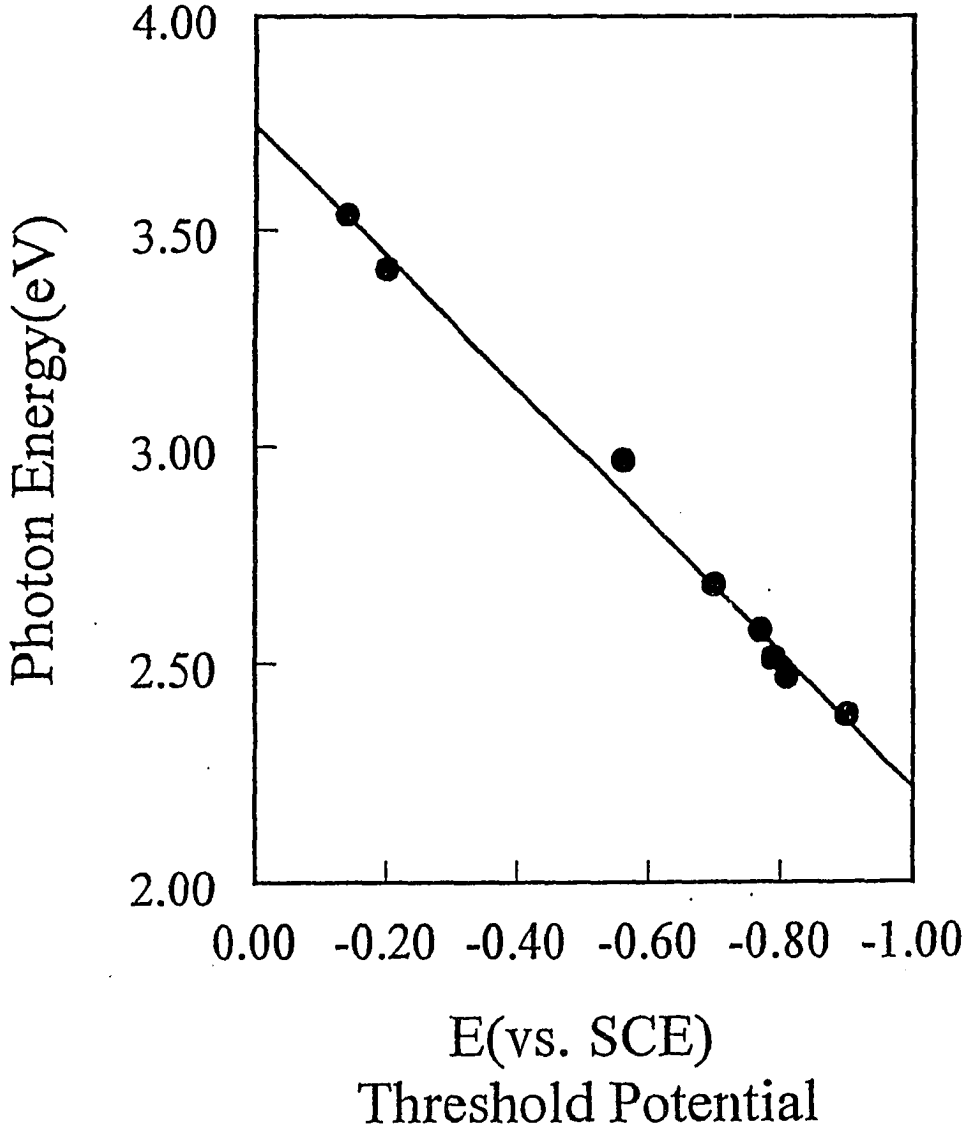

Figure 6. Photon energy dependence of onset potential. Data obtained from Figure 2 and 3.

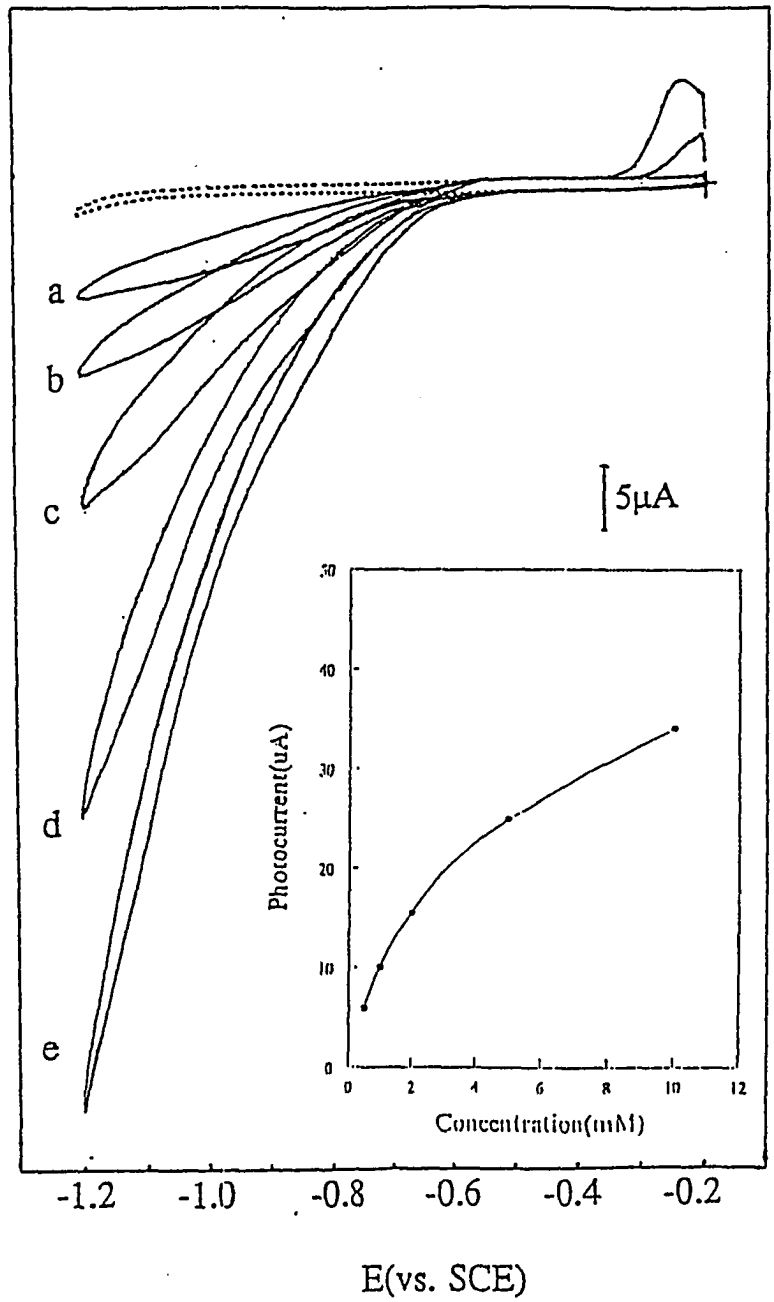

Figure 7. Cyclic voltammograms of $NaNO_2$ with different concentration at the roughened Ag electrode with 413 nm irradiation. Dashed curve: dark. (a) 0.5 mM (b) 1 mM (c) 2 mM (d) 5 mM (e) 10 mM. Insert: Plot of photocurrent at -1.0 V versus concentration.

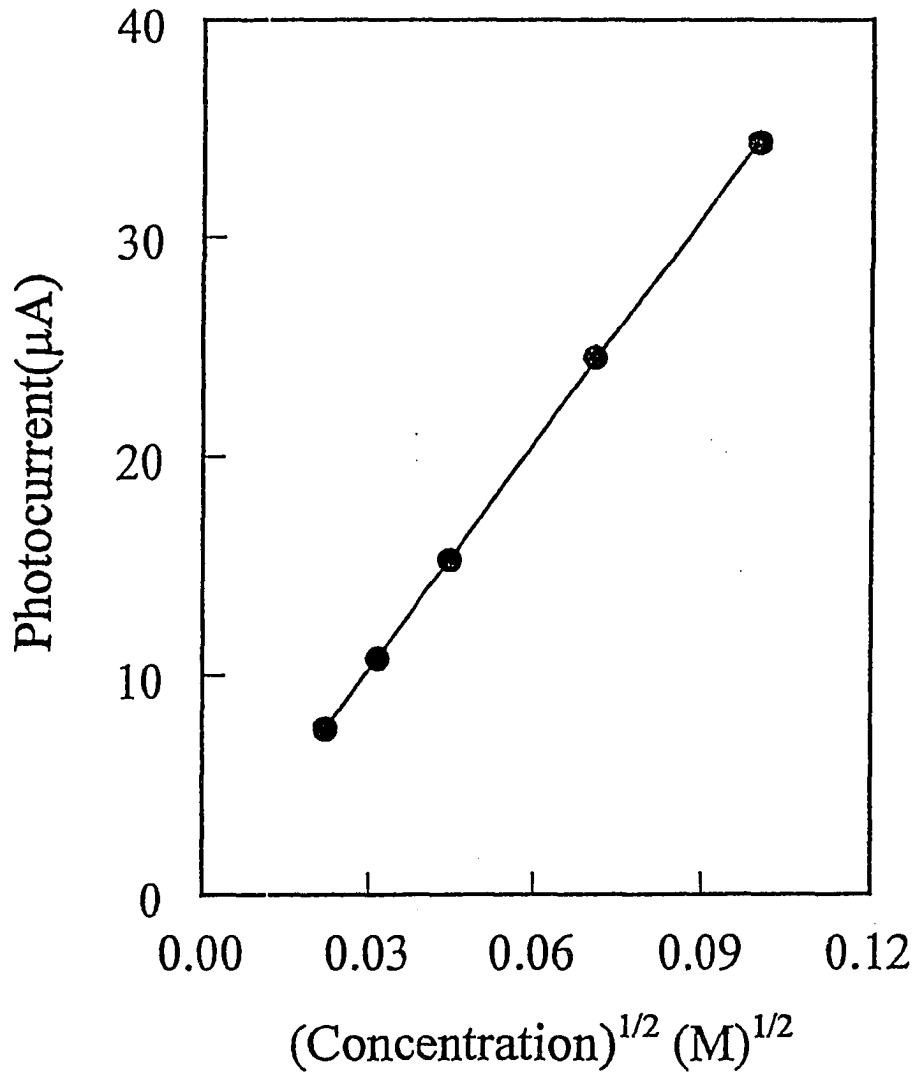

Figure 8. Plot of photocurrent as a function of $C^{1/2}$. Data obtained from Figure 7.

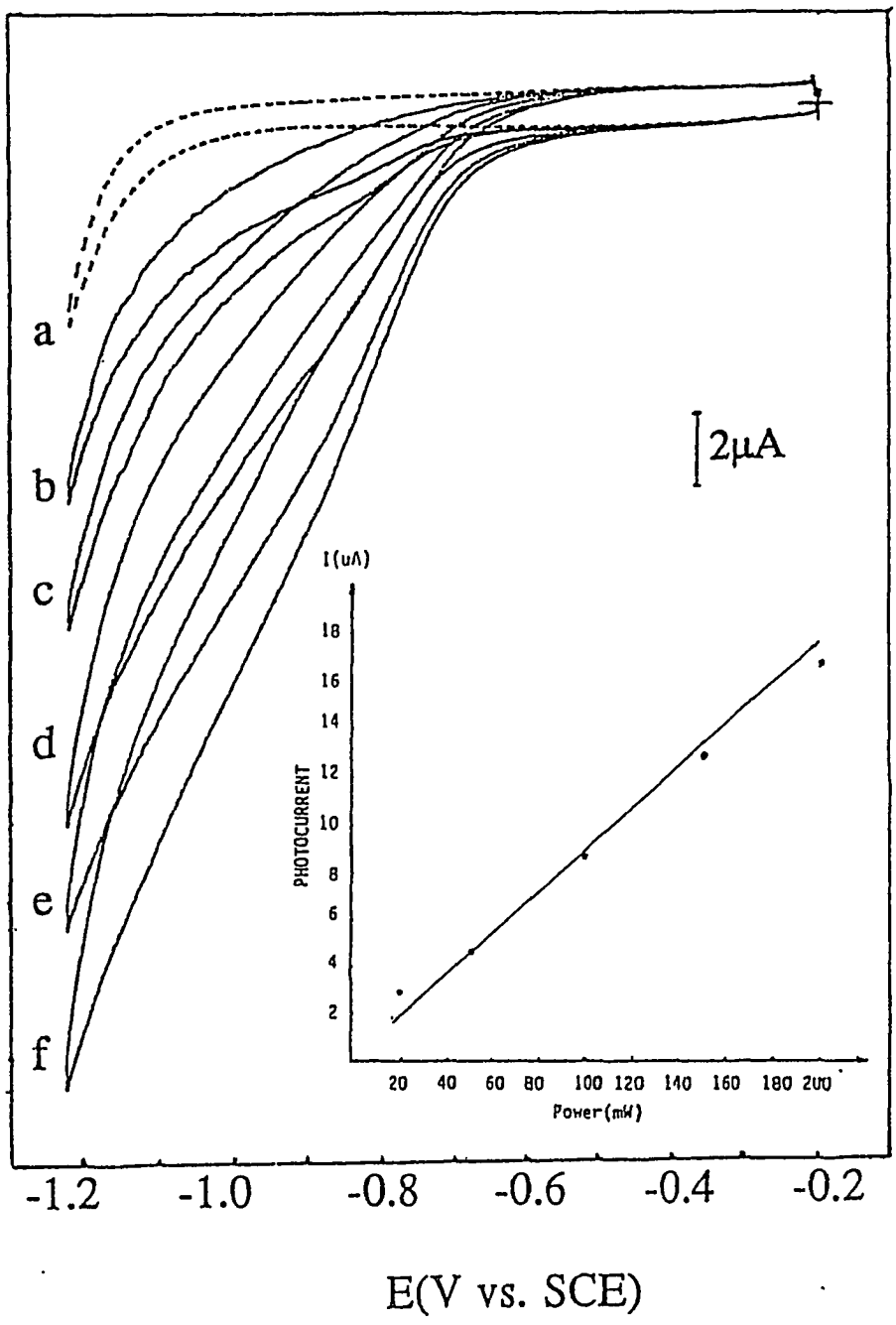

Figure 9. Power dependence of cyclic voltammograms of 1 mM $NaNO_2$ in 0.1 M Na_2SO_4 solution at the roughened Ag electrode with 413 irradiation. Insert: Plot of photocurrent at -1.0 V versus power of irradiation.

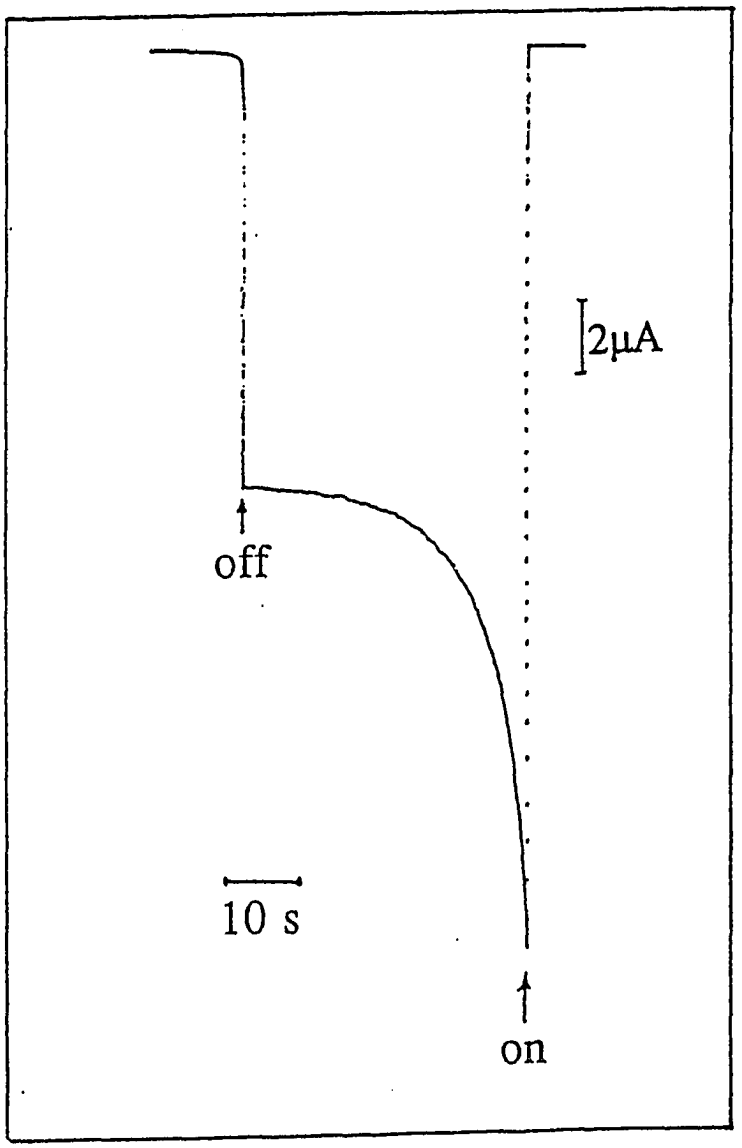

Figure 10. Photoresponse of 1 mM $NaNO_2$ in 0.1 M Na_2SO_4 solution at -1.0 V at the roughened Ag electrode with 413 nm irradiation.

indicating little or no poisoning of the electrode surface by reaction intermediates or products. Electrolysis experiments at the controlled potential were further performed under the irradiation with 413 nm light and ammonia was detected as one of the products.

Based on the experimental results, possible mechanisms for the photoelectrochemical reduction of nitrite at roughened silver electrode are proposed. Photogenerated hydrated electrons $e^-(aq)$ are captured by nitrite to form NO_2^{2-} which undergoes the hydrolysis. Following this initial photochemical step, several electrochemical reactions take place:

$$NO_2^- + e^-(aq) \rightarrow NO_2^{2-}$$

$$NO_2^{2-} + H_2O \rightarrow NO + 2\,OH^-$$

$$NO + e^- \rightarrow NO^{-\bullet}$$

$$NO^{-\bullet} + 2e^- \rightarrow NH_2OH$$

$$NH_2OH + 2e^- \rightarrow NH_3$$

It is important to emphasize that the measured current is the sum of the photocurrent and the current due to subsequent electrochemical reactions. This issue must be taken in to account when determining the photoelectrochemical efficiency. In the proposed mechanism the total number of the electrons crossing the interface is six and only one electron is photogenerated.

Even though no measurements of nitrogen gas were performed in this study, its formation could also take place. As the concentration of $NO^{-\bullet}$ product in the diffusion layer increases, the dimeric species $(N_2O_2)^{2-}$ can be formed with further decomposition into N_2O [27]. Nitrous oxide can then react with the hydrated electron and undergo the following reactions:

$$N_2O + e^-(aq) \rightarrow N_2O^-$$

$$N_2O^- + H_2O \rightarrow N_2 + OH^\bullet + OH^-$$

$$OH^\bullet + e^- \rightarrow OH^-$$

Three photoelectrons among total of six are required for the reduction of $2NO_2^-$ to nitrogen gas N_2 according to this scheme. Finally, any electrochemical reaction following the photochemical step can "utilize" hydrated electrons as well. This fact complicates even more the exact determination of the number of photoelectrons that contribute to the measured photocurrent making calculations of the photoefficiency difficult. Nevertheless, we estimated the quantum efficiency of about 0.04% for nitrite photoreduction on the electrochemically roughened silver surface. The estimate is based exclusively on the assumption that only one photoelectron is captured.

Effect of pH. The pH of the solution strongly affects the reduction potential of nitrite, as demonstrated for a number of different electrodes [28-31]. For the silver electrode, Cattarin [6] reported that the nitrite reduction in the 1 M NaOH begins in the potential region of hydrogen evolution, ca. – 1.4 V. The product formed was identified as ammonia. Our results obtained in the dark in 1 mM $NaNO_2$ and 0.1 M NaOH solution are consistent with that report (Figure 11, dashed curve). However, when irradiated with 413 nm light the onset potential for the reduction was shifted to –0.6 V (Figure 11, solid curve). Comparing to that at neutral pH (Figure 1, C), two new features at –1.08 and –1.35 V appeared in the cathodic scan. These features could represent the reduction of different intermediates, reduction potentials of which are shifted to more positive values in alkaline pH. It should be noted that under irradiation the onset potentials for the nitrite reduction were the same at -0.6 V in both neutral and alkaline solutions, thereby indicating that the photoemission process is essentially independent on pH.

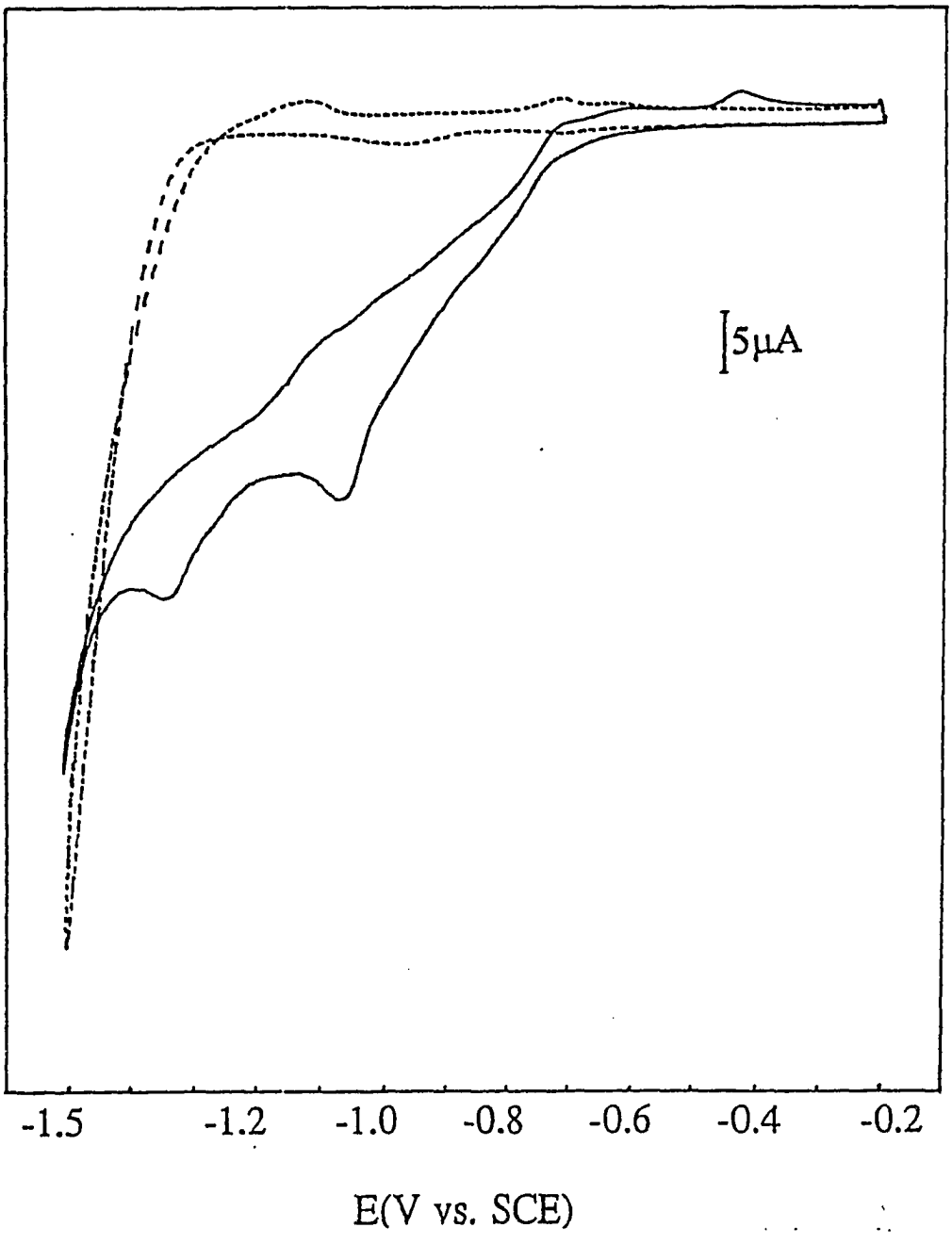

Figure 11. Cyclic voltammograms of 1 mM $NaNO_2$ in 0.1 M NaOH solution at the roughened Ag electrode. Dashed curve: in dark. Solid curve: with 413 nm irradiation.

Reduction of Nitrate. A photoelectrochemical response was also observed in the solution of nitrate (Figure 12). Nitrate can be electrochemically reduced to nitrite without irradiation via two-electron step process (Figure 12, dashed curve). The reduction peak at -1.1V reflects a large overpotential that is required for this reaction because of the rapid reoxidation of high energy, NO_3^{2-} intermediate ion [27]. Since no light is required to convert nitrate to nitrite, the observed photocurrent was attributed mainly to the photoelectrochemical reduction of nitrite according to mechanisms described above. The limiting step in overall reaction is the electrochemical reduction of NO_3^- to NO_2^- that occurs at the potentials more negative than the onset potential for the photoelectrochemical reduction of NO_2^-. For this reason, no dependence of the onset potential on irradiation is expected. Indeed, the reduction current under irradiation (Figure 12, solid curve) increased ca. twice relative to the dark current with no or very little shift in the onset potential. A small shift that can be assumed in Figure 12 is due to the fact that the reduction of nitrate to nitrite can also occur by capturing hydrated electrons generated by photoemission. This reaction will compete with the electrochemical reduction of nitrate and, depending upon relative contributions of these two pathways, more or less shift in the onset potential will be observed.

Conclusions

Enhanced photoelectrochemical reduction of nitrite and nitrate was observed on roughened silver surfaces compared to "smooth" silver and mercury when irradiated with light in the blue-green spectral region. In the case of nitrite, the irradiation resulted in an increase of the reduction current along with a shift of the onset potential, as was determined from the comparison of CVs measured in the dark and under illumination conditions. It was

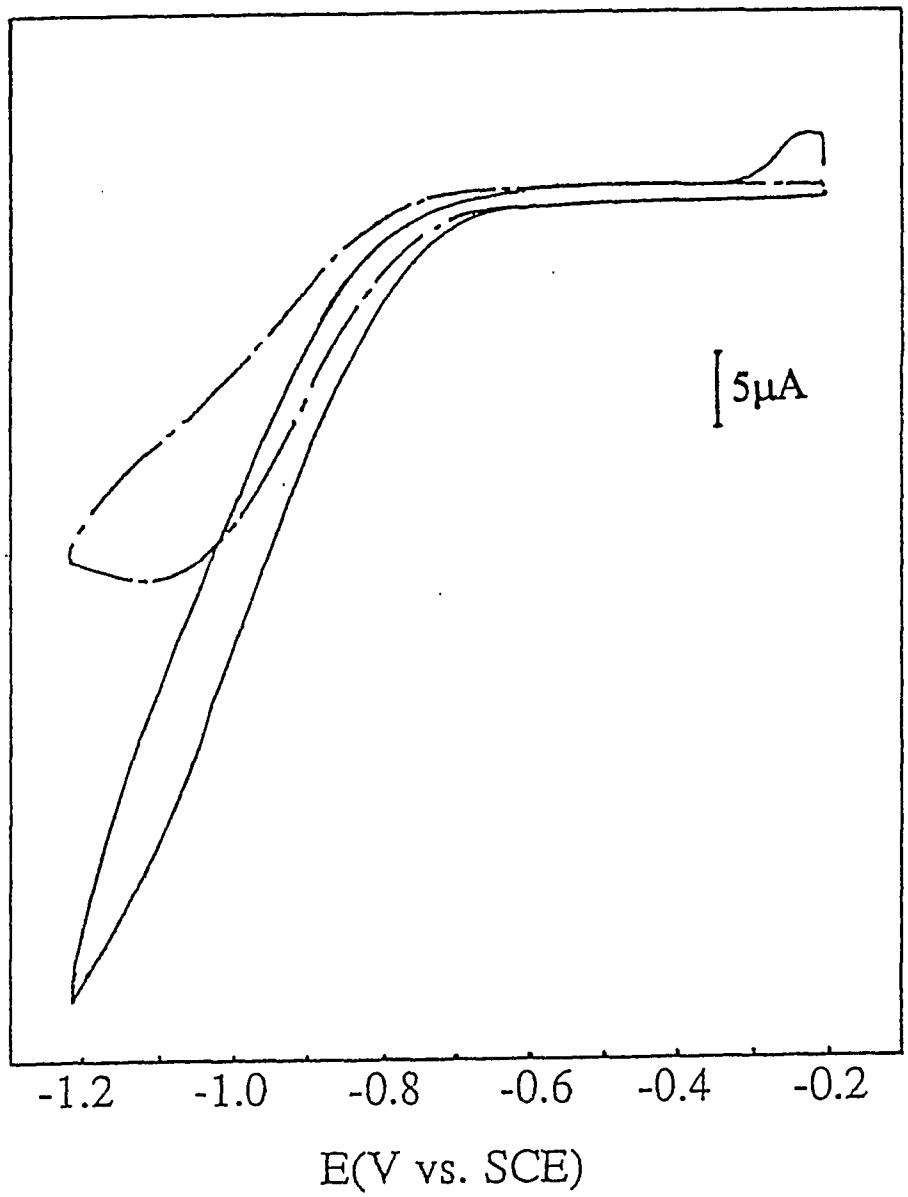

Figure 12. Cyclic Voltammograms of 1 mM $NaNO_3$ in 0.1 M Na_2SO_4 solution at the roughened Ag electrode. Dashed curve: in dark. Solid curve: with 413 irradiation.

determined that the photocurrent is proportional to the 5/2 power of the applied potential and to the square root of the nitrite concentration in the solution. Based on these data as well as on the linear relationship between the onset potential and photon energy, it was concluded that the photoelectrochemical reduction involves a photoemission process from the metal followed by capture of the hydrated electrons by nitrite. The dependence of the photocurrent on irradiation power and wavelength suggests a one-photon process that involves the excitation of plasmon resonances in nanoscale metal structures on the roughened silver surface. Electrolysis experiments at the controlled potential and under irradiation revealed ammonia as one of the products. Two mechanisms are proposed for nitrite reduction. In the case of nitrate reduction, it is suggested that nitrate was first reduced to nitrite via two-electron electrochemical step followed by photoelectrochemical reduction of nitrite.

Acknowledgement

Research at Ames Laboratory is supported by the Division of Chemical Sciences, Office of Basic Energy Sciences, U.S. Department of Energy. Ames Laboratory is operated for U.S. Department of Energy by Iowa Sate University under Contract No. W-7405-Eng-82.

References

1. Genders, J.D.; Hartsough, D.; Hobbs, D.T. *J. Appl. Electrochem.* **1996**, 26, 1.
2. Coleman, D.H.; White, R.E.; Hobbs, D.T. *J. Electrochem. Soc.* **1995**, 142, 1152.
3. Van de Moesdijk, C.G.M. *Chem. Ind.* **1984**, 18,189.
4. Strehlitz, B.; Grundig, B.; Schumacher, W. *Anal. Chem.* **1996**, 68, 807.
5. Wu, Q.; Storrier, G.D.; Pariente, F. *Anal. Chem.* **1997**, 69, 4856.

6. Cattarin, S. *J. Appld. Electrochem.* **1992**, 22, 1077.

7. Nishimura, K.; Machida, K.; Enyo, M. *Electrochim. Acta* **1991**, 36, 877.

8. Xing, X.-K.; Scherson, D.A. *J. Electroanal. Chem.* **1986**, 199, 485-488.

9. Taniguchi, I.; Nakashima, N.; Matsushita, K.; Yasukouchi, K. *J. Electroanal. Chem.* **1987**, 224, 199-209.

10. Fung, C.-S.; Wong, K.-Y. *J. Electroanal. Chem.* **1996**, 401, 263.

11. Halman, M.; Tobin, J.; Zuckerman, K. *J. Electroanal. Chem.* **1986**, 209, 405.

12. Baldwin, R.P.; Perone, S.P. *J. Electrochem. Soc.* **1976**, 123, 1647.

13. Babenko, S.D.; Benderskii, V.A.; Zolotovitskii, Y.A.M.; Krivenko, A.G. *J. Electroanal. Chem.* **1977**, 76, 347.

14. Becquerel, E. *Compt. Rend.* **1839**, 9, 145.

15. Brodsky, A.M., Pleskov, Y.V. *Surface Sci.* **1972**, 2, 1.

16. Barker, G.C.; Gardner, A.W.; Sammon, D.C. *J. Electrochem. Soc.* **1966**, 113, 1183.

17. Berg, H. *Rev. Polarograph, Kyoto* **1963**, 11, 29.

18. Heyrovsky, M.; Norrish, R.G.W. *Nature* **1965**, 200, 1356.

19. Brodsky, A.M.; Gurevich, Y. Y. *Soviet Phys. JETP* **1968**, 54, 213.

20. Sass, J.K.; Sen, R.K.; Meyer, E.; Gerischer, H. *Surface Sci.* **1974**, 44, 515.

21. Corrigan, D.S.; Weaver, M.J. *J. Electroanal. Chem.* **1987**, 228, 265.

22. Kostecki, R.; Augustynski, J. *J. Appl. Phys.* **1995**, 77, 4701.

23. Marczenko, Z. *Separation and Spectrophotometric Determination of Elements*, Masson, M., Ed.; Ellis Harwood Limited, Chichester, England, 1986, chapter 35.

24. Fowler, R.H. *Phys. Rev.* **1931**, 38, 45.

25. Pleskov, Y.V.; Rotenberg, Z.A. *J. Electroanal. Chem.* **1969**, 20, 1.

26. Gurevich, Y.Y.; Pleskov, Y. V.; Rotenberg, Z.A. *Photoelectrochemistry*, Wroblowa, H.S.; Conway, B.E., Eds.; Consultants Bureau: New York, 1980, chapter 4.

27. Benderskii, V.A.; Benderskii, A.V. *Laser Electrochemistry of Intermediates*; CRC Press: New York, 1995, chapter 7.

28. Ehman, D. L.; Sawyer, D. T. *J. Electroanal. Chem.* **1968**, 16, 541.

29. Vicente, F.; Garcia-Jareño, J.J.; Tamarit, R.; Cervilla, A.; Domenech, A. *Electrochim. Acta* **1995**, 40, 1121.

30. Reuben, C.; Galun, E.; Cohen, H.; Tenne, R.; Kalish, R.; Muraki, Y.; Hashimoto, K.; Fujishima, A.; Butler, J.M.; Lévy-Clément, C. *J. Electroanal. Chem.* **1995**, 396, 233.

31. Fung, C.-S.; Wong, K.-Y. *J. Electroanal. Chem.* **1996**, 401, 263.

CHAPTER 3

PHOTOELECTROCHEMICAL REDUCTION OF CO_2 MEDIATED WITH METHYLVIOLOGEN AT ROUGHENED SILVER ELECTRODES

A paper submitted to the *Journal of Electroanalytical Chemistry*

Junwei Zheng, Tianhong Lu, Therese M. Cotton and George Chunanov

Abstract

The photoelectrocatalytic effects for the reduction of CO_2 mediated with methylviologen (MV) was studied at the mercury, polished silver and roughened silver electrodes using the electrochemical and surface-enhanced Raman scattering (SERS) techniques. the large photoelectrocatalytic effect for the reduction of CO_2 in the presence of MV was observed at the roughened silver electrode. The fact that no or small photoelectrocatalytic current was obtained on mercury and polished silver electrodes indicates that the surface plasmon resonance of the nanoscaled silver particles responses for the photoelectrocatalytic effect on roughened silver electrode. The surface adsorbed complexes, $MV^{\bullet+}$-Ag and MV^{0}-Ag, played the role as the mediators for the photoinduced electron transfer to CO_2 in the solution via vibronic coupling between the CO_2 molecule and the excited complex.

Introduction

The photoelectrochemistry and photoemission of metal electrodes has been widely studied since the first observation of the photoemission current upon illumination of the electrodes immersed in dilute acids in 1839 [1-5]. One of the most interested subjects is the

photoelectrochemical effect due to the surface plasmon of metal electrodes, such as Cu, Au, Al and Ag [6-10]. It has been suggested that the optically excited surface plasmon of a metal may be decomposed to transfer the energy to a single electron. If the decomposition energy exceeds the work function of the metal, the electron could be emitted from the metal. The explanations of the phenomena occurring on the electrode surface upon the illumination, so far, can be classified into two groups. The first group is associated with the concepts of electron photoemission from metal to solution, where the hydrated electron could be formed [11-13]. The second one includes the concepts of heterogeneous photochemical reactions and processes of formation and disintegration of charge-transfer complexes on the electrode surfaces, or the electron is directly ejected from the metal electrode to the species in the solution, as recently reported by Wavier and other researchers [14-17]. In order to obtain a measurable photocurrent, the excited electrons have to be captured by some species acting as the scavengers, such as proton, N_2O and NO_3^- [18,19]. Recently, the particularly interesting study reported by Kostecki and Autustynski [20] demonstrated that very strong cathodic photoeffect of the silver electrode can be obtained for the reduction of carbon dioxide. However, it has also been suggested that the photoactive molecules adsorbed on a metal electrode should be much less efficient in a photochemical event than that on a semiconductor electrode, mainly owing to the rapid energy quenching of the excited molecules at the metal electrodes.

Recent works in this group on the study of surface-enhanced Raman scattering (SERS) spectra of methylviologen (MV) [21] and cytochrome c [22] on the roughened silver surfaces have demonstrated photoinduced charge transfer from the metal to the adsorbate. The charge separation was found to be stable indefinitely at low temperatures. The presence of nanosized metal clusters on the surface was determined to play a critical role in this process.

Using iodide ions as the model species, the effect of cluster size on electronic properties of the silver surface was unambiguously demonstrated [22].

In this paper, the photoelectrochemical reduction of CO_2 mediated with MV was studied at metal electrodes. Methylviologen has been widely used as the mediator in photochemical reduction of CO_2 in the presence of photosensitive catalysts such as $Ru(bpz)^{2+}$and $Ru(bpy)^{2+}$ [23,24]. The main product of the photochemical reductions was identified as formic acid. A comparison of the effects of the photoelectrochemical reduction of CO_2 at different electrodes indicates that the roughened silver surface plays an essential role in the enhancement of the photoelectrochemical reduction of CO_2 mediated by methylviologen.

Experimental

Chemicals. Methylviologen dichloride (MV^{2+}) was purchased from Sigma Chem. Co. and used without further purification. The other chemicals are all reagent grade. The solutions were prepared with Millipore water. The solutions usually contained 0.5 mM MV^{2+} + 0.1 M Na_2SO_4. In order to remove the oxygen dissolved in the solutions, the solutions were purged with nitrogen for 30 min prior the measurements. When the electrochemical reduction of CO_2 were studied, the solutions were purged with CO_2 for 30 min before measurements.

Apparatus and methods. The electrochemical measurements were performed on BAS-100 electroanalytical instrument connected with a PC computer. The laser power dependence measurements were carried out with a Princeton Applied Research model 173 potentiostat/galvanostat interfaced with a model 175 universal programmer. A conventional three-electrode electrochemical cell was used in all measurements. The scan rate used for the cyclic voltammetric measurements is usually 20 mV/s. A platinum wire was used as the

auxiliary electrode. A saturated calomel electrode (SCE) served as the reference electrode. All the potentials were reported with respect to the SCE. The working electrode is a mercury, or polished silver, or roughened silver electrode.

The Hg electrode was prepared by dipping a polished gold electrode in mercury for few min. The polished silver electrode was constructed from a polycrystalline wire sealed in a glass tubing with Torr Seal (Vaian). The electrode surface was sequentially polished with 5.0, 0.3 and 0.05 um alumina/water slurries until a shiny, mirror-like finish was obtained. It was then sonicated twice in Millipore water and washed thoroughly with Millipore water. The roughened silver electrode was prepared as follows. The polished silver electrode was roughened in 0.1 M Na_2SO_4 by oxidation-reduction cycle (ORC). This consisted of a double potential step from -0.55 to +0.50 V, where 250 uC charge was passed. Then the electrode potential was stepped back to -0.55 V. The electrochemical roughening increased the surface area of the electrode from 0.09 to 0.15 cm^2 as determined by underpotential lead deposition [25].

In the photoelectrochemical measurements, a light of 413 nm from krypton ion laser (Innova 100-K 3) was used as the excitation source. The power of the laser light at the sample was about 100 mW.

The Raman instrument included a spectrograph (Spex Triplemate 1377) interfaced to a liquid nitrogen-cooled CCD detector (Princeton Instruments Model LN1152) and an Innova 100-k3 krypton ion laser as an excitation source. The surface enhanced Raman scattering (SERS) and surface enhanced resonance Raman scattering (SERRS) spectra of MV were obtained by excitation with 413 nm radiation. The laser power used was about 2 mW at the samples. The resolution of the Raman instrument was ca. 2 cm^{-1} at the excitation wavelength used here. The scattered light was collected in a backscattering geometry. The Raman spectra

were calibrated with indene. The roughened silver electrode was used for the SERS and SERRS measurements of MV. The electrode was firstly dipped in the 0.5 mM MV^{2+} + 0.1 M Na_2SO_4 solution for 30 min. Then, the electrode was placed in the 0.1 M Na_2SO_4 solution for the SERS and SERRS measurements at the different potentials.

Results

The cyclic voltammogram (CV) of MV^{2+} in 0.1 M Na_2SO_4 solution at a mercury electrode is shown in Figure 1 Curve (a). The CV is in good agreement with that reported in literatures [26-29]. A pair of redox peaks was observed in the -0.60 to -0.70V region, corresponding to the reversible one-electron electrochemical redox reaction that is associated with the formation of the cation radical ($MV^{\bullet+}$). In the -0.80 to -1.10 V region, a cathodic and three anodic peaks were observed. The cathodic peak is due to the reduction of $MV^{\bullet+}$ to the neutral viologen (MV^0). The complication of the corresponding cathodic peaks is due to the phase transfer of MV^0 deposited on the electrode surface during the reduction process. Different phases of MV^0 were electrochemically oxidized at the different potentials.
As the solution was saturated with CO_2, except the two cathodic peaks of MV^{2+}, a new cathodic peak at about -1.08 V due to the reduction of CO_2 was observed and the three anodic peaks due to the oxidation of MV^0 completely disappeared, as shown in Figure 1, Curve (b). This indicates that at the mercury electrode, CO_2 can be electrocatalytically reduced with MV^0 as an electron transfer mediator. The catalytic current for the reduction of CO_2 only slightly increased at the potentials more negative than -1.0 V as the electrode was irradiated with a 413 nm light (Figure 1, Curve c). The small increase in reduction current could result from either the excitation of MV^0 by absorption of the light or the photoemission of the electron from

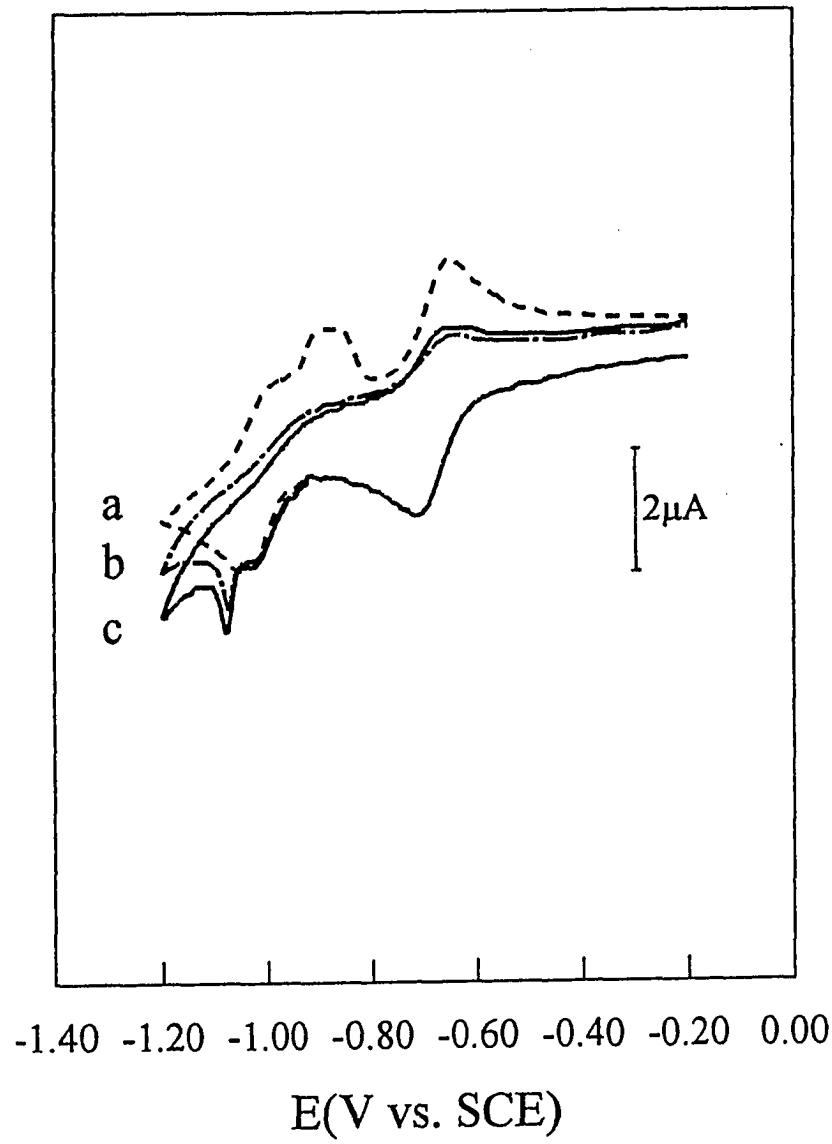

Figure 1. The CVs of the 0.5 mM MV^{2+} solution with 0.1 M Na_2SO_4 at the mercury electrode. (a) without CO_2 saturated in the solution and without the irradiation of 413 nm laser light; (b) with CO_2 saturated in the solution and without the irradiation of the 413 nm laser light; (3) with CO_2 saturated in the solution and with the irradiation of the 413 nm laser light.

mercury electrode. As demonstrated by Richardson [30], the photoemission and scavenging with MV may occur at potential more negative than -1.1 V at mercury electrode.

A similar CV of MV^{2+} was obtained at a polished silver electrode, as shown in Figure 2, Curve (a). However, only one oxidation peak of MV^0 was observed at about -0.90 V. This may resulted from the faster phase transformation of MV^0 deposit at the polished silver electrode than that at the mercury electrode. When the solution was saturated with CO_2, a relative large cathodic peak was observed at ca. -1.00 V and the anodic peak at about -0.90 V disappeared, corresponding to the electrocatalytic reduction of CO_2. The onset potential of the reduction peak of CO_2 positively shifted to ca. -0.60 V and overlapped with the reduction of $MV^{\bullet+}$, compared to that at the mercury electrode (Figure 1, Curve (b)). Furthermore, the current of the oxidation peak of $MV^{\bullet+}$ also slightly smaller than that for the solution without CO_2 (Figure 2, Curve (a)). These results indicate that the electrocatalytic ability of the polished silver electrode for the reduction of CO_2 is better than that of the mercury electrode and $MV^{\bullet+}$ may also have the electrocatalytic activity for the reduction of CO_2. Under the irradiation, an increase in the reduction current of CO_2 was observed (Figure 2, Curve (c)), indicating that the polished silver electrode possesses the photocatalytic ability for the reduction of CO_2.

Comparing with the CV of MV^{2+} at the polished silver electrode (Figure 2, Curve (a)), the CV of MV^{2+} at the roughened silver electrode (Figure 3, Curve (a)) shows an additional pair of redox peaks appeared at -0.52 V. This pair of peaks was suggested to be associated with the redox reactions of the adsorbed MV^{2+} because of the strong adsorption ability of MV^{2+} at the roughened silver electrode [26-29]. The corresponding peak currents at the roughened silver electrode were larger than that at the polished silver electrode, due to an approximately 1.6 times of increase in the electrode surface area from the roughening procedure. In the presence of CO_2

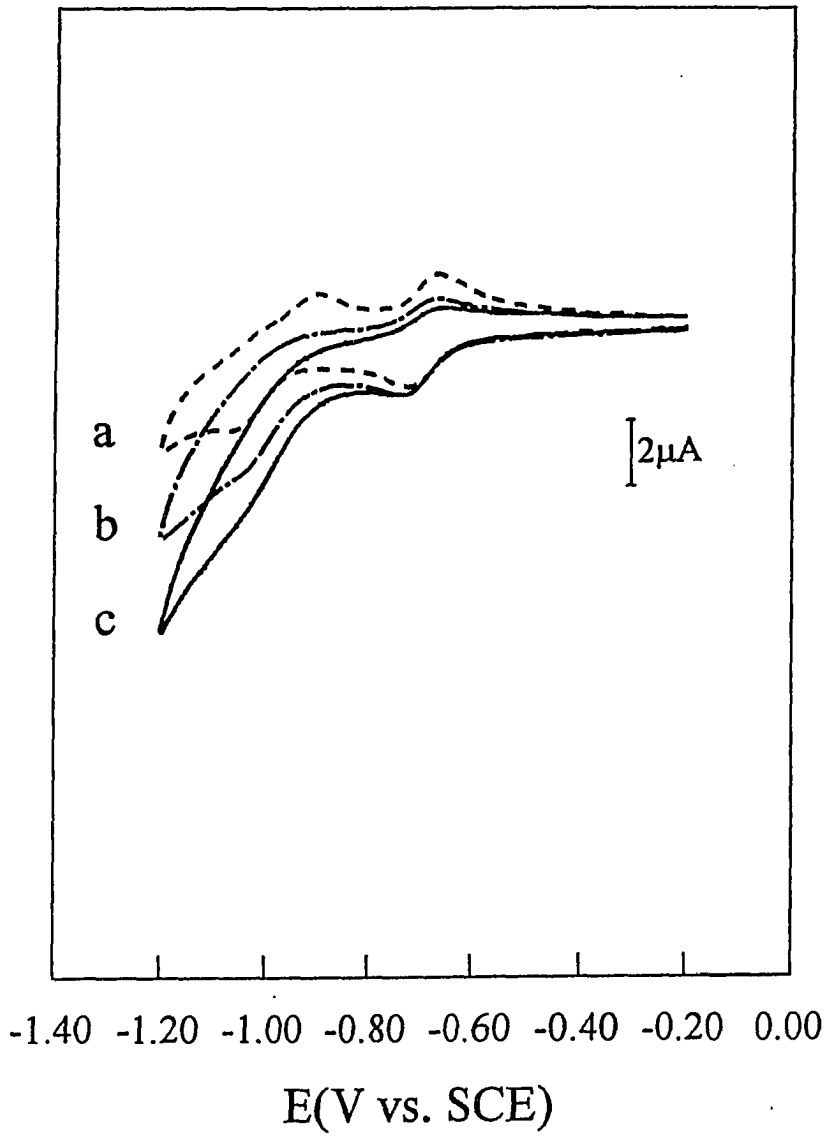

Figure 2. The CVs of the 0.5 mM MV^{2+} solution with 0.1 M Na_2SO_4 at the polished silver electrode. (a) without CO_2 saturated in the solution and without the irradiation of 413 nm laser light; (b) with CO_2 saturated in the solution and without the irradiation of the 413 nm laser light; (3) with CO_2 saturated in the solution and with the irradiation of the 413 nm laser light.

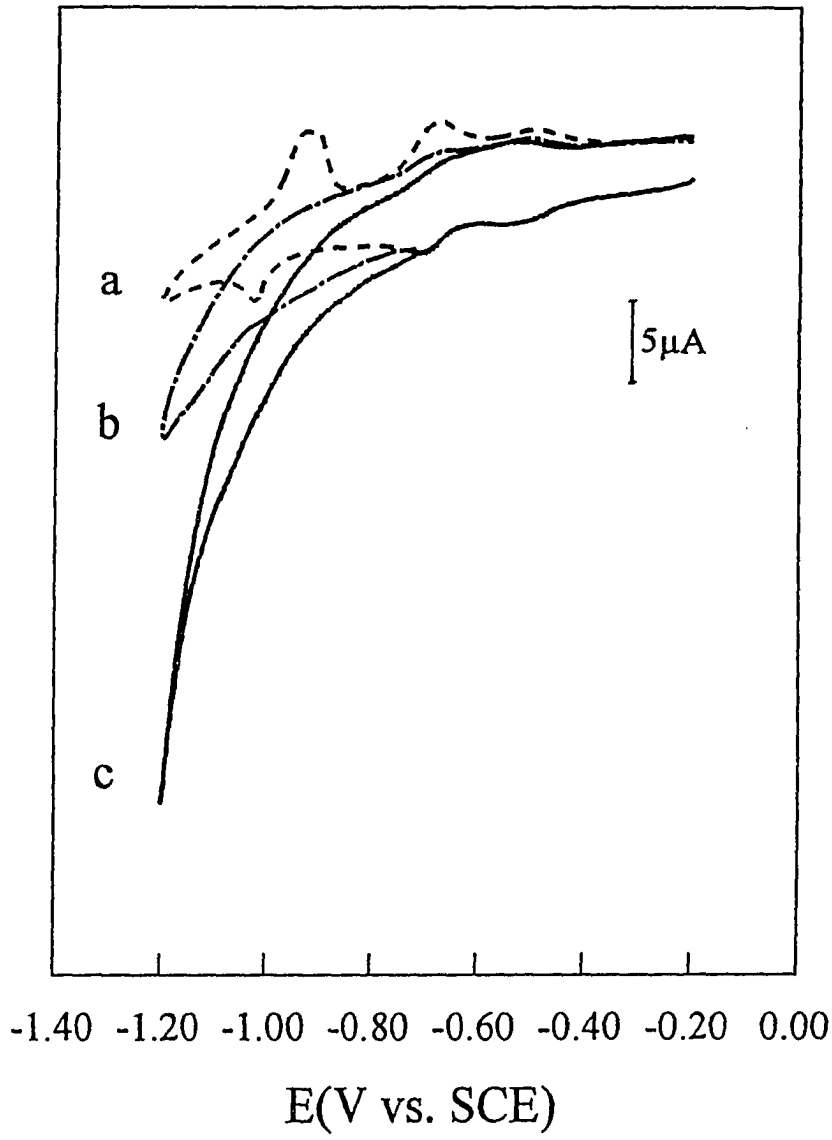

Figure 3. The CVs of the 0.5 mM MV^{2+} solution with 0.1 M Na_2SO_4 at the roughened silver electrode. (a) without CO_2 saturated in the solution and without the irradiation of 413 nm laser light; (b) with CO_2 saturated in the solution and without the irradiation of the 413 nm laser light; (3) with CO_2 saturated in the solution and with the irradiation of the 413 nm laser light.

in solution, a larger catalytic current was observed (Figure 4, Curve b), relative to that at the polished silver electrode. However, considering the real surface areas of the two electrodes, the increase in electrocatalytic current for the reduction of CO_2 at the roughened silver electrode is simply the result of the large real surface area due to the surface roughness features. In other words, the electrocatalytic ability of the roughened silver electrode for the reduction of CO_2 is similar to that of the polished silver electrode.

A very large cathodic current for the CO_2 reduction was obtained at the roughened silver electrode under the irradiation (Figure 3, Curve c). The increase in the photoelectrocatalytic current for CO_2 reduction was not likely only due to the increase in the electrode surface area. As mentioned above, the roughness only increases about 1.6 times in the real surface area of the electrode, while the photoelectrocatalytical current at the roughened silver electrode at -1.2 V (Figure 3, Curve c) is about 4.0 times as large as that at the polished silver electrode. Therefore, it seems that the surface roughness plays an important role in the photoelectrocatalytic reduction of CO_2 mediated with MV.

An additional experiment was performed to determine the effect of irradiation on the electrochemical response of MV without CO_2 in solution. The result is shown in Figure 4. It can be clearly seen that under the illumination of the 413 nm laser light, the CV of MV (Figure 4, Curve b) is similar to that obtained in the dark (Figure 4, Curve a). This implies that there is no photoelectrocatalytic effect for the redox reaction of MV itself.

To visualize better the difference between the photoelectrochemical effect at different electrodes, the CVs measured in the dark were subtracted from the corresponding CVs obtained under irradiation, the results are shown in Figure 5. It is obvious that there is almost no photoelectrocatalytic effect for the reduction of CO_2 at the mercury electrode; a small

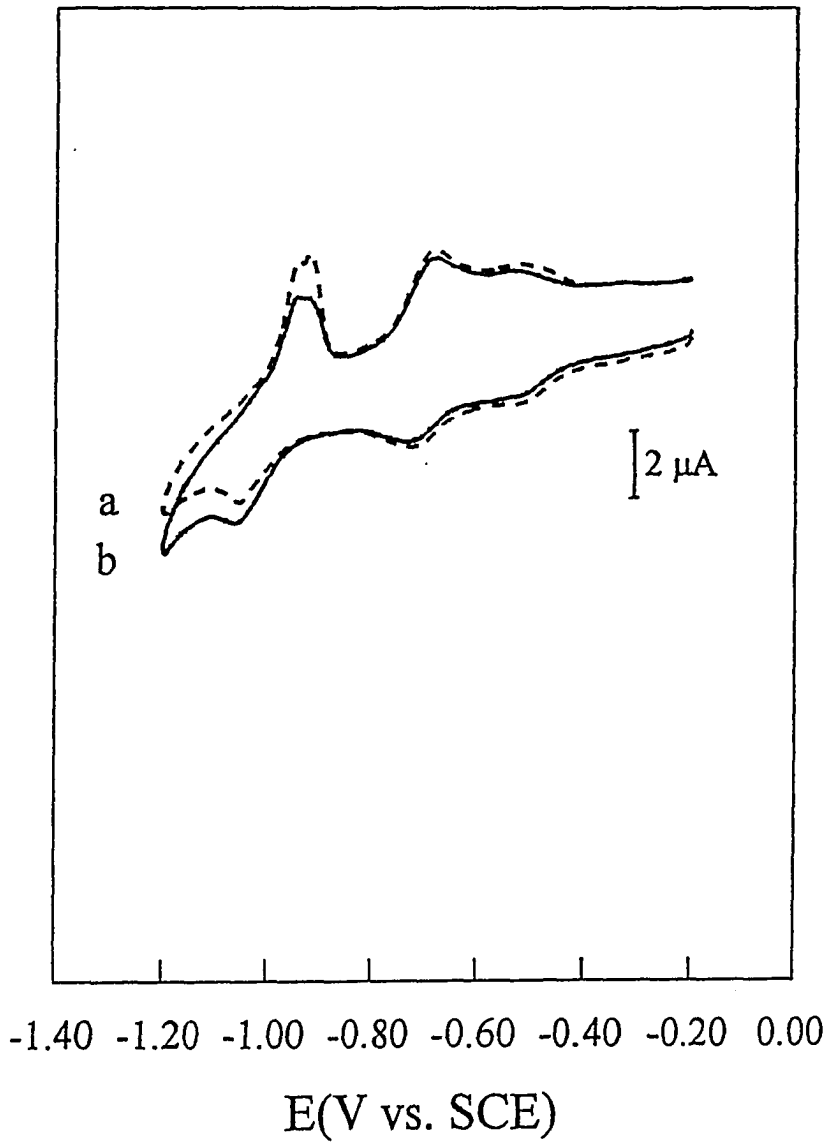

Figure 4. The CVs of the 0.5 mM MV^{2+} solution with 0.1 M Na_2SO_4 at the roughened silver electrode. (a) without the irradiation of 413 nm laser light; (b) with the irradiation of the 413 nm laser light.

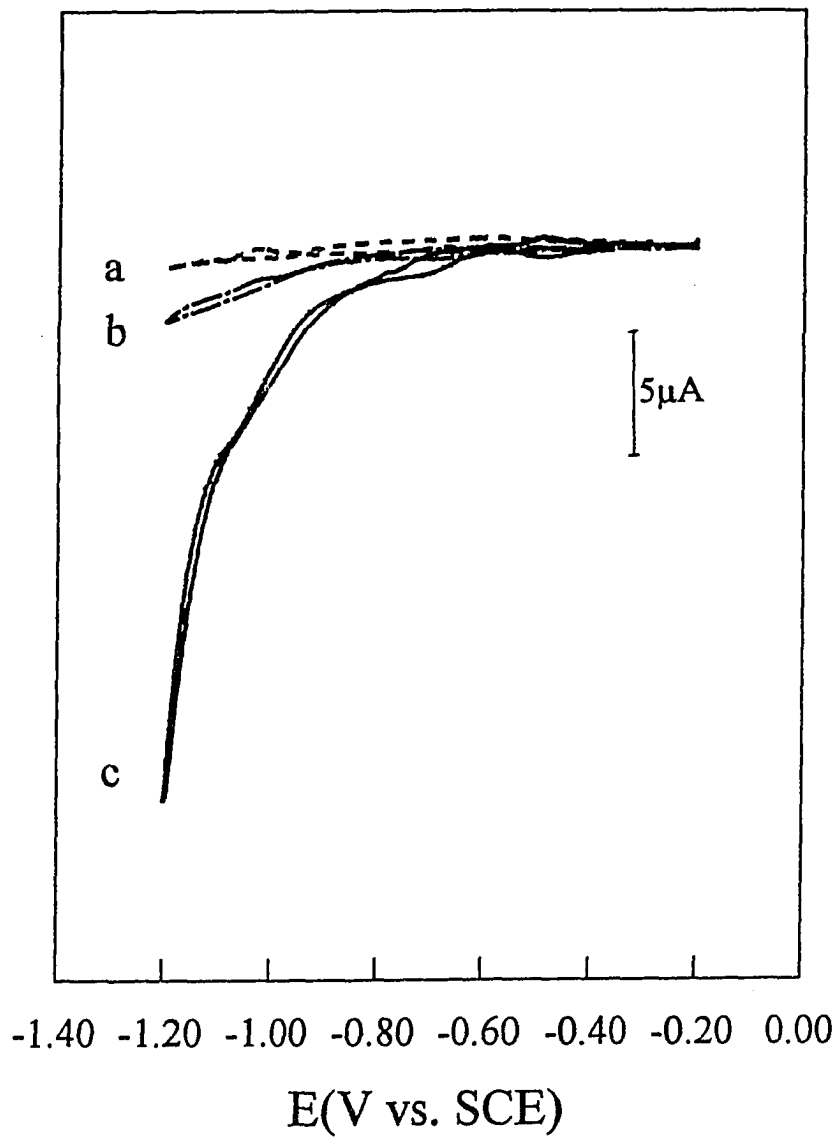

Figure 5. The difference between the CVs of 0.5 mM MV^{2+} solution with 0.1 M Na_2SO_4 and saturated CO_2 without and with the irradiation of the 413 nm laser light at (a) the mercury electrode; (b) the polished silver electrode; (c) the roughened silver electrode.

photoelectrocatalytic effect was observed at the polished silver electrode, while there is a large photoelectrocatalytic effect at the roughened silver electrode.

The CVs of CO_2 at the roughened silver electrode in the presence of MV^{2+} in the solution with the different irradiation power is shown Figure 6. The reduction current of CO_2 varied linearly with the irradiation power. This further demonstrates that the reduction of CO_2 is indeed related to the photocatalytic effect.

From the above experimental results, it seems that the methylviologen species adsorbed on the roughened Ag electrode surface played a role in the enhancement of photoinduced electrochemical reduction of CO_2. A further experiment was performed with an Ag electrode roughened in the solution containing 0.5 mM MV and 0.1 M Na_2SO_4 so that the MV can be strongly adsorbed on the electrode surface. The CV clearly shows that a large photoelectrocatalytic reduction current can be obtained in the solution only with supporting electrolyte and CO_2 (Fig. 7 (c)), compared to those obtained in the dark (Fig. 7 (a) and (b)).

Figure 8 (A) shows the SERS spectra of MV adsorbed on the roughened silver electrode at the different potentials in the 0.1 M Na_2SO_4 solution. The spectra are similar to that reported in the previous papers [28,29]. Corresponding to the CV of MV^{2+} at the roughened silver electrode (Figure 3, Curve a), the SERS spectra of MV^{2+} (Figure 8 A, a and b) were observed at the potential more positive than -0.40 V. When the potential was at -0.60 V, the SERRS spectrum of $MV^{\bullet+}$ (Figure 8A, c) was observed, as indicated by the characteristic bands at 1662, 1534, 1356 and 1028 cm^{-1}. As the potential stepped to -0.8 V, except for the above bands, two new bands at 1601 and 993 cm^{-1} appeared in the SERRS spectrum (Figure 8A, d). The two bands are characteristic bands of MV^0, indicating the formation of MV^0. It should be noted that

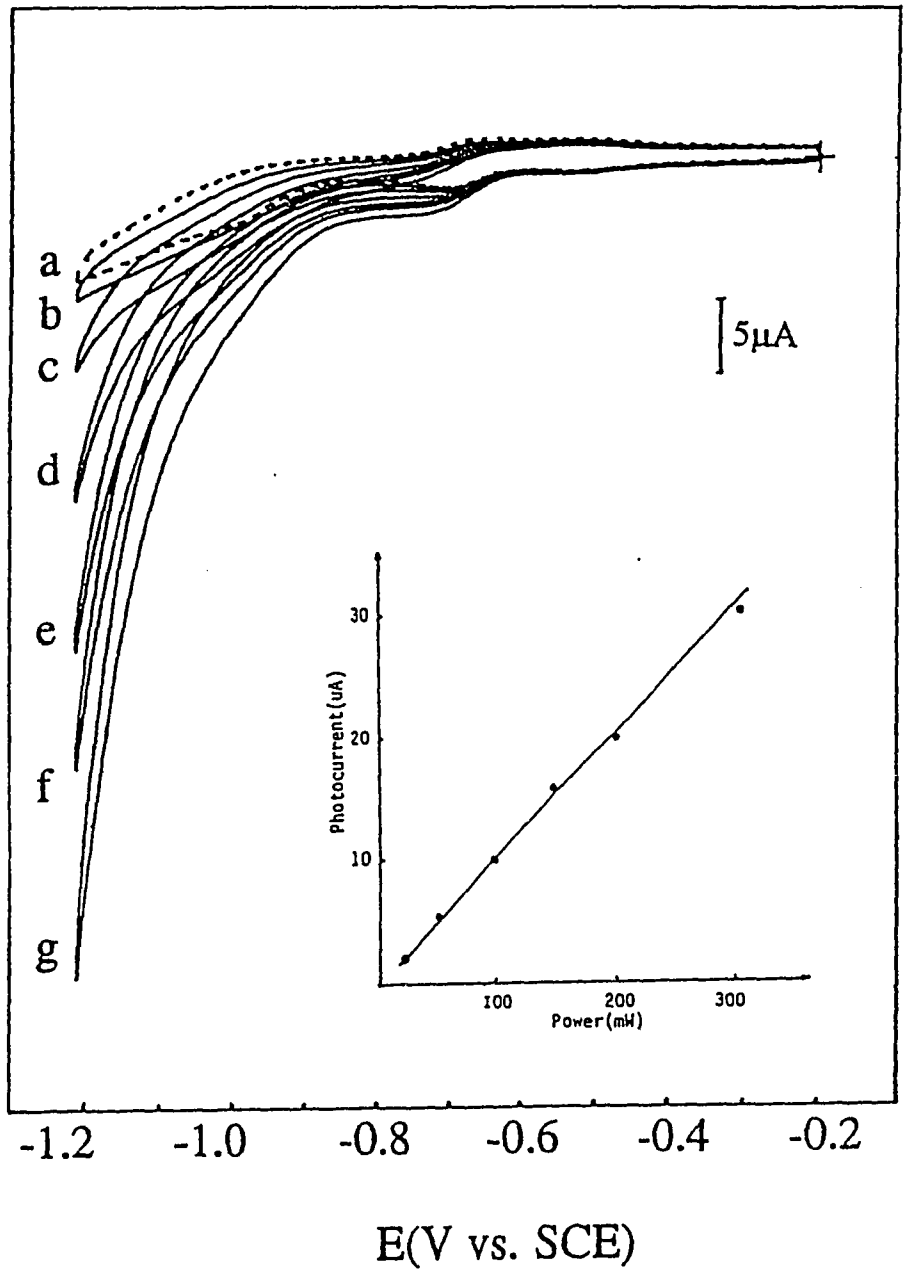

Figure 6. The CVs of the 0.5 mM MV^{2+} solution with 0.1 M Na_2SO_4 and the saturated CO_2 at the roughened silver electrode with the irradiation of 413 nm laser light with (a) 0; (b) 25; (c) 50; (d) 100; (e) 150; (f) 200; (g) 300 mW.

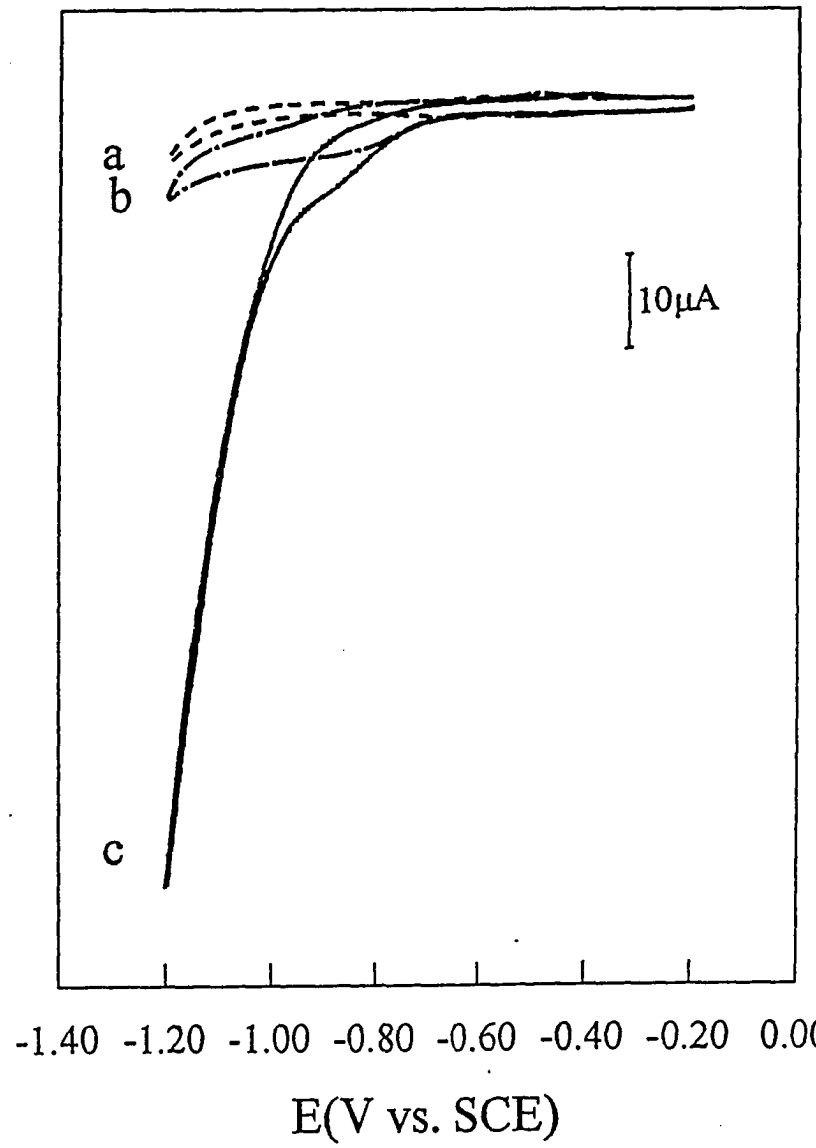

Figure 7. The CVs of Ag electrode roughened in 0.5 mM MV + 0.1 M Na_2SO_4. (a) in 0.1 M Na_2SO_4, dark; (b) in 0.1 Na_2SO_4 saturated with CO_2, dark; (c) in 0.1 M Na_2SO_4 saturated with CO_2, under irradiation of 413 nm laser light.

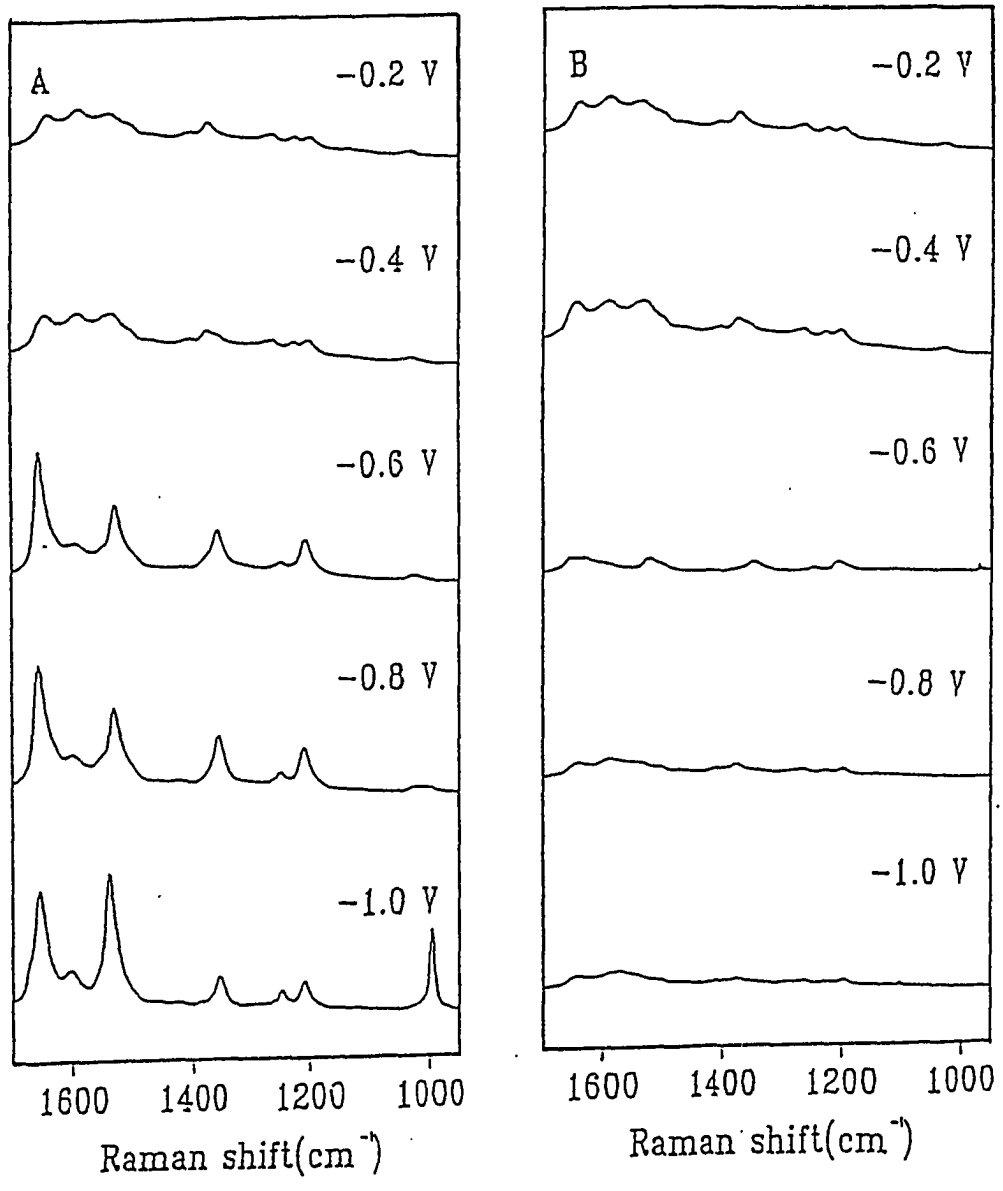

Figure 8. The SERS spectra of MV at the roughened silver electrode without (A) and with (B) the saturated CO_2 in the solution at (a) -0.20; (b) -0.40; (c) -0.60; (d) -0.80; (e) -1.00 V.

the intensities of the SERRS spectra of $MV^{\bullet+}$ and MV^0 are much higher than that of the SERS spectra of MV^{2+} because of the resonance enhancement.

When the solution is saturated with CO_2, the characteristic bands for $MV^{\bullet+}$ were still observed at -0.6 V (Figure 8B, c), but the intensities are much weaker than that in the corresponding spectrum without CO_2 (Figure 8A, c). This further demonstrates that the photoelectrocatalytic reduction of CO_2 starts at -0.6 V and $MV^{\bullet+}$ act as a mediator. The remaining of weak $MV^{\bullet+}$ bands indicates that the reduction rate of CO_2 is quite low at -0.6 V. When the potential was stepped at -0.8 V, no characteristic SERRS bands for $MV^{\bullet+}$ or MV^0 were observed, but only the characteristic SERS bands of MV^{2+} appeared, indicating that both $MV^{\bullet+}$ and MV^0 acted as the mediators for the photoelectrocatalytic reduction of CO_2. It should be noted that Curve d and e in Figure 8 B can only obtained with the solution being stirred or bubbling with CO_2 continuously. This means that the reduction reaction rate of CO_2 is much high at the potential more negative then -0.8 V, so that CO_2 in the double layer near the electrode surface could be completely exhausted in the static solution. The photoelectrochemical reduction therefore is controlled by the diffusion of CO_2 in double layer.

Discussion

Several important issues should be emphasized according to above experimental results. The photoelectrocatalytic effect for the reduction of CO_2 mediated with MV only occurred at the roughened silver electrode, although relatively small electrocatalytic effect for the reduction of CO_2 mediated with MV was observed at all the electrodes studied in this work. The photoelectrocatalytic effect obviously depended on the material and surface state of the

electrode. The photoelectrocatalytic effect was not observed at the mercury electrode; there was only small photoelectrocatalytic effect at the polished silver electrode. Both adsorbed $MV^{\bullet+}$ and MV^0 can act as the mediators for the photoelectrocatalytic reduction of CO_2. In the case of $MV^{\bullet+}$, the reduction reaction was relatively slow, while an accelerated reaction can be achieved at more negative potential where MV^0 was formed.

Photoinduced charge transfer mechanisms of surface complexes formed between electrode surfaces and adsorbates have been suggested for both photoemission [31-34] and surface-enhancement Raman scattering [35,36]. The adsorption of a molecule on metal surface results in the overlap of the electronic wavefunctions of the metal and adsorbate. The electronic states of adsorbate are shifted and broadened by the interaction with the surface of metal, or new electronic states are generated and act as the resonant intermediate state due to the chemisorption of the adsorbate. As a result, the interaction of incident photon with the electron in the Feimi level of the metal produces the excited electron, which can be tunneled into a charge transfer state of the adsorbed molecule and, in turn, transferred either to electrode (anodic current) or adsorbed species (cathodic current). Accordingly, the mechanism of the photoelectrocatalytic reduction of CO_2 in this case can be inferred in terms of charge transfer between the nanoscaled silver particles and the strong adsorbed species MV. The fact that no or small photoelectrocatalytic effect on mercury and polished silver electrodes, respectively, reveals that $MV^{\bullet+}$ and MV^0 in the solution is unlikely to serve as the real mediators in the photoelectrocatalytic reduction processes of CO_2. Reasonably, the surface complex formed between silver particles and adsorbed MV actually acts as the mediators. The formation of the surface complex has been demonstrated with SERS studies

and was considered to be the origin of the chemical enhancement for the SERS effect [37]. The pair of strong adsorption redox peaks in the CV of MV^{2+} at the roughened silver electrode (Figure 3) is also an evidence of the formation of the surface complexes. Moreover, as indicated in Figure 3 and 6, $MV^{\bullet+}$-Ag and/or MV^{0}-Ag complexes can also formed due to the reduction of adsorbed MV^{2+} when the potential shifts to more negative than -0.5 V. On other hand, the energy of surface plasmon at silver-vacuum interface is approximate 3.6 eV, only 0.5 eV below the threshold for the electron emission, and the threshold can be further reduced by adsorption of molecules or ions on the surface [38]. Accordingly, the photoelectrocatalytic effect of roughened silver surface can be attributed to surface plasmon resonance excitation followed by electron transfer to the adsorbate. The complexes formed between the adsorbed molecules and Ag may be easy to be excited or the energy level of the excited state of the complexes may match well with that of CO_2. Thus, the illumination of the laser light produces the excited states of the complexes. Then the photoexcited electron in silver metal is tunneled through the surface MV complexes to CO_2 molecule in the solution via vibronic coupling between the CO_2 molecule and the excited complexes, which results in the reduction of CO_2.

For the polished silver electrode, it is not easy to form the surface complex, probably because of the lack of the active sites. However, it should be pointed out that the surface of the polished silver electrode is not absolutely smooth; there are always some defects on the surface. As a result, some surface complexes can be formed and a small photoelectrocatalytic effect was observed at the polished silver electrode, as shown in Figure 2. However, it is not likely to form such kind of surface complex on the smooth surface of the liquid mercury electrode, or even the surface complex is formed, the energy level of the excited state of the mercury

complex may not match well with that of CO_2. Therefore, the photoelectrocatalytic effect for the reduction of CO_2 was not observed at the mercury electrode.

In our previous paper [21], we demonstrated that MV^{2+} adsorbed on the roughened silver surface can be reduced to $MV^{\bullet+}$ upon irradiation with laser light at liquid nitrogen temperature. However, at the room temperature such phenomenon can not be observed. The possible explanation for that phenomenon is that the captured photoelectron is frozen in a state that minimizes interaction with the metal surface; at room temperature the system is more fluid. Similarly, no photoelectrocatalytic effect for the redox reaction of MV was observed in Figure 5. This implies that under the experimental conditions the fast back electron transfer from adsorbed MV to silver particles may cancel the increase in the forward electron transfer rate resulting from the photo excitation, due to the high reversibility of the MV redox reactions. In other word, the presence of a reaction system, which can undergo an irreversible chemical reaction after receiving photoemitted electrons, is a necessary condition for gaining the photoelectrocalytic effect. Yamada and Kaneko [39,40] reported a similar conclusion in study of the effect of photoexcited $MV^{\bullet+}$ on the electroreduction of O_2 at indium tin oxide electrodes. They demonstrated that even though $MV^{\bullet+}$ and MV^0 could partially absorb the excitation light and some of $MV^{\bullet+}$ and MV^0 species could be excited to the excited state, the excited $MV^{\bullet+}$ and MV^0 species do not have any contribution to the photocurrent in the absence acceptors, such as oxygen.

Kostecki and Autustynski [20] recently reported the direct photoelectrocatalytical reduction of CO_2 at the roughened silver electrode. Our results (Figure 3) indicate that in the presence of MV, the onset potential for the photoelectrocatalytic reduction of CO_2 was approximately located at -0.6 V, which is about 300 mV more positive than that without MV

reported previously [20]. It means that it is more effective for CO_2 to be photoelectrocatalytically reduced with MV as the mediator.

Conclusion

The large photoelectrocatalytic effect for the reduction of CO_2 mediated with MV occurred at the roughened silver electrode. The surface plasmon resonance contribution of nanoscaled silver particles is attributed to the photoelectrocatalytic effect. According to the experiment results, the mechanism is inferred for the photoelectrocatalytic reduction of CO_2. The surface complexes, $MV^{\bullet+}$-Ag and MV^0-Ag, may play the role as the mediator transfer the photoexcited electrons to CO_2 in solution by a vibronic coupling between surface adsorbed complexes and CO_2 molecules.

Acknowledgement

Research at Ames Laboratory was supported by the Division of Chemical Sciences, Office of Basic Energy Sciences, U.S. department of Energy. Ames Laboratory is operated for U.S. Department of Energy by Iowa Sate University under Contract No. W-7405-Eng-82.

References

1. E. Becquerel, Compt. Rend. 9(1839)145.
2. Y. Y. Gurevich, Y. V. Pleskov and Z. A. Rotenberg, Photoelectrochemistry, H. S. Wroblowa and B. E. Conway (Eds.), Consultants Bureau, New York, 1980.
3. B. Feuerbacher, B. Fitton and R. F. Willis, Photoemission and the electronic properties of surface, John Wiley & Sons, New York, 1978.

4. J. M. Ziman, Electrons and photons, W. Marshall and D. H. Wilkinson (Eds.), Oxford, London, 1979.
5. S. R. Morrison, Electrochemistry at semiconductor and oxidized metal electrodes, Plenum Press, New York, 1980.
6. J. K. Sass, R. K Sen, E. Meyer and H. Gerischer, Surf. Sci. 44(1974)515.
7. J. Crowell and R. H. Ritchie, J. Am. Chem. Soc. 60(1970)794.
8. H. Ehrenreich and H. R. Philipp, Phys. Rev. 128(1962)1622.
9. E. A. Stern and R. A. Ferrell, Phys. Rev. 120(1960)130.
10. N. D. Lang and W. Kohn, Phys. Rev. B3(1971) 1213.
11. Y. Harima, H. Sato and K. Suga, J. Phys. Chem. 93(1989)6418.
12. J. H. Richardson, S. M. George, J. E. Harrar and S. P. Perone, J. Phys. Chem. 82(1978)1818.
13. Y. A. Benderskii, S. D. Babenko, Y. M. Zolotoviskii, A. G. Krivenko and T. S. Rudenko, J. Electroanal. Chem. 56(1974)325.
14. D. S. Corrigan, and M. J. Meaver, J. Electroanal. Chem. 228(1987)265.
15. L. Rips and M. I. Urbakh, J. Chem. Phys. 95(1991)2975.
16. J. G. Gordon and H. O. Finklea, J. Phys. Chem. 83(1979)1834.
17. H. Berg, and P. Reissmann, J. Electroanal. Chem. 24(1970)427.
18. V. V. Konovalov and A. M. Raitsimring, Chem. Phys. Lett. 171(1990)326.
19. Y. V. Pleskov and Z. A. Rotenberg; J. Electroanal. Chem. 20(1969)1.
20. R. Kostecki and J. Augustrynski, J. Appl. Phys. 77(1995)4701.
21. F. Hannah, G. Chumanov and T. M. Cotton, J. Phys. Chem. 100(1996)4937.
22. M. S. Sibbaid, G. Chumanov and T. M. Cotton, J. Phys. Chem. 100(1996)4672.
23. N. Kitamura; S. Tazuke, Chem. Lett. 1983, 227.

24. M. Venturi; Q.G. Mulazani; M. Ciano; M.Z. Hoffman, Inorg. Chem. 25(1986)4493.

25. A. Vashkyalis and O. Demontaite, Elektrokhimiya, 14(1978)1213.

26. R. M. Elofson and R. L. Edsberg, Can. J. Chem. 35(1957)646.

27. M. Ito and T. Kuwana, J. Electroanal. Chem. 32(1971)415.

28. T. Lu, R. L. Birke and J. R. Lombardi, Langmuir 2(1986)305.

29. Q. Feng, W. Yue and T. M. Cotton, J. Phys. Chem. 94(1990)2082.

30. J.H. Richardson, L.J. Kovalenko, S.B. Deutscher, J.E. Harrar J. Electroanal. Chem. 106(1980)263.

31. M. Heyrovsky, Nature 200(1965)1356.

32. M. Heyrovsky, Nature 209(1966)708.

33. M. Heyrovsky, Proc. R. Soc.(Londen) Ser. A 301(1967)411.

34. M. Heyrovsky, Croat. Chem. Acta 45(1973)247.

35. A. Otta, J. Raman Spectrosc. 22(1991)743.

36. A. Campion, P. Kambhampati, Chem. Soc. Rev. 27(1998)241.

37. R. L. Birke, T. Lu and Lombardi, J. R. Techniques for Characterization of Electrodes and Electrochemical Processes, R. Varma, J. R. Selman, (Eds.), John & Sons Inc.: 1990, p. 211.

38. U. Even, K. A. Holcomb, C. W. Snyder, P. R. Antoniewicz, J. C. Thompson, Surf. Sci. 165(1986)L35.

39. M. Kaneko and D. Wohrle, J. Electroanal. Chem. 307(1991)209.

40. K. Yamada, C. B. Lin, N. Kolayashi, K. Ikeda, R. Hirahoshi and M. Kaneko, J. Electroanal. Chem. 370(1994)59.

CHAPTER 4

PHOTOINDUCED ELECTRON TRANSFER AT THE SURFACE OF NANOSIZE SILVER PARTICLES AS MONITORED BY EPR SPECTROSCOPY

A paper submitted to the *Journal of Physical Chemistry*

Junwei Zheng, Therese M. Cotton, George Chumanov,

Tijana Rajh and Marion Thurnauer

ABSTRACT

EPR spectroscopy was employed in study of photoinduced electron transfer on nanosized silver particles. Radicals were observed for the silver colloid with methylviologen, nitrophenol and methanol with irradiation of UV lights. The wavelength dependence of EPR spectra of silver colloid with methanol indicates that plasmon resonance may be critical for the formation of the radicals on the nanosized silver particles.

INTRODUCTION

Recent surface-enhanced Raman scattering studies of methylviologen and iodide adsorbed on nanostructred silver surfaces have revealed photoinduced charge transfer from the metal to the adsorbate [1,2]. Charge separation was found to be stable indefinitely at low temperatures. The presence of nanosized metal clusters on the surface was determined to play a critical role in this process. Using iodide as a model species, the effect of cluster size on optical properties of the surface was unambiguously demonstrated [3].

In order to obtain further insights into the nature and properties of the charge separated species photogenerated at the nanostructured silver surface, EPR spectroscopy was

employed. Here we report preliminary EPR results obtained from silver colloids in the dark and under illumination. EPR has a long and successful history in the study of photoproduced organic radicals. It has also been used to characterize the nature of silver atoms and clusters formed by γ irradiation of Ag salts in alcohol solution, clays as well as silver-exchanged zeolite materials [4-8]. However, to the best of our knowledge, the potential of this technique for monitoring photoprocesses at nanosize metal particles in colloidal suspensions has not been explored prior to now. The results suggest EPR as a new tool that is potentially capable of characterizing surface species formed in heterogeneous electron transfer reactions at metal surfaces.

EXPERIMENTAL METHODS

Silver colloids were prepared by literature procedures using chemical reduction of silver salts. Chemicals of the highest available purity were used as received for the preparation of colloids and EPR samples. Deionized 18 MΩ water was used in all preparations.

EPR spectra were obtained from samples contained within 4 mm Suprasil quartz tubes. A Bruker ESP 300E instrument was used to acquire the spectra. Spectra were recorded in a liquid He Dewar at 4.2-10K. In most of the spectra shown here, the parameters were as follows: modulation frequency = 100 kHz; modulation amplitude = 12 G; frequency 9.14 GHz; power ≤ 2 mW. Typically, 10 scans were signal averaged.

RESULTS AND DISCUSSION

Figure 1 depicts a typical dark EPR spectrum obtained from silver colloids. A very weak, narrow band (8 G) was observed that has the same intensity at 77K and is characteristic of conduction electron spin resonance (CESR) [9]. It is known that the linewidth and intensity of the signal are related to the size of the particles. Large particles (> 100 nm) and bulk metals produce asymmetric lines (Dysonian line shape) and detune the cavity, thereby decreasing the instrument sensitivity. Very small particles, on the other hand, produce stronger symmetric bands at low temperatures. It should be noted that the dark signal did not change with addition of the electron acceptors (methylviologen and nitrophenol) and donor (methanol) used in these experiments.

EPR spectrum of the colloidal suspension irradiation with 308 nm light at 4.2 K for 8 minutes is shown in Figure 2. The measurements were performed in the dark. The CESR spectrum was stronger than that in Figure 1 by at least one order of magnitude; in addition, the hyperfine structure can be observed. The increase in the intensity resulted from electron ejection from the particles, possibly a photoemission process or charge transfer to surface species. Conceivable explanations for the hyperfine structure include the presence of a surface impurity or charged silver clusters larger than 6 atoms [7,8].

Addition of low concentration ($< 10^{-4}$ M) of methylviologen (MV) dication to the silver colloid had no effect on the dark signal, but irradiation with 308 nm light for 16 minutes produced the spectrum shown in Figure 3. The sample exhibited the characteristic blue color of the one-electron reduced methylviologen cation radical. The hyperfine structure superimposed with the strong CESR signal is distinct from that

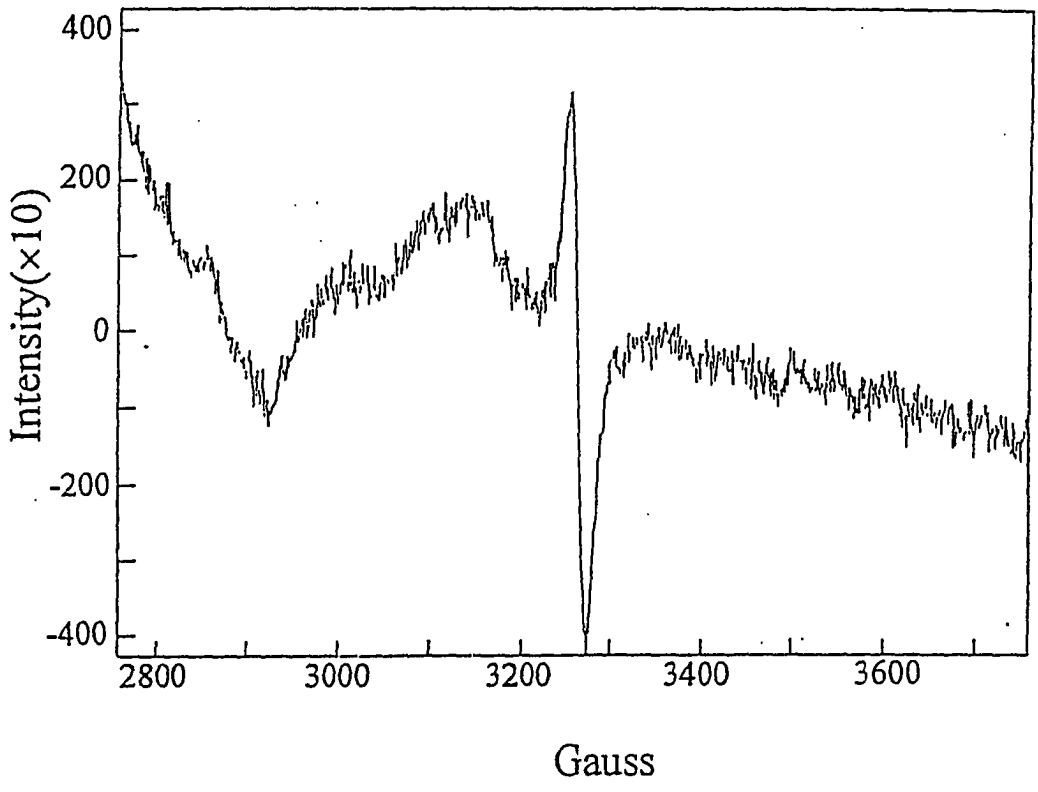

Figure 1. EPR spectrum of Ag colloid. Conditions:10 scans, 4.2 K, in dark.

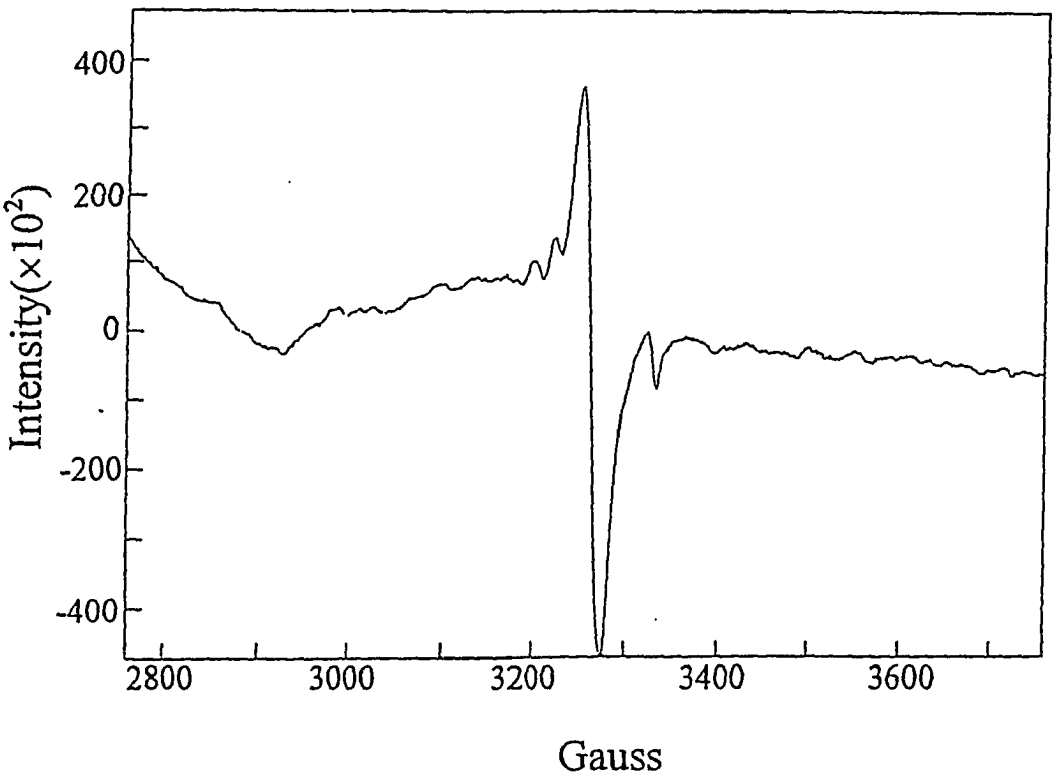

Figure 2. EPR spectrum of Ag colloid. Conditions: 10 scans, 4.2 K, irradiation with 308 nm for 8 min

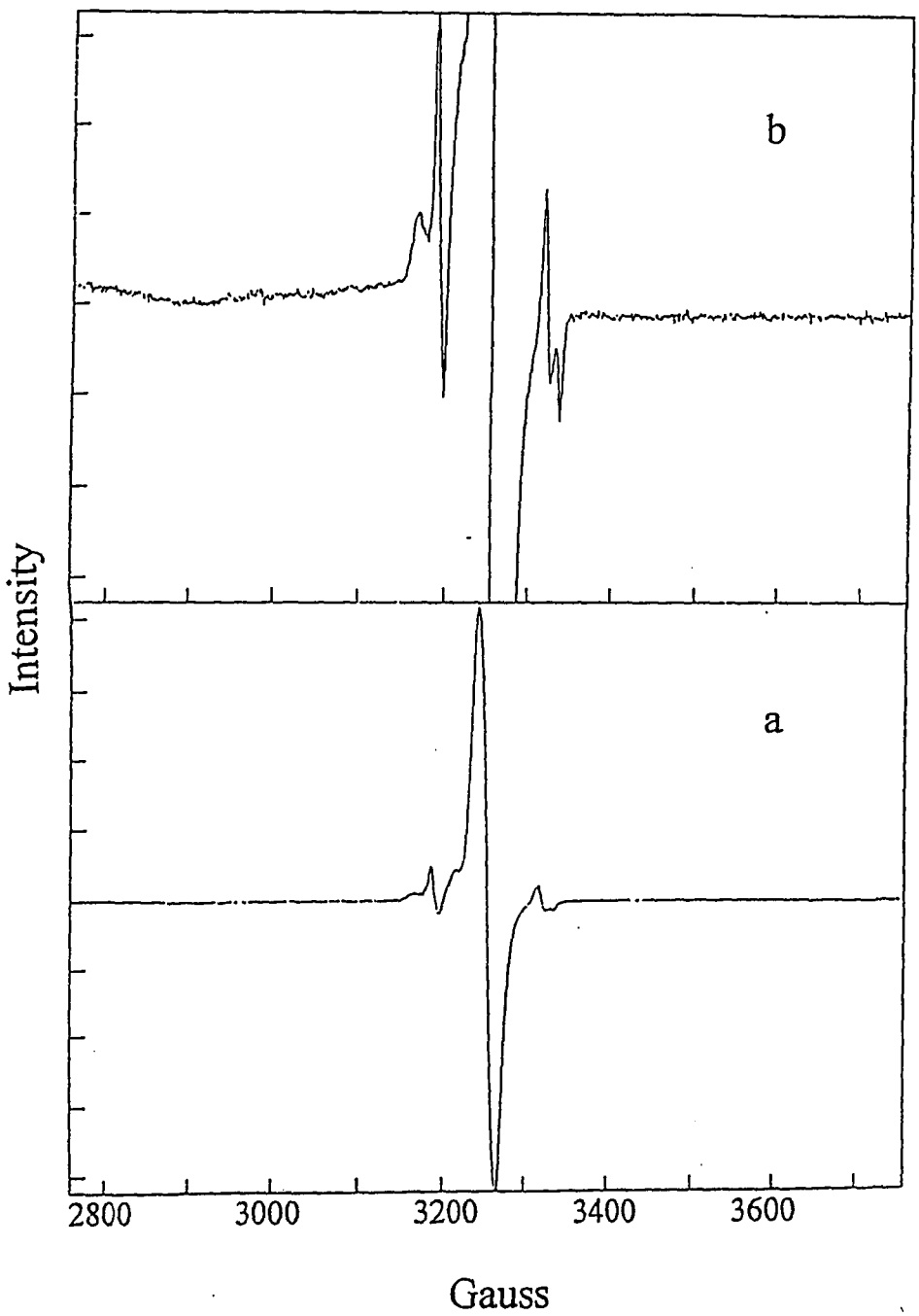

Figure 3. EPR spectra of Ag colloid with methylviologen. (a) 10 scans (b) 30 scans. Temperature: 4.2 K, irradiation with 308 nm for 16 min.

observed for the pure metal colloid and is tentatively assigned to an Ag-viologen complex. At high concentration of MV the EPR spectrum was dominated by a strong band characteristic of the radical in solution (spectrum is not shown) that can be formed without metal colloid. Relatively week hyperfine structure from the complex can not be distinguished in the presence of this strong band. The formation of MV radical in solution with 308 nm irradiation in the absence of silver colloids was confirmed in a control experiment. EPR spectrum of MV radical in solution was also previously reported [10].

Because UV light can produce MV radical in the absence of silver colloid it is not clear whether photoinduced electron transfer takes place from the metal particle to the adsorbed species. Exploring a more interesting possibility of utilizing the plasmon resonance for the enhancement of photochemistry, experiments were performed with a different electron acceptor exciting in the different spectral region. EPR spectrum of the Ag colloid in the presence of nitrophenol as the electron acceptor measured after irradiation with 420 nm light is shown in Figure 4. As in the case of MV hyperfine structure was observed. However, it is distinct from that of MV. No dark signal was observed and no signal was observed using wavelengths longer that 450 nm. It is important to emphasize that no photoreduction of nitrophenol was detected under the same conditions without the silver colloid.

Experiments were undertaken to study photoinduced hole transfer from silver nanoparticles to adsorbed species. EPR measurements were performed on silver colloids in 50% methanol/water irradiated with wavelength from 500 nm to 420 nm (Fig. 5). No

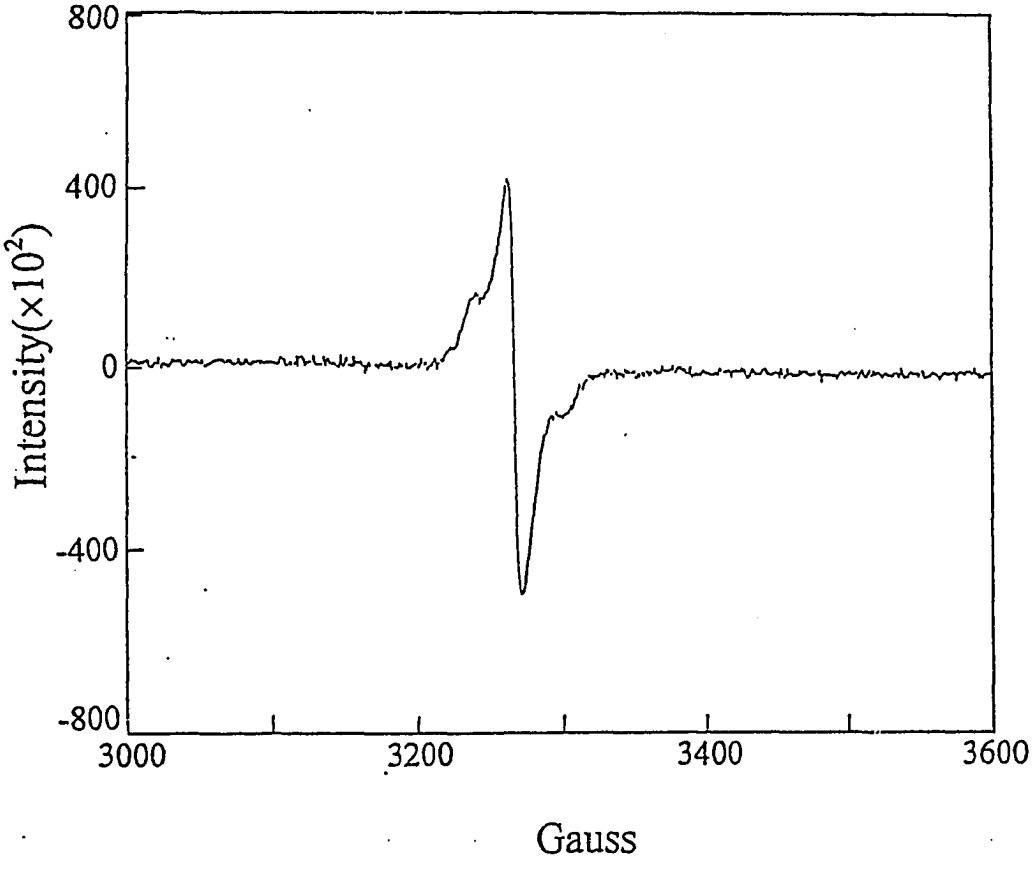

Figure 4. EPR spectrum of Ag colloid with nitrophenol. Conditions: 10 scans, 4.2 K, irradiation with 420 nm for 10 min.

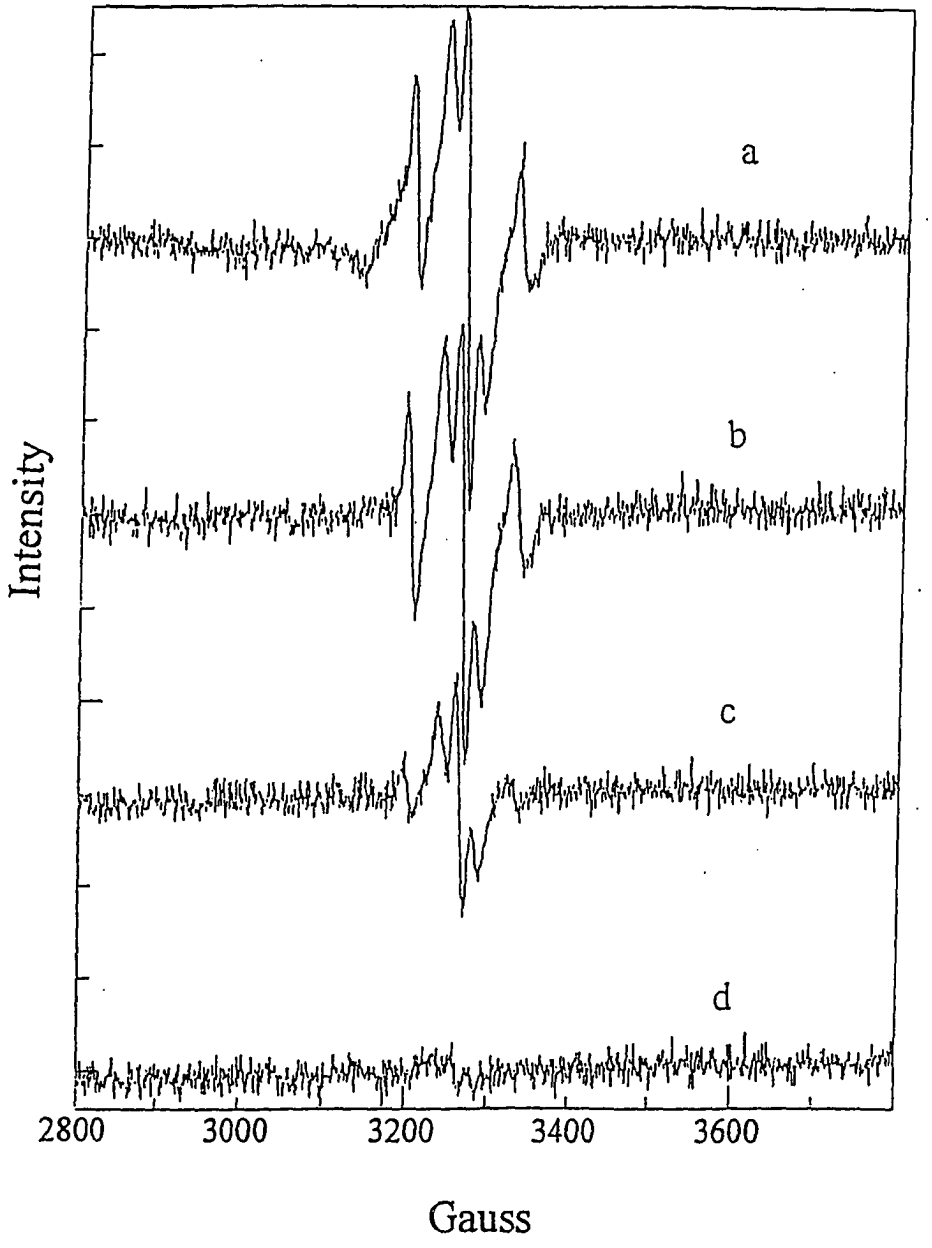

Figure 5. Wavelength dependence of EPR spectra of Ag Colloid with 50% methanol. Conditions: 10 scans, 4.2 K, irradiation with (a) 420 (b) 430 (c) 450 (d) 500 nm for 10 min.

signal could be observed after 500 nm irradiation; however the signal intensity increased dramatically as irradiation was gradually tuned from 450 to 420 nm. It should be noted that the signal-noise-ratio is much lower in these spectra because only 0.2 mW of power was used for EPR measurements to obtain better resolution of hyperfine structure. The outermost doublet in the spectra has been assigned to a Ag-CH_2OH^+ radical [8]. Other features include the CESR and signals from other radical species, possibly CH_3. Control experiments in the absence of colloid produced no signal at any of these wavelengths. Clearly, excitation into the plasmon resonance (maximum near 400 nm) is critical for the formation of the radical species.

In conclusion, EPR spectroscopy can be used to monitor the formation of radicals on the surface of metal nanoparticles in colloidal suspensions. Irradiation of silver nanoparticles in resonance with plasmon frequency resulted in the photoinduced electron and hole transfer from the metal to nitrophenol and methanol, correspondingly.

REFERENCES

1. Sibbald M. S.; Chumanov, G. and Cotton, T. M., *J. Phys. Chem.*, **1996**, 100, 4672.
2. Feilchennfeld, H.; Chumanov, G., and Cotton, T.M., *J. Phys. Chem.*, **1996**, 100, 4937.
3. Sibbald, M.S., Chumanov, G. and Cotton, T.M., *J. of Chem. Phys.*, **1998**, 109, 753-762.
4. Hermerschmidt, D. and Haul, R. *Ber. Bunsenges. Phys. Chem.* **1980**, 84, 902.
5. Janes, R.; Stevens, A.D. and Symons, M.C.R. *J. Chem. Soc. Farday Trans.* **1989**, 1, 85, 3973.
6. Wasosicz, G.; Mikosz, J.; Sadlo, J. and Michalik, J. *J. Chem. Soc. Perkin Trans.* **1992**, 2, 1487.

7. Michalik, J.; Azuma, N.; Sadlo, J. and Kevan, L. *J. Phys. Chem.* **1995**, 99, 4679.

8. Michalik, J.; Yamada, H.; Brown, D.R. and Kevan, L. *J. Phys. Chem.* **1996**, 100, 4213.

9. Edmonds, R.N.; Harrison, M.R. and Edwards, P.P. *Annu. Rep. Prog. Chem.* **1985**, C82, 265.

10. Mcmanus, J.D.; Finel, C. and Kevan, L. *Radiat. Phys. Chem.* **1995**, 45, 761.

CHAPTER 5

ELECTROCHEMISTRY AND SURFACE-ENHANCED RRESONANCE RAMAN SCATTERING SPECTRA OF MICROPEROXIDASE-11

Part of this chapter was published in "*Spectrscopy of Biological Molecules: Modern Trends*" P. Carmona, R. Navarro, and A. Hernanz, Ed., Kluwer Academic Publishers: Dordrecht, Netherland, 1997, p 171

Junwei Zheng, Richard Walsh, Tianhong Lu, George Chumanov, Therese M. Cotton

Abstract

The electrochemical reactions and surface enhanced resonance Raman scattering (SERRS) spectra of microperoxidase-11 (MP-11) were studied at silver electrodes. The redox properties of MP-11 are affected by coordination state and the sixth ligand of heme iron. From the change in the position of the SERRS bands sensitive to the oxidation state of MP-11, the SERRS spectra of the adsorbed MP-11 molecules in the reduced and oxidized states were ascertained. Using SERRS spectroscopy, it was demonstrated that the photo-reduction of the MP-11 molecules adsorbed on the surface of the roughened silver electrode occurs. The mechanism of photoreduction of the adsorbed MP-11 molecules is considered to be the result of the photoejection of free electrons from the roughened silver electrode.

Introduction

MP-11, which is obtained from proteolytic digestion of cytochrome c with pepsin, provides us with a good potential model for c-type heme enzymes [1,2]. This heme-containing undecapeptide retains amino acid residues 11-21 of cytochrome c. The heme group remains linked through thioether bonds to the α-carbon atoms of the saturated vinyl groups of two

adjacent pyrrole moieties to Cys-14 and Cys-17, while His-18 serves as the proximal ligand. The sixth coordination site can be occupied by numbers of exogenous ligands, such as an NH_2 group from Val-11 or lys-13 of another MP-11 molecule because MP-11 molecules usually exist as aggregates in the neutral solution.

The electrochemistry of MP-11 has been studied by several groups [3-9]. The reversible electrochemical reaction of MP-11 at the glass carbon electrode was first reported by Santucci [3]. Afterwards, they reported the electrochemical reaction of MP-11 at the bare and the gold-plated reticulated vitreous carbon electrodes [4]. Razumas et al. [5,6] reported the electrochemical reaction of MP-11 at the silver electrode. In their studies, methanol was added into the aqueous solution of MP-11 in order to prevent MP-11 molecules from aggregating. Recently, they reported the direct electrochemistry of MP-11 at a gold electrode modified with a self-assembled monolayer of 4,4'-dithiodipyridine and 1-octadecanethiol [7]. Lötzbeyer et al. [8] observed the direct electron transfer of MP-11 at a cystamine-modified gold electrode, where MP-11 is covalently immobilized on the electrode surface via the amide bonds. The MP-11 immobilized electrode shows high bioelectrocatalytic activity for the reduction of H_2O_2, even at a very positive electrode potential. Das and Medhi [9] studied the effect of surfactant and pH on the redox potential of MP-11 in aqueous micellar solutions.

Although RR and SERRS spectra of c-type heme proteins have been extensively studied during the past decades, the RR and SERRS spectra of MP-11 have scarcely been investigated. Only a recent work by Wang et al. [10] has shown that MP-11 exhibits the typical RR characteristics of a c-type heme group. Under normal conditions, the heme group of MP-11 is in the ferric, six-coordinate, low-spin state. Thus, the molecules of MP-11 tend to aggregate in

neutral aqueous solutions. Only Razumas et al. [6, 11] reported the SERRS spectra of MP-11 on the silver hydrosol.

In this paper, the electrochemical reactions, RR and SERRS spectra of MP-11 were studied. The SERRS spectra of adsorbed MP-11 molecules in the reduced and oxidized states were ascertained. Using SERRS spectra of MP-11, the photo-induced electron transfer from the roughened silver electrode to MP-11 adsorbed on the electrode surface was observed.

Experimental Section

Materials and Solutions. MP-11 was purchased from Sigma and used without further purification. Other chemicals used were all reagent grade. All the solutions were prepared with deionized water.

Apparatus and Procedures. The electrochemical measurements were carried out using a potentiostat (EG & G Model 176), a signal generator (EG & G Model 175), a X-Y recorder (Omnigraphic 100 recorder) and a traditional three-electrode electrochemical cell. A silver disk electrode with a silver wire sealed in a glass tube with Torr Seal was used as the working electrode. The roughened silver electrode was prepared using an oxidation and reduction cycle (ORC) procedure [12], in which the electrode potential was stepped from -0.55 V to +0.6 V, then after a certain time, back to -0.55 V. During the ORC process, 250 uC charge was allowed to pass the electrode. A Pt wire was used as the auxiliary electrode. A saturated calomel electrode served as the reference electrode.

The Raman instrument included a spectrograph (Spex Triplemate 1377) interfaced to a liquid nitrogen-cooled CCD detector (Princeton Instruments Model LN1152) and an Innova 100-k3 krypton ion laser as an excitation source. The RR and SERRS spectra were obtained by

excitation with 413 nm radiation. The laser power used was about 10 mW at the samples for the RR spectra and 1 mW for the SERRS spectra. The resolution of the Raman instrument was ca. 2 cm^{-1} at the excitation wavelength used here. The scattered light was collected in a backscattering geometry. The Raman spectra were calibrated with indene.

The electrochemical and RR measurements were carried out in the 1×10^{-4} M MP-11 + 0.025 M phosphate buffer (pH 7.0) + 0.1 M $NaClO_4$ solution. For the SERRS measurements, the roughened silver electrode was dipped in the 1×10^{-4} M MP-11 + 0.025 M phosphate buffer (pH 7.0) + 0.1 M $NaClO_4$ solution for about 30 min and then to transfer the electrode into 0.025 M phosphate buffer solution with 0.1 M $NaClO_4$ for the measurements. All the solutions were purged with bubbling with high-purity nitrogen prior to measurements to remove the oxygen dissolved in the solutions.

Results and Discussion

Electrochemistry of MP-11. A pair of redox peaks was observed in the cyclic voltammograms (CVs) of MP-11 (Figure 1, Curve a) at a polished silver electrode for the 100 mV/s scan rate. The anodic peak is located at -0.34 V and the cathodic peak is at -0.44 V. The formal redox potential of MP-11 calculated from $E^0 = (E^a_p+E^c_p)/2$, is constant with a value of -0.39 V for the scan rates from 10 to 200 mV/s. This is in good agreement with that reported at the glass carbon electrode [3] and at the silver electrode [5,6]. The difference between anodic and cathodic peak potentials is about 100 mV, slightly larger than that for the reversible electrochemical reaction. The anodic peak current is almost equal to the cathodic peak current. Both the anodic and cathodic peak currents vary linearly with the square root of the scan rates, indicating that the electrochemical reaction is diffusion-controlled. These results demonstrated

that a quasi-reversible electrochemical reaction of MP-11 was observed at the polished silver electrode in the 1×10^{-4} M MP-11 + 0.1 M $NaClO_4$ + 0.025 M phosphate buffer solution (pH 7.0).

The CV of MP-11 at the roughened silver electrode shows that the anodic peak is located at -0.38 V and the cathodic peak is at -0.42 V (Figure 1, Curve b). The peak positions are somewhat different from that at the polished silver electrode (Figure 1, Curve a). In addition, no linear relationship could be obtained between the peak current and the scan rate or the square root of the scan rates from the CVs with different scan rates. Thus, the electrochemical reaction of MP-11 at the roughened silver electrode is not simply controlled by diffusion or non-diffusion surface redox couple.

After the roughened silver electrode was immersed in 0.1 mM MP-11 solution for 30 min, the CV was measured in the solution without MP-11 (Figure 1, Curve c). Both the cathodic and anodic peaks are located at about -0.34 V. The current of the cathodic peak is almost equal to that of the anodic peak. Both the cathodic and anodic peak currents are proportional to the scan rates. These results demonstrate that MP-11 is strongly adsorbed on the surface of the roughened silver electrode and that the reversible electrochemical reaction of adsorbed MP-11 occurs. A -0.34 V of the formal redox potential of the adsorbed MP-11 is slightly more positive than that for the MP-11 in the solution. The factors that caused the difference in formal redox potential will be discussed later. Thus, the broad electrochemical response of 1×10^{-4} M MP-11 at the roughened silver electrode in the 0.025 M phosphate buffer solution (pH 7.0) with 0.1 M $NaClO_4$ was contributed from both MP-11 in the solution and adsorbed species on the electrode surface.

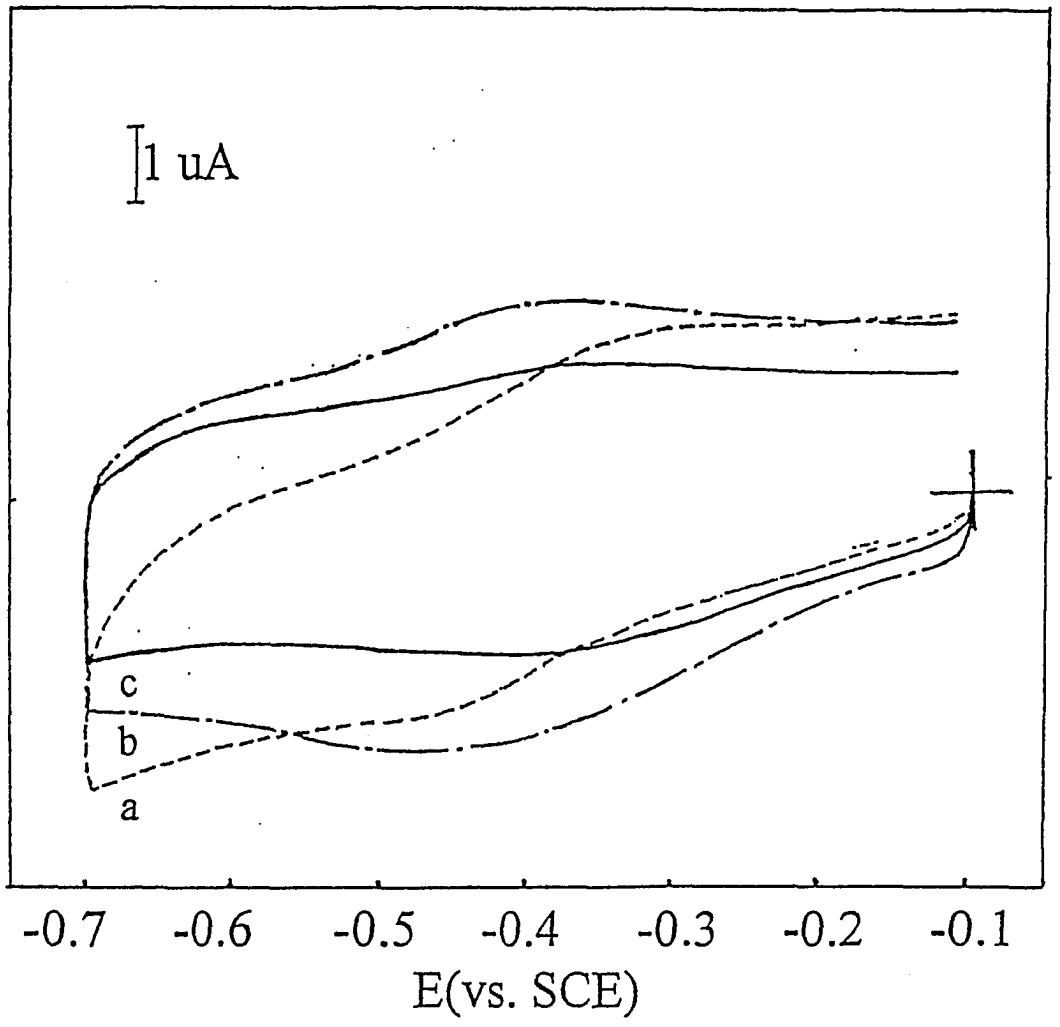

Figure 1. The CVs of (a) 0.1 mM MP-11 in 0.025 phosphate buffer solution with 0.1 M $NaClO_4$ at the polished silver electrode, (b) 0.1 mM MP-11 in the 0.025 phosphate buffer solution with 0.1 M $NaClO_4$ at the roughened silver electrode, (c) MP-11 adsorbed on the surface of the roughened silver electrode in the 0.025 phosphate buffer solution with 0.1 M $NaClO_4$. The scan rate: 100mV/s.

RR spectra of MP-11. Resonance Raman spectrum of 1×10^{-4} M MP-11 in the 0.025 M phosphate buffer solution (pH 7.0) with 0.1 M $NaClO_4$ is shown in Figure 2. The spectrum is similar to that reported by Wang et al. [10]. No change in the RR spectrum was observed with the addition of 20% methanol to the solution, indicating that methanol does not affect the aggregated state of MP-11 molecules in the 1×10^{-4} mM MP-11 solution. It is generally accepted [13-15] that the ν_4 band in the 1350-1380 cm^{-1} region is sensitive to the oxidation states of the heme iron for heme proteins. The reduction of the heme iron produces its shift towards a low-frequency region. Since the ν_4 band was observed at 1373 cm^{-1}, MP-11 is in its oxidized state [13-15]. The appearance of the spin and coordination marker bands at 1639 (ν_{10}), 1585 (ν_2) and 1504 (ν_3) cm^{-1} implies that MP-11 exists in the low spin, six-coordination state [13-15]. Therefore, it can be concluded from the RR spectrum of MP-11 that when MP-11 concentration is as high as 1×10^{-4} M, the MP-11 molecules in the aqueous solution exist as in the ferric, low spin, six-coordination state. In other words, it is in the oxidized, low spin, aggregated state, even in the presence of methanol.

SERRS Spectra of MP-11. The SERRS spectrum of MP-11 at -0.2 V is shown in Figure 3, Spectrum a. Comparing with the RR spectrum of MP-11 (Figure 2), it was found that except the bands corresponding to that observed in RR spectrum, some new bands, such as 1625, 1576 and 1493 cm^{-1} appeared in the SERRS spectrum at -0.2 V. These bands correspond to the ν_{10}, ν_2 and ν_3 band, respectively, and are sensitive to the spin and coordinated state of the heme iron. It was reported that the ν_3 band is most sensitive to the spin and coordinated state. It is located at about 1502 cm^{-1} for low spin and six-coordinated state, at about 1491 cm^{-1} for the

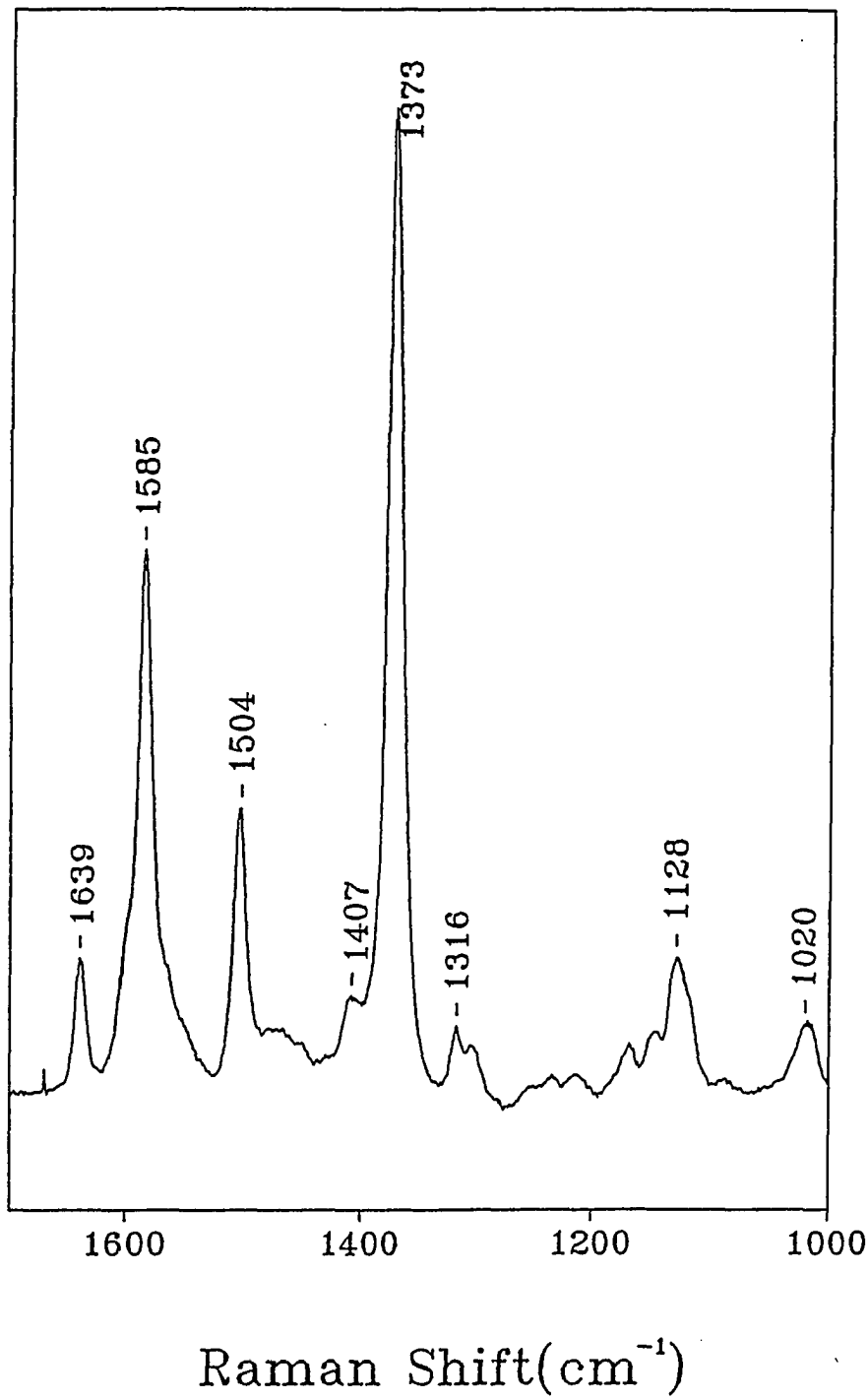

Figure 2. The RR spectrum of 0.1 mM MP-11 in the 0.025 phosphate buffer solution with 0.1 M $NaClO_4$.

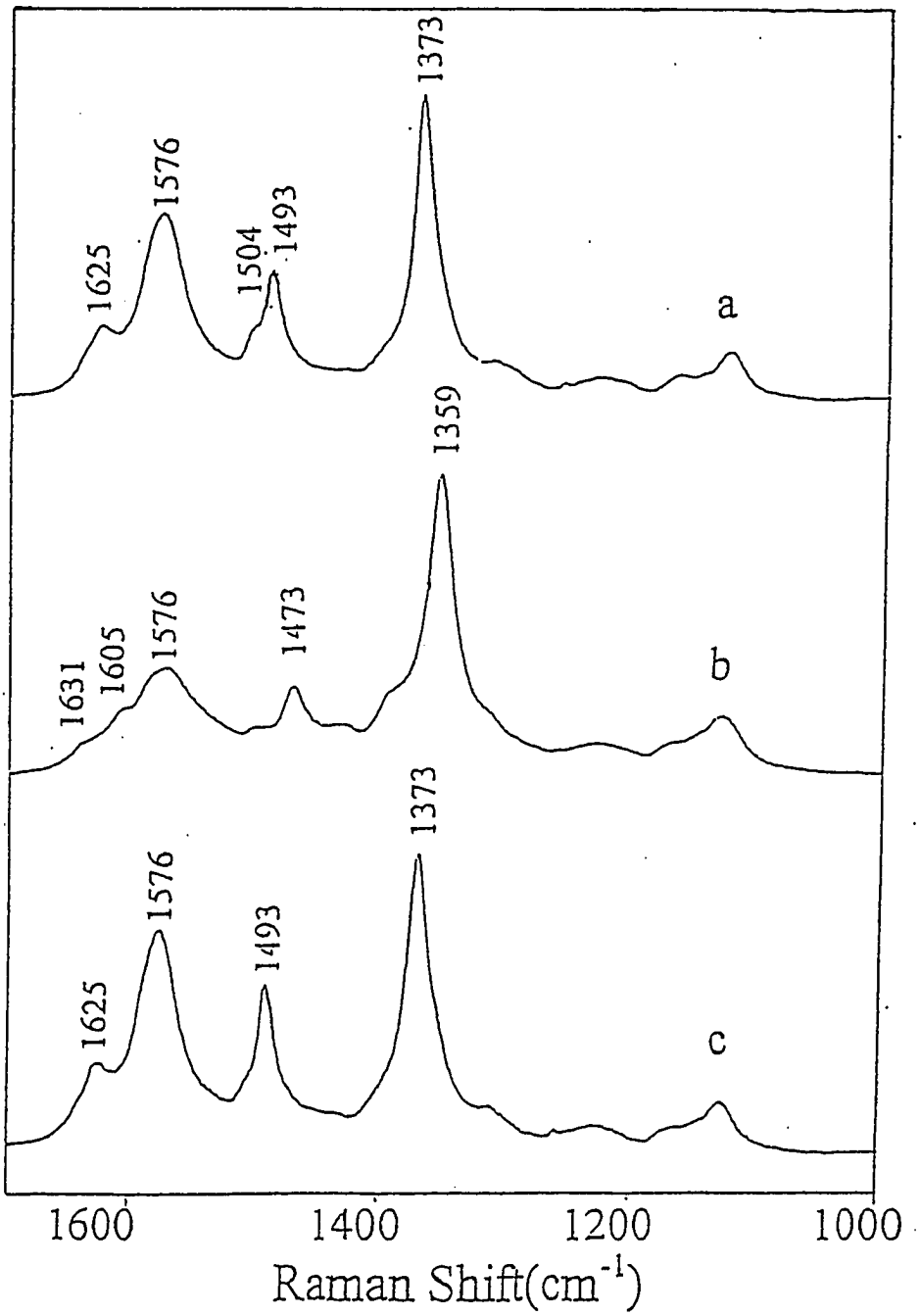

Figure 3. The SERRS spectra of MP-11 adsorbed on the surface of the roughened silver electrode at (a) -0.2 V, (b) -0.5 V, (c) back to -0.2 V.

high spin and five-coordinated state and at about 1480 cm^{-1} for the high spin and six coordination state [14]. Thus, the appearance of the ν_3 band at 1493 cm^{-1} definitely indicated the existence of the high spin and five-coordinated state of MP-11 adsorbed on the roughened silver electrode. Accordingly, the ν_{10} band related to the high spin and five-coordinated state was observed at 1625 cm^{-1}. The band at about 1580 cm^{-1} is broad due to the overlap of the ν_2 and ν_{19} bands [14] so that the bands at 1585 and 1576 cm^{-1} can not be distinguished. Thus, the coexistence of the bands at 1639 and 1504 cm^{-1} with the bands at 1625 and 1491 cm^{-1} illustrates that when MP-11 molecules with the low spin, six-coordinated state are adsorbed on the roughened silver electrode at -0.2 V, they are partially decomposed to form the high spin, five-coordinated state species.

When the electrode potential was stepped from -0.2 to -0.5 V, the oxidation sensitive band at 1373 cm^{-1} disappeared and a band at 1359 cm^{-1} was observed (Figure 3, Spectrum b), indicating that the MP-11 is in its fully reduced form [14]. Furthermore, the bands at 1504 and 1493 cm^{-1} disappear and a band at 1474 cm^{-1} was observed. The ν_3 band at 1474 cm^{-1} represents the high spin, five-coordination form for a reduced heme protein. For the low spin and six-coordinated state or high spin and six-coordinated state, the ν_3 band should be located at about 1493 or 1463 cm^{-1}, respectively [14]. Accordingly, the ν_{10} band appears at 1605 cm^{-1}. All the above results demonstrate that the adsorbed MP-11 molecules can be reduced at potentials as negative as -0.5 V, accompanying their complete transformation from the low spin, six-coordinated state to the high spin, five-coordinated state.

When the electrode potential was switched back to -0.2 V, the low spin and six-coordination marker band at 1504 cm^{-1} completely disappeared and only the band at 1493 cm^{-1}

corresponding to the high-spin, five-coordination state are observed (Figure 3, Spectrum c). Therefore, it can be concluded that the aggregates of the MP-11 molecules adsorbed on the electrode surface can be transformed to the monomer through the reduction-oxidation cycle.

For heme proteins, the conversions in the spin and coordination states have been suggested for several studies, particularly for cytochrome c [16-18]. Hibdebrandt et al. [17] in their SERRS study of cytochrome c suggested that the conversion behavior in the spin and coordination states for cytochrome c molecules may be the results of the electrostatic interaction between the cytochrome c chromophore and the charged electrode/electrolyte interface. The interaction may cause certain changes in the orientation of cytochrome c molecules on the electrode surface and decrease the ligand field strength in cytochrome c molecules. Hence, a thermal equilibrium can be established between the five-coordination and six-coordination states of cytochrome c molecules. This assumption was confirmed by the temperature and electrode potential dependence of the spin-state contribution of cytochrome c [18]. However, the sixth coordinated ligand of the MP-11 molecule is contributed from the amino acid residues of another molecule. When the coordination bond is broken, a change in the conformation or the orientation of the MP-11 molecule on the electrode surface could occur. This may be the reason for the irreversible conversion of the coordination states of the MP-11 molecules.

Figure 4 shows the SERRS spectra of the adsorbed MP-11 at the roughened silver electrode at different potentials. It can be clearly seen from Figure 3, Spectrum b or Spectrum d that the MP-11 molecules adsorbed on the roughened silver electrode were fully oxidized at -0.2 V, as indicated by the redox marker band appearing at 1373 cm^{-1}. When the electrode potential was more negative than -0.3 V, the adsorbed molecules started to be reduced, because the band at 1359 cm^{-1} started to appear at -0.3 V. The band at 1373 cm^{-1} completely disappeared at -0.5

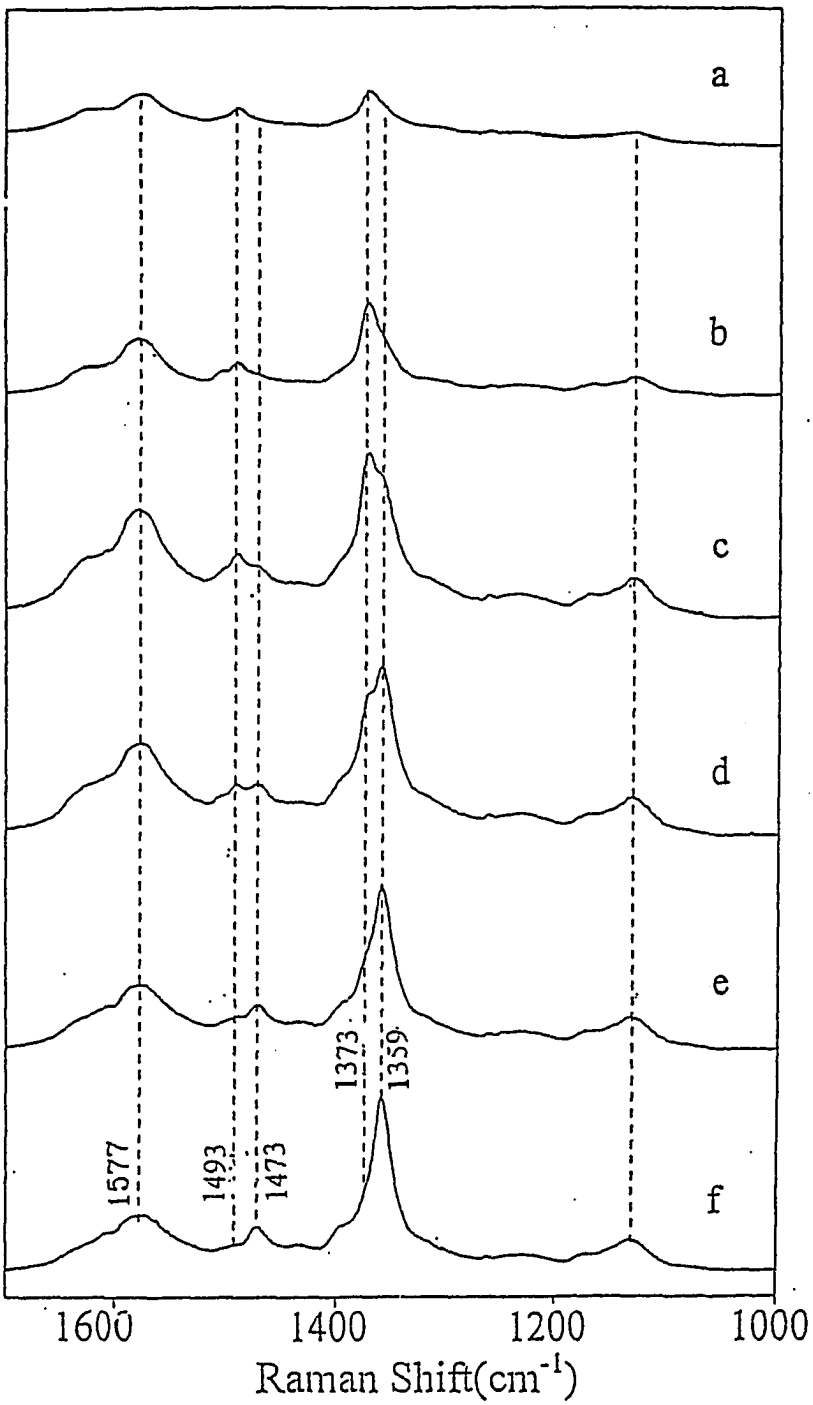

Figure 4. The SERRS spectra of MP-11 adsorbed on the surface of the roughened silver electrode at (a) -0.25, (b) -0.30 V, (c) -0.35 V, (d) -0.40, (e) -0.45, (f) -0.5 V.

V, implying that the MP-11 molecules are totally reduced at this potential. When the normalized intensities of the bands at 1373 and 1359 cm^{-1} were plotted against the electrode potential, respectively, the intersect of two curves is at -0.34V (Figure 5). This value is consistent with that of CV measurement. Usually, it may be considered as the formal redox potential of the adsorbed molecules [12]. However, there is 50 mV difference between the formal redox potentials for MP-11 in solution and adsorbed on roughened silver electrode surface. The possible explanation is that adsorbed species are partially or totally converted to five-coordinate, high-spin state, which may be easier reduced, compared to the solution species which mainly exist in six-coordinate, low-spin state.

Photo-induced Reduction of MP-11. Figure 6 shows the time dependence of SERRS spectra of MP-11 molecules adsorbed on the surface of the roughened silver electrode at open circuit. At the beginning, the spectrum obtained is as the same as Spectrum a in Figure 3, in which only the bands at 1373 and 1474 cm^{-1} appear, indicating that all the adsorbed MP-11 molecules are in the oxidation state. Under the continuous illumination of the laser light, however, it was observed that the intensities of the bands at 1491 and 1373 cm^{-1} decrease, while the bands at 1474 and 1359 cm^{-1} appear and the intensity of the two bands increases with the illumination time. After 30 min, the spectrum (Figure 6, Spectrum c) is the same as Spectrum c in Figure 3, indicating that the adsorbed MP-11 molecules are completely reduced at the open circuit after 30 min continuous illumination of the laser light. Therefore, it is demonstrated that the photo-induced reduction of the MP-11 molecules adsorbed on the surface of the roughened silver electrode occurs.

Heme proteins, such as hemoglobin and cytochrome c can undergo photoreduction under the illumination of light, particularly under the illumination of ultraviolet light [19-21]. It

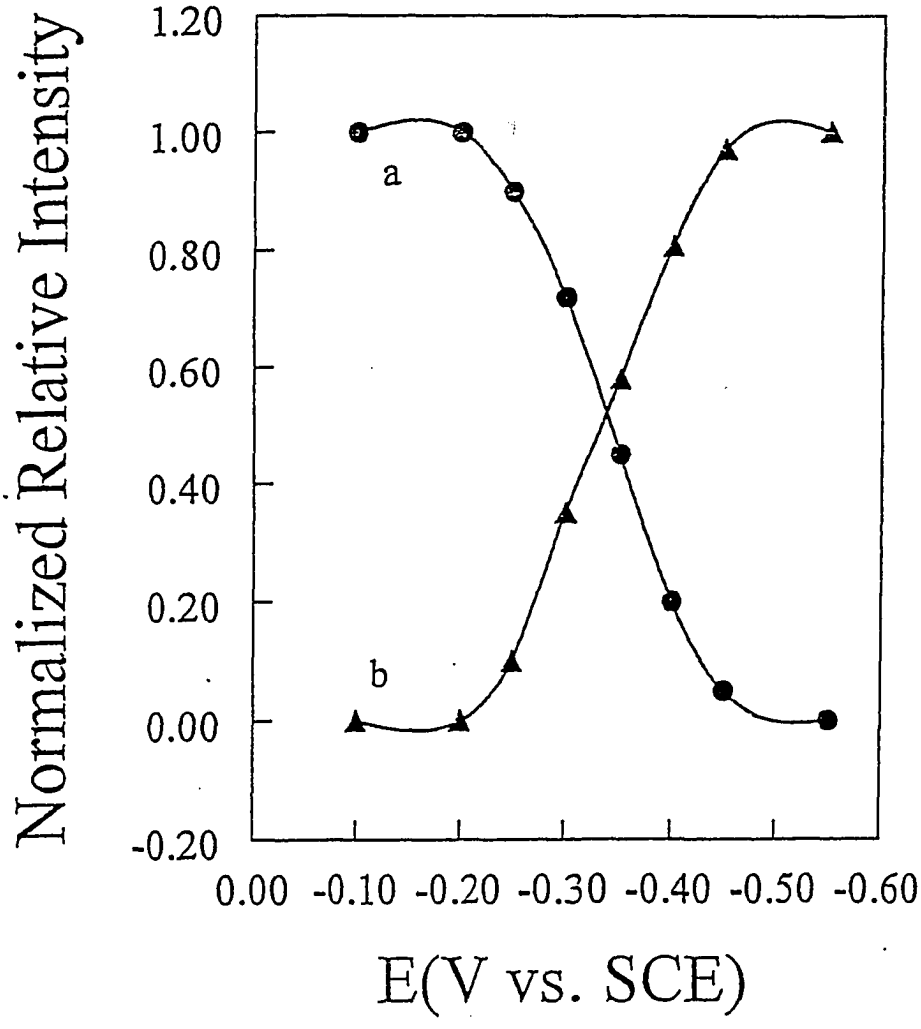

Figure 5. The plot of the relative intensity of the bands at (a) 1373, (b) 1359 cm^{-1} against the electrode potential according to Figure 4.

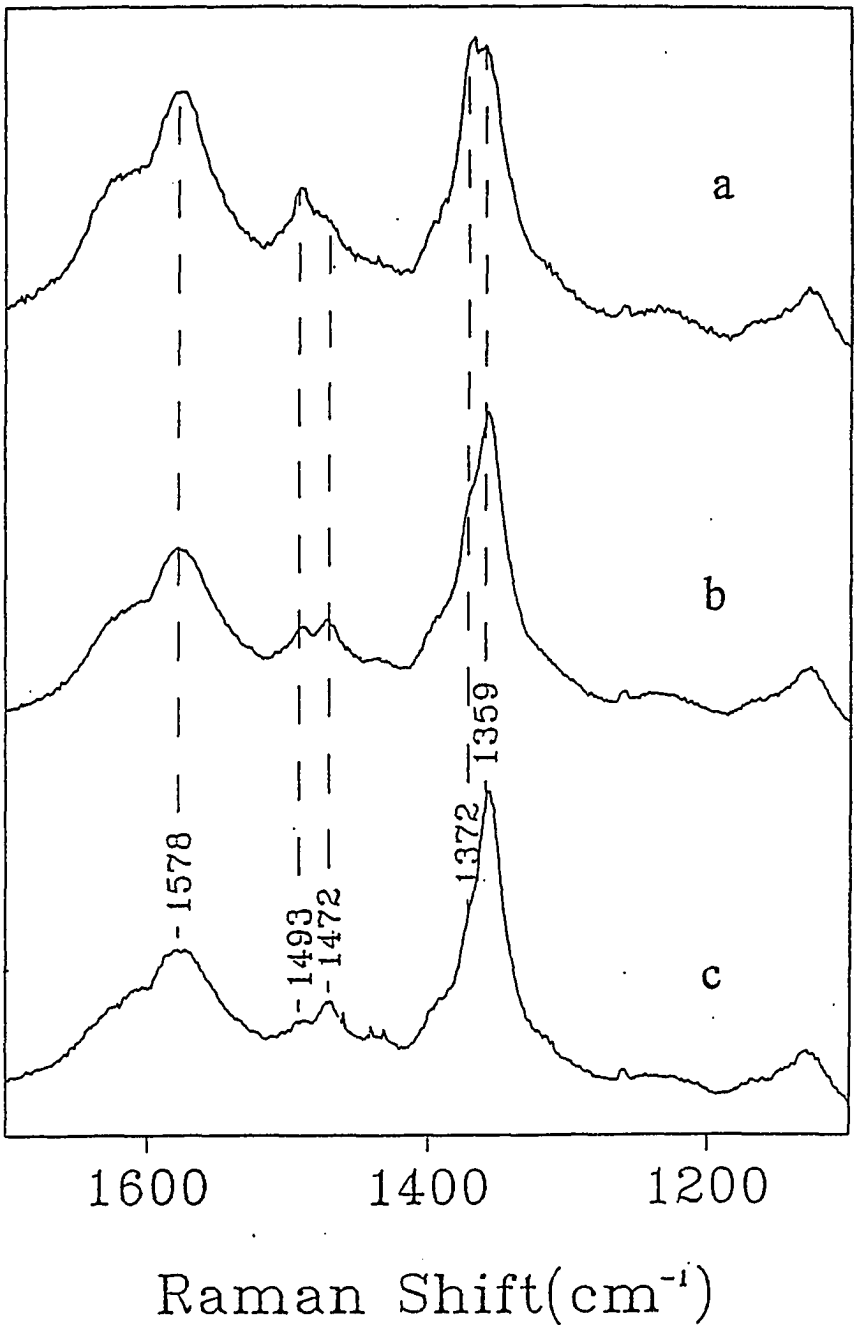

Figure 6. Time dependence of SERRS spectra of MP-11 adsorbed at the surface roughened silver electrode under continuous irradiation of 413 nm laser.

has generally been accepted that the sixth axial ligand of the heme group or aromatic amino acid residues may play the role as the electron donors [22,23]. However, this is not possible for MP-11 molecules, because the adsorbed MP-11 molecules are in five-coordination state in both oxidized and reduced forms. In addition, no aromatic amino acid residues are present in the structure of the MP-11 molecule.

Based on the above consideration, it is assumed that the photo-induced reduction of the adsorbed MP-11 molecules results from the photoejection of the free electron in silver to the adsorbed MP-11 molecules. It is generally accepted that the free electron in a metal can be excited under the illumination of light. The excited electron may escape from the metal to outside. The escaped electron may be captured by an acceptor molecule, resulting in the reduction of the acceptor molecule. The similar phenomena have been reported by several groups [24-26]. A recent work from this group also reported the photo-induced reduction of methylviologen at a roughened silver electrode under the liquid nitrogen temperature [27]. Therefore, in this case, the photoejection of free electrons from silver metal is considered to be responsible for the reduction of adsorbed MP-11 molecules.

Conclusion

The study of the electrochemical reactions, RR and SERRS spectra of MP-11 indicates that the coordination state and spin state of heme iron largely determine the redox properties of MP-11. The adsorbed MP-11 can undergo photo-reduction on the roughened silver electrode. The mechanism of photoreduction of the adsorbed MP-11 molecules is considered to be the result of the photoejection of free electrons from the roughened silver electrode.

Acknowledgement

The Financial support of the National Institutes of Health (GM35108) and National Natural Science Foundation of China is gratefully acknowledged.

References

1. J. Aron, D.A. Baldwin, H.M. Marques, J.M. Pratt, P.A. Adams. J. Inorg. Chem. 27(1986) 227.
2. M.T. Wilson, Eur. J. Biochem. 77(1977)193.
3. R. Santucci, H. Reinhard, M. Brunori, J. Am. Chem. Soc.110(1988)8536.
4. S. Zamponi, R. Santucci, M. Brunori, R. Marassi, Biochem. Biophys. Acta 1034(1990)294.
5. V.J. Razumas, A.V. Gudavicius, J.D. Kazlauskaite, J.J. Kulys, J. Electroanal. Chem. 271(1989)155.
6. V. Razumas, J. Kazlauskaite, T. Ruzgas, J. Kulys, Bioelectrochem. Bioenerg. 28(1992)159.
7. V. Razumas, T. Arnebrant, J. Electroanal. Chem. 427(1997)1.
8. T. Lotzbeyer, W. Schuhmann, E. Katz, J. Falter, H.L. Schmidt, J. Electroanal. Chem. 377(1994)291.
9. D.K. Das, O.K. Medhi, J. Chem. Soc., Dalton Trans., (1998)1693.
10. J.S. Wang, H.E.V. Wart, J. Phys. Chem. 93(1989)7925.
11. V.J. Razumas, J.D. Kazlauskaite, G.J.A. Vidugiris, J. Kulys, J. Bioorg. Khim.,15(1989)40.
12. R.L. Birke, T. Lu, J.R. Lombardi, in R. Varma, J.R. Selman(Ed.), Techniques for Characterization of Electrodes and Electrochemical Processes, John & Sons Inc., New York, 1990, p. 211.

13. B. Cartling, in T.G. Spiro(Ed.), Biological Applications of Raman Spectroscopy, John Wiley & Sons, Inc., New York, 1988, p. 217-248.

14. P. Hildebrandt, M. Stockbuger, in H.D. Bist(Ed.), Raman Spectroscopy: Sixty Years on Vibrational Spectra and Structure, Elsevier Science, Netherlands, 1989, vol. 17A, 443.

15. T.G. Spiro, in A.B.P. Lever, H.B. Gray(Ed.), Iron Porphyrins, Addison-Wesley Publishing Company, Inc., Massachuusetts, 1983, 89-159.

16. P.R. Carey, in Biochemical Applications of Raman and Resonance Raman Spectroscopies, Academic Press, Inc. (London) Ltd. New York, 1982.

17. G. Simulevich, T.G. Spiro, J. Phys. Chem. 89(1985)5168.

18. P. Hildebrandt, M. Stockburger, J. Phys. Chem. 90(1986)6017.

19. P. Hildebrandt, M. Stockburger; Biochem. 28(1989)6710.

20. J.T. Sage, D. Morikis, P.M. Champion, J. Chem. Phys. 90(1989)3015.

21. C. Bartocci, A. Maldotti, V. Carassiti, O. Traverso, A. Ferri, Inorg. Chim. Acta 107(1985)5.

22. M.A. Cusanovich, T.E. Meyer, G. Tollin, Biochemistry 24(1985)1281.

23. Y. Gu, P. Li, T. Sage, P.M. Champion, J. Am. Chem. Soc. 115(1993)4993.

24. Y. Ozaki, K. Iriyama, H. Ogoshi, T. Kitagawa, J. Am. Chem. Soc.109(1987)5583.

25. D.S. Corrigan, M.J. Weaver, J. Electroanal. Chem. 228(1987)265.

26. J.G. Gordon, H.O. Finkea, J. Phys. Chem. 83(1979)1834.

27. H. Berg, P. Reissmann, J. Electroanal. Chem. 24(1970)427.

28. F. Hannah, G. Chumanov, T.M. Cotton, J. Phys. Chem. 100(1996)4937.

CHAPTER 6

RESONANCE RAMAN STUDY OF CYTOCHROME C WATER MUTANTS

A paper published in the *Journal of Raman Spectroscopy*, 1998, 29, 955

Chengli. Zhou, Junwei Zheng, Abel Schejter, Wenying Qin, Emanuel Margoliash and Therese, M. Cotton

ABSTRACT

Resonance Raman studies of three mutants of cytochrome c demonstrated the sensitivity of the spectra to mutations that affect the interactions of the heme peripheral substituents with the protein matrix. The most dramatic differences in the spectra of the reduced mutant cytochromes, as compared with that of wild-type cytochrome c, are observed in the low-wavenumber region of the reduced proteins. The bands that are most strongly affected include bending modes of the thioether linkages and propionic acid side-chains. These modes are activated by the distortion of saddling of the heme macrocycle in the protein pocket. The high-wavenumber region of the mutants is nearly identical with that of wild type. The spectral changes are pronounced in the oxidized form of the mutant cytochromes. This observation is consistent with the more open structure of ferricytochrome c than ferrocytochrome c.

INTRODUCTION

Mitochondrial cytochrome c is one of the most extensively characterized proteins both because its physicological role as an electron carrier in the respiratory chain and also because it provides a model for the development of experimental approaches that can be

applied to proteins in general[1]. The primary goal of many of the prior investigations has been to correlate the structural aspects of the protein with its function. The crystal structures of both oxidized and reduced form of the protein have provided detailed structural information[2]. Its functional behavior has been monitored by a number of spectroscopic techniques, including UV-visible[3], circular dichromism[4] and resonance Raman[5], that are capable monitoring redox reactions at the heme prosthetic site and, in some cases, changes in the protein structure that accompany the electron transfer processes. In spite of considerable amount of information that exists concerning the spectroscopic and structural aspects of the protein, a detailed understanding of the electron transfer mechanism is not yet available. In particular, the role of the protein or specific amino acid pathways in intraprotein (from the heme to redox labels on the surface of the protein) or interprotein electron transfer is under intense scrutiny[6].

Site-directed mutagenesis has emerged as a powerful method for probing the effect of specific amino acids, especially those which have been evolutionally conserved, on the structure and function of cytochrome c. A few selected examples of this approach are cited here. The effect of mutating proline-71 to valine, threonine or isoleucine on the folding and unfolding kinetics of iso-1-cytochrome c was studied by Nall and co-workers[7]. They proposed that mechanistic studies of the folding of mutant proteins may assist in determining the code which relates amino acid sequence to tertiary structure and function. In another study, the effects of specific point mutations on the redox potential of yeast iso-1-cytochrome c and yeast cytochrome c peroxidase were examined[8]. A continuum model was used to calculate the effects of the mutations on the redox potential of the proteins and on their complex formation. The theoretical results were compared with experimental data. Factors

that were included in the analysis included the charge and polarity of a surface residue, the size of a surface residue controlling the exposure of the heme to the solvent and polarity of an interior residue. Mutation of Phe-82, a residue which controls heme exposure, to a smaller Ser residue results in the formation of a solvent channel[9], leading a -35 mV change in the reduction potential[10]. A more drastic change in the cytochrome c reduction potential was observed for axial ligand mutants prepared by semisynthesis[11]. The reduction potential of a mutant in which cysteine was substituted for Met-80 is -390 mV vs. the normal hydrogen electrode or more that 600 mV lower than that of the native protein.

Margoliash et al.[12] utilized sit-directed mutagenesis to prepare a number of rat cytochrome c mutants. Rather than substitute the axial ligands which would lead to profound changes in the properties of the mutant and complicate the interpretation of these effects, 'second tier' residues were modified. These are residues that interact with the heme ligands, but not with the heme itself. The effects of these substitutions were surprising in that, in some cases, the mutant exhibited the expected variations in heme-related physico-chemical properties that can be related to the strength of the sulfur-iron bond in function (Pro-30), whereas in others the bond displayed great stability than the wild-type protein. The latter include mutations at Tyr-67 and Asn-52, so-called 'water mutants' because the residues of the wild-type protein are hydrogen bonded to a molecule of water in the interior of the protein. The effect of the amino acids substitutions on both the local (strength of the iron-sulfur bond) and global (overall conformational energy) stability was determined. The former can be evaluated by pH and thermal titrations[13-15]. In the equilibrium:

(Met)S–Fe^{3+}–imidazole ⇆ X–Fe^{3+}–imidazole (His)

the 695 nm band in the electronic absorption spectrum is present as long as the methionine sulfur is coordinated to heme iron and disappears when this bond is broken. The coordination of Met-80 to ferric cytochrome c is sensitive to a number of experimental variables, including pH (acid and alkaline), increases in temperature, urea and the presence of exogenous ligands[16]. Thus, loss of the 695 nm band provides a convenient method for monitoring the effect of site-directed mutations on the local stability of the protein and, in turn, the contribution of the iron-methionine bond to overall stability[14,17]. The global stability of the proteins was evaluated by measuring its unfolding in the presence of denaturants, i.e. urea[13-15] or guanidine hydrochloride[14]. Protein folding changes were followed by fluorescence spectroscopy [14,15] or ultraviolet circular dichroism[13]. In the case of the Tyr-67 to Phe mutant, a comparison of NMR spectra of the mutant and native proteins also provided preliminary structural information about changes in the protein environment near the heme group as a result of the amino acid replacement[13].

The independent nature of the effects of mutations on local and global stability was emphasized in the mutant in which Asn-52 is replaced by isoleucine. In this case, the Fe-S bond strength is increases[15], whereas the global stability is decreases in the mutant rat protein[18]. A similar independence is observed in a recently described study of a His-33 mutant[19]. Substitution of His-33 with Phe increased the stability of rat cytochrome toward heat and denaturants. However, no change was observed in the stability of iron-methionine bond. This residue is highly variable in the protein and the increase in global stability, which was observed for the first time, was totally unexpected.

In contrast, replacement of the invariant His-26 with Val results in a protein with decreases local and global stabilities. This residue forms two hydrogen bonds, to the backbone amide of Asn-31 and carbonyl of Pro-44, that appear to have structural and/or functional significance.

Resonance Raman spectroscopy[20] has been used extensively in the characterization of heme proteins. The initial research in this field has underscored the potential of this technique for monitoring the oxidation state of the heme and coordination interactions of the protein ligands with central iron. More recent applications of Raman spectroscopy to mutant heme proteins have illustrated its potential for monitoring the effects of amino acid replacements on the heme-protein interactions. These substitutions need not involve residues directly in contact with the heme in order to have an effect on the RR spectrum. For example, in a study of Phe-82 mutants, Hildebradt et al.[21] concluded from changes in the RR spectrum that Ser substitution resulted in an opening of the heme crevice and a weakening of the iron-methionine bond. However, the changes were not attributed to differences in the heme pocket in the vicinity of the mutation, but rather were indicative of structural differences remote from the mutation site. In another case, RR spectra of the semisynthetic Met80Cys horse heart cytochrome c mutant provided information about the active site and also the protein-heme interactions[22]. The high-wavenumber skeletal modes were found to be characteristic of a thiolate anion as the sixth ligand, whereas the low-wavenumber region of the spectrum indicated a lessening of the protein-induced heme distortion as compared with the wild-type cytochrome.

In the present study, RR spectroscopy was used to evaluate the effects of substitution of second tier amino acids on the heme-protein interactions. These include the water mutants, in which a non-polar amino acid is substituted for one of the polar residues that is normally hydrogen bonded to one of the interior water molecules and the His-26Val mutant. The results further emphasize that RR spectroscopy can provide information regarding not only the effect of local mutations on heme-protein interactions, but also structural effects that result from mutations distant from the heme. The low-wavenumber region of the heme spectrum is exquisitely sensitive to interactions between the heme substituents and protein, and also to the overall distribution of the heme structure by the protein pocket. In essence, this region of the spectrum is sensitive to both the local and global stability of the protein.

EXPERIMENTAL

The procedure for preparing the mutant cytochromes has been described previously[14,15,23,24]. Solutions (0.1 mM) of the cytochromes were deposited on a stainless-steel sample holder and submerged directly into liquid nitrogen in a Dewar vessel containing a transparent window for Resonance Raman measurements.

Resonance Raman spectra were obtained by excitation with 413 nm radiation from a krypton ion laser. A backscattering geometry was used for collecting the scattered light. The Raman instrumentation included a spectrograph (Spex Triplemate 1377) interfaced to a liquid nitrogen-cooled CCD detector (Princeton Instruments Model LN1152). Typically, the spectra were acquired with ca. 1 mW of power and a total acquisition time of less than 2 min. The resolution of the Raman instrument was ca. 2 cm^{-1} at the excitation wavelengths used here. Indene was used to calibrate the Raman spectra.

RESULTS AND DISCUSSION

The water mutants consist of three site-directed mutants of rat cytochrome c expressed in *S. cerevisiae*. Polar amino acids on the 'left' side of the heme plane that are hydrogen bonded to a single water molecule near the 'lower' edge of the heme plane, in the hydrophobic pocket of the protein, have been replaced with non-polar residues12. These include tyrosine-67 to phenylalanine (Y67F) at 'top left' and asparagine-52 to isoleucine-52 (N52I) at 'bottom left' of the heme crevice [Fig. 1(A)]. Another mutation, of His-26 to Val(H26V) was performed on the right-side middle loop of the protein [Fig. 1(B)]. In all three cases, the mutants sustained normal growth of the yeast cultures.

Assignments of the RR bands in the wild type and mutant cytochromes are based on the recent complete normal coordinate analysis by Hu et al.[25]. Figure 2 illustrates the atom designations of the heme. In Figure 3 and 4 the RR spectra of the oxidized and reduced forms of the wild type and mutant cytochromes in high-wavenumber region are presented. These spectra were recorded with 413.1 nm excitation and at 77 K. The low-temperature spectra are essentially identical with those taken at room temperature, except that the bands are significantly sharper and the resolution is superior at liquid nitrogen temperature.

A comparison of the spectra of the reduced proteins shows few differences in the spectral region between 1600 and 600 cm^{-1} (Fig. 3). The most notable is the change in relative intensities of the ν_2 and ν_{19} bands at 1594 and 1587 cm^{-1}, respectively. In the wild type [Fig. 3(a)] ν_{19} is the most intense, whereas ν_2 is the most intense in the mutant [Fig 3(b) and (c)]. As noted previously [25], the ν_{19} band is sensitive to heme distortion, hence this difference suggests that the heme is less distorted in mutants. It may be that this will also

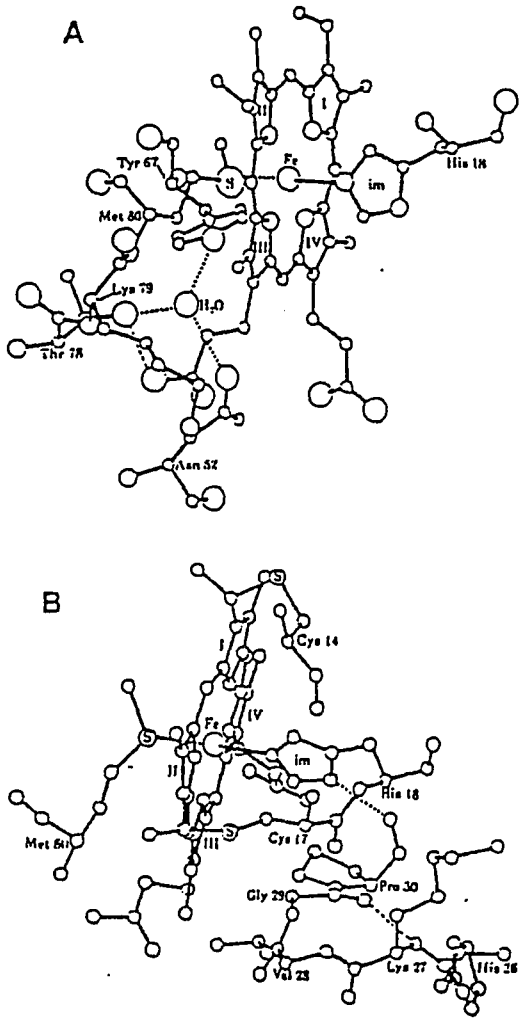

Figure 1. Diagrams of the structure of cytochrome c in the region important to the water mutations studied here. Fe indicates the heme iron atom, im shows the imidazole side-chain of histidine-18 and S is the sulfur atom of methionine-80. These are axial ligands of heme iron atom, from the 'right' and the 'left' sides of the protein molecule, respectively. I, II, III and IV indicate the corresponding pyrrole rings of the heme. The amino acid residues are indicated in three-letter code placed near their α-carbon atoms. (A) Part of the 'left' side of the protein relevant to the effects of the Y67F substitution. The molecule is viewed from the 'front', defined as the area containing the solvent-accessible edge of the heme plane, containing pyrrole ring II and III. The heme plane is slightly tilted to the left, so that the imidazole axial ligand on the right side has moved closer to the viewer than the sulfur ligand on the other side of the heme plane. H2O marks the internal water molecule hydrogen-bonded (dotted lines) to the side-chains of asparagine-52, tyrosine-67 and threonine-78. (B) Part of the 'right' side of the protein showing the histidine 26 residue.
Reprinted with permission from Ref. 14.

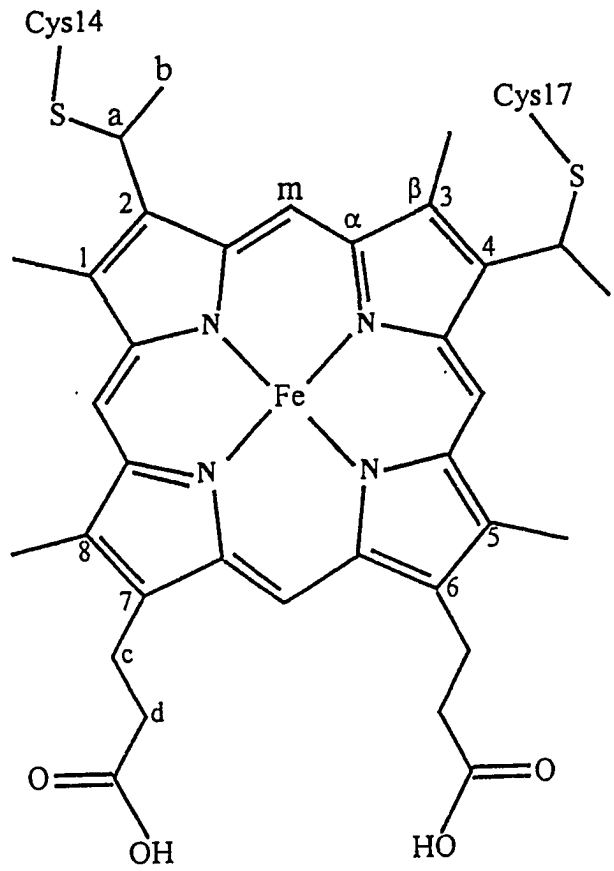

Figure 2. The heme labeling scheme and atom designations for cytochrome c

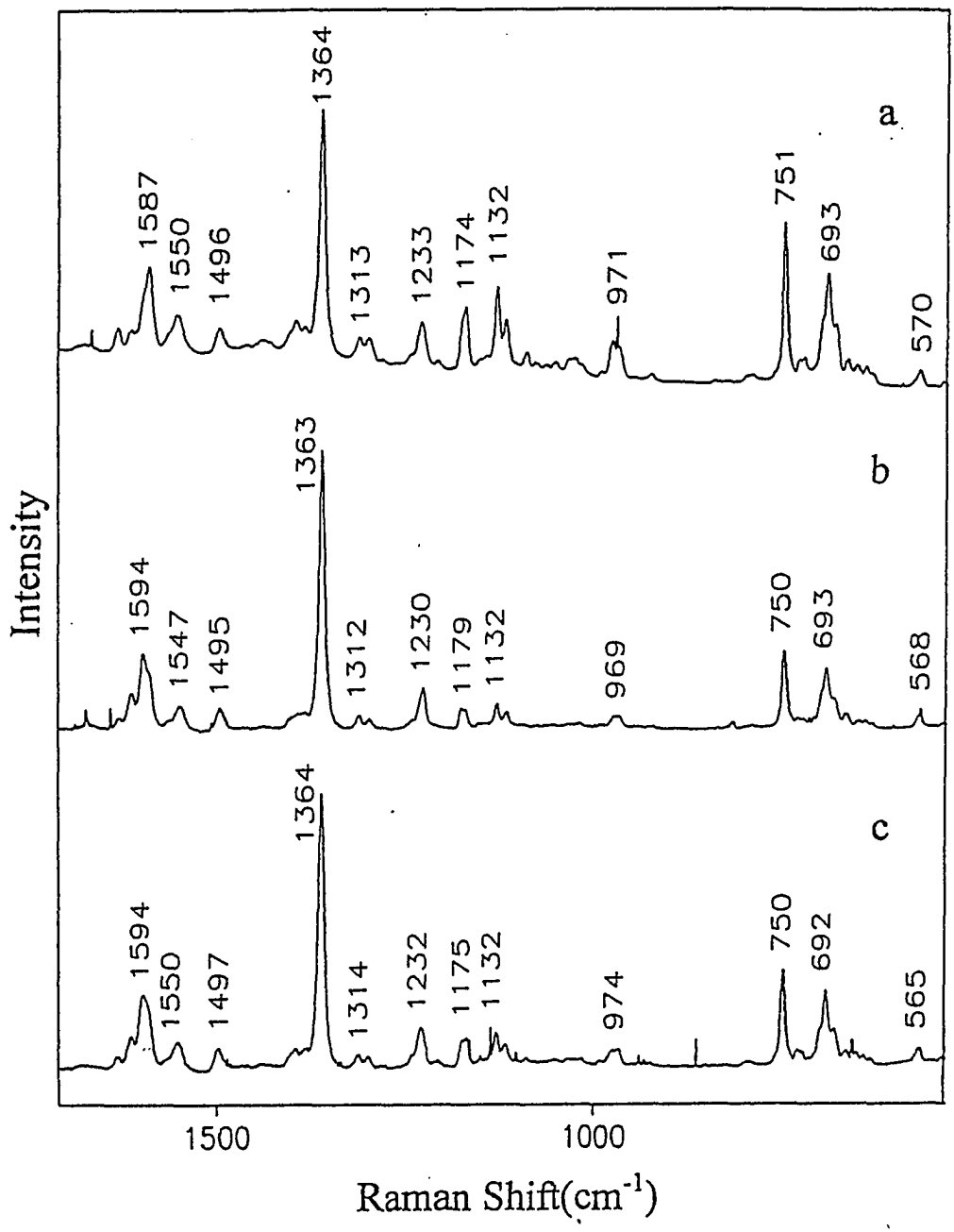

Figure 3. Resonance Raman spectra in the high-wavenumber region of 0.1mM solution of reduced cytochromes at 77 K: (a) wild type; (b) Y67F mutant; (c) N52I mutant. The spectra were obtained with 413.1 nm excitation and 1 mW power.

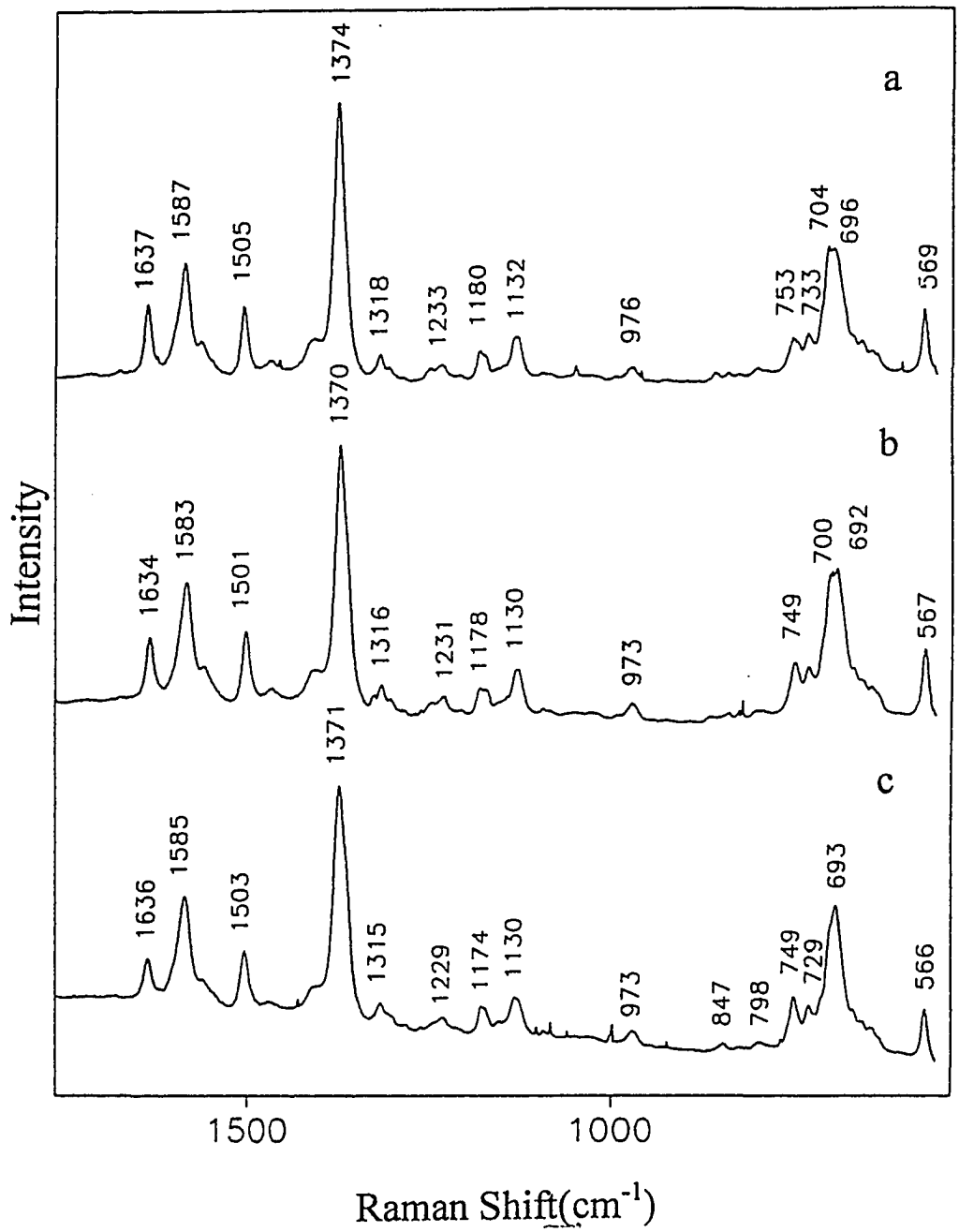

Figure 4. Resonance Raman spectra in the high-wavenumber region of 0.1 mM solution of oxidized cytochromes at 77 K: (a) wild type; (b) Y67F mutant; (c) N52I mutant. Experimental conditions as in Fig. 3.

effect the enhancement of heme peripheral modes in the mutants relative to that of the wild type. The spectrum of the wild type is in agreement with that reported previously[25].

The effect of mutations on the RR spectra of the oxidized proteins in the high-wavenumber region (Fig. 4) is even less significant. Oxidation produces the expected shifts in the oxidation state-sensitive bands, but the only significant difference in the spectra is in the split 704/696 cm^{-1} band in the wild type. The former band is assigned to ν_7, a symmetric, in-plane pyrrole deformation mode. The latter band, the C_a-S stretch, is dominant in the N52I [Fig 4(c)]. The observation that the mutations described above have no effect on the RR spectrum of the heme in the high-wavenumber region is not expected. These modes reflect the inner and outer ring stretching vibrations of the heme and are sensitive to core size, spin and oxidation state of the central Fe atom. Because the amino acids that are substituted in the water mutants are not directly in contact with the heme macrocycle, it is reasonable that this region of the spectrum is unchanged.

In contrast, the low-wavenumber spectra of the mutants (Figs 5 and 6) show considerable variation compared with that of the wild type. Many of these bands have been assigned to modes involving the peripheral substituents of the heme, in particular bending modes of the thioether and propionic acid side-chains[25]. The substitution of amino acids containing side-chains capable of hydrogen bonding with non-polar residues affects not only the direct interaction of these groups with the interior water molecule, but also perturbs the hydrogen-bonding network involving the propionic acid side-chains of the heme. Differences in the RR spectra of the wild type and the various mutants provide support for the recent low-wavenumber assignments. The spectra of the individual mutants are

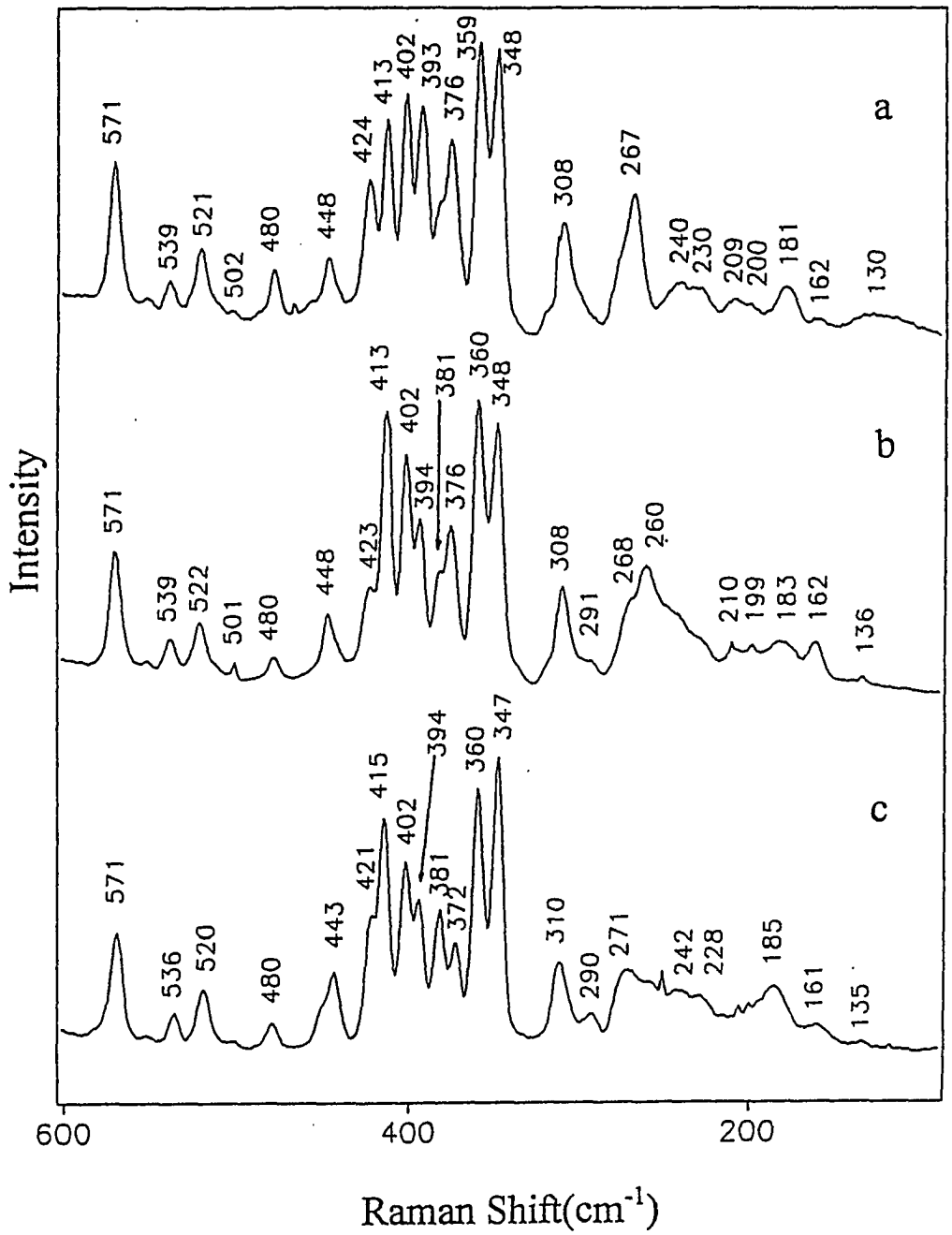

Figure 5. Resonance Raman spectra in the low-wavenumber region of 0.1 mM solution of reduced cytochromes at 77 K: (a) wild type; (b) Y67F mutant; (c) N52I mutant. Experimental conditions as in Fig. 3.

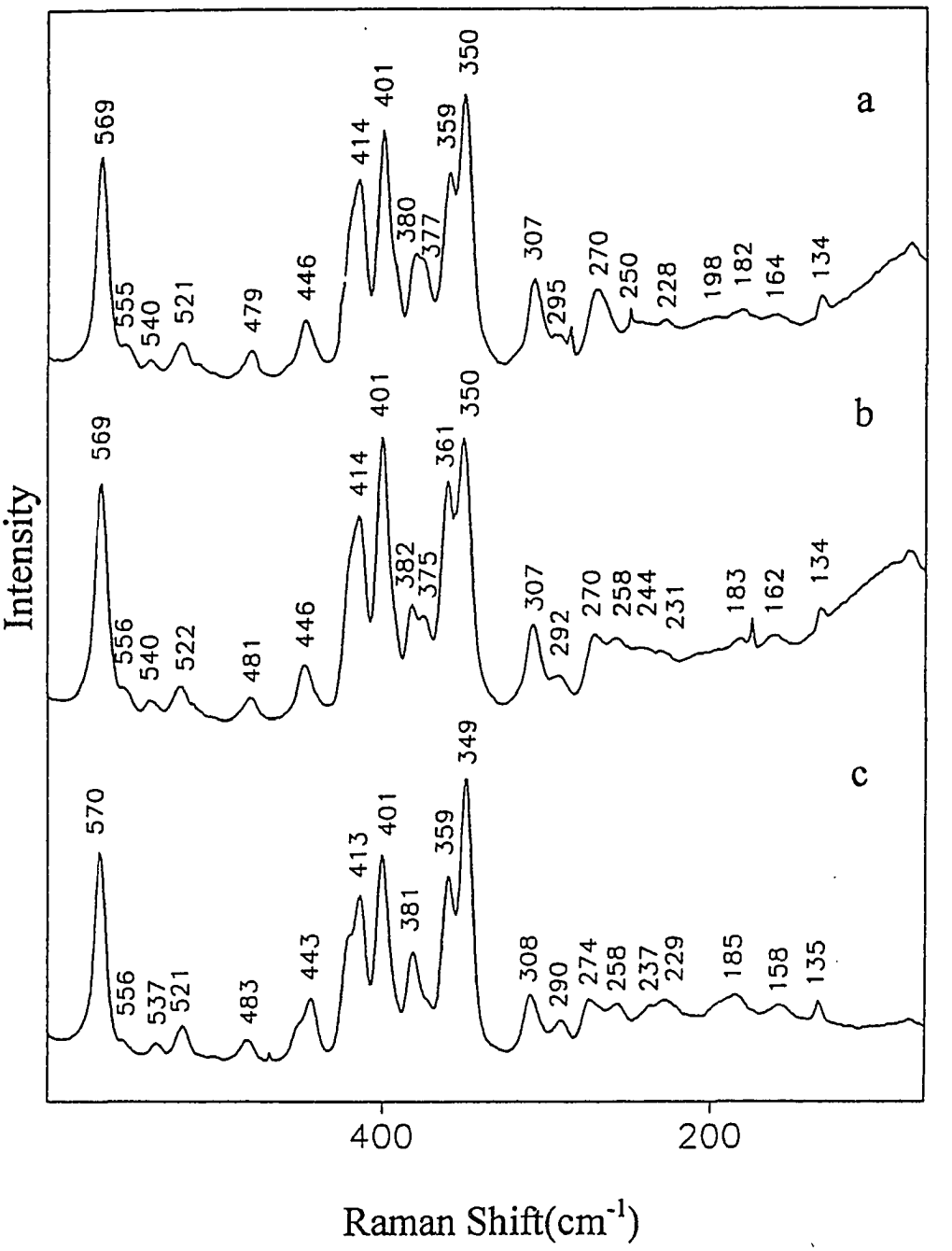

Figure 6. Resonance Raman spectra in the low-wavenumber region of 0.1 mM solution of oxidized cytochromes at 77 K: (a) wild type; (b) Y67F mutant; (c) N52I mutant. Experimental conditions as in Fig. 3.

discussed below. The band assignments are given in Table 1 according to the literature assignments[25,26].

Tyrosine-67 to phenylalanine

As noted above, the hydroxyl group of this acid is hydrogen bonded to the internal water molecule of cytochrome and may also be hydrogen bonded to the sulfur atom of methionine-80, the heme ligand. Thus, it was originally thought that Tyr-67 may have a stabilizing influence on the ligand interaction. Unexpectedly, loss of the phenyl OH resulted in an even stronger Met-Fe bond. In order to explain this result, Luntz et al.[13] hypothesized that the water is expelled with this mutation, because it is held in the mutant by only two hydrogen bonds, whereas three are required to maintain its presence in the hydrophobic pocket. The loss of water also frees the Asn-52 and Thr-78 side-chains leading to structural rearrangements in the lower region of the protein.

The RR spectrum of the reduced protein [Fig. 5(b)] shows changes in modes associated with thioether substituents, $\delta(C_\beta C_a C_b)$: an increase in the 413 cm^{-1} band and a decrease in 423 cm^{-1} band. A decrease occurs in the $\delta(C_\beta C_a S)$ mode at 394 cm^{-1}. Also, a strong new band appears at 260 cm^{-1}. This may be due to an intensification and shift of the 267 cm^{-1} band in the wild type, which is one of a group bands (308, 260, 240 and 181 cm^{-1}) that are assigned to the peripheral CH_3 group bending modes. In the case of the oxidized protein, only very minor differences are observed as compared to the wild type protein [Fig. 6(a) and (b)].

Asparagine-52 to isoleucine

Mutation of Asn-52 to isoleucine was found to increase the stability of the cytochrome c closed-heme crevice[15]. The increased stability can be attributed to the

hydrogen-bonding effects with the interior water or to an increase in hydrophobicity in the region of the protein where the mutation occurs. In this study, both rat cytochrome and yeast SC-iso1c were employed. Unlike the ferric vertebrate proteins, the Asn-52 residue of SC-iso1c is not hydrogen bonded to the interior water (W-1), but instead it hydrogen bonds with Ser-40 and backbone amide of Gly-41[27]. In the vertebrate proteins, the Asn-52 side-chain is hydrogen bonded to W-1 and to the propionyl side-chain of pyrrole ring IV. Consequently, W-1 occupies a large cavity in the case of the yeast protein. The two mutants behave differently, with the yeast exhibiting a greater increase in stability as compared with the rat. This is attributed to the greater decrease in cavity size in the case of the yeast. Computer graphics analysis suggests that rupture of the Met-80 bond could result in a rotation about its C_α-C_β bond with the formation of a hydrogen bond to Tyr-67. Thr-78 may then rotate and hydrogen bond to its own amide group instead of the anterior heme propionic group (ring III)[15].

An analysis of the RR spectrum of the reduced mutant shows little difference in high-wavenumber region of the spectrum [Fig. 3(c)] compared with that of the wild type [Fig. 3(a)], except for the change in relative intensities of the ν_2 and ν_{19} bands discussed above. In low-wavenumber region [Fig. 5(c)] an increase is observed in the 415 cm^{-1} band [$\delta(C_\beta C_a C_b)$] relative to that in the wild type, in addition to a decrease in the 376cm^{-1} band and a shift to 372 cm^{-1}. This band is attributed to a bending mode of the propionic acid side-chain [$\delta(C_\beta C_c C_d)$]. A decrease is also observed in the 267 cm^{-1} band [$\delta(C_\beta C_1)$] which shifts to 271 cm^{-1} in the mutant. A new band is evident at 290 cm^{-1} which may be due to an out-of-plane (oop) mode ($\gamma C_\alpha C_m$). The changes in bending modes involve peripheral substituents and reflect changes in the constraints imposed upon the heme by the protein, as a result of the

mutation. It is significant that a loss of hydrogen bond between the propionic acid side-chain and Thr-78 has been proposed and this may be correlated with a decrease in the band at 376 cm^{-1}, the bending mode associated with this functionality.

Differences in the RR spectra of the oxidized wild type [Figs 4(a) and 6(a)] and mutant [Figs 4(c) and 6(c)] are much smaller as compared with their reduced forms. Once again a significant decrease in the 377 cm^{-1} band is observed, consistent with the loss of hydrogen bond between the propionic acid side-chain and Thr-78 in the yeast mutant.

Histidine-26 to valine

The conserved imidazole group of His-26 is believed to have special structural and/or functional significance in cytochromes from vertebrates, invertebrates and higher plants. This residue hydrogen bonds with backbone atoms of Pro-44 and Asn-31, bridging the lower and middle loops on the right side of the protein. Substitution of this residue by valine results in a protein with decreased stability of Fe-Met bond. The interior of the protein is probably more hydrated in its mutant because of the increased mobility of the lower loop; this increased mobility may affect a series of hydrogen bonds with the heme (Thr-49 with the anterior propionyl side-chain and Tyr-48 and Gly-41 with the posterior heme propionyl side-chain)[19].

The RR spectra of reduced cytochrome c from H26V mutant in the high- and low-wavenumber region are shown in Figure 7(b) and (c). As in the water mutants, no significant changes are observed in the high-wavenumber region of the spectrum with the substitution. The low-wavenumber region is more perturbed, and the 401 cm^{-1} band is dominant. The bands assigned to propionic acid bending modes are diminished in the intensity, in support of the change predicted from the stability studies discussed above. The RR spectrum of the

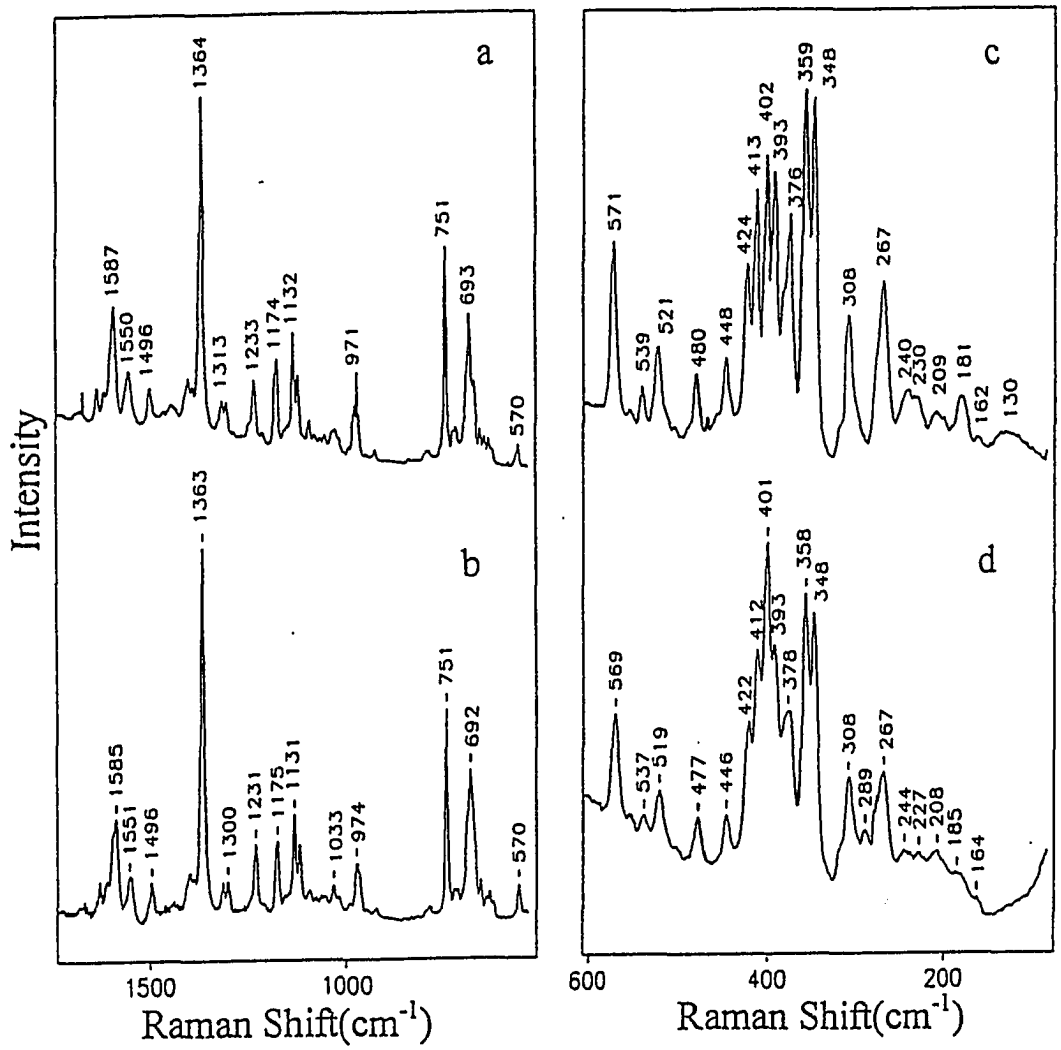

Figure 7. Resonance Raman spectra of 0.1 mM solution of reduced cytochrome c: (a) and (c) wild type; (b) and (d) H26V mutant. Experimental conditions as in Fig. 3.

oxidized protein is very similar to that of the wild type [Fig. 8(a) and (c) and 8(b) and (d)], respectively.

CONCLUSIONS

The high-wavenumber RR spectra of the cytochrome c water mutants Y67F and N52I and the right side mutant, H26V, are largely unaffected by second tier amino acid substitutions. In sharp contrast, the low-wavenumber spectra of each of the three mutants are unique in the reduced state of these proteins, but not in oxidized state. This spectral region is strongly influenced by the conformation of the heme. As pointed out by Hu et al.[25], the saddling or distortion of the macrocycle from planarity within the protein pocket results in the activation of out-of-plane modes. The richness of this spectral region can also be attributed to the interaction of the heme substituents with nearby protein residues. Bending modes of the thioether linkages and propionic side-chains are strongly enhanced in the wild-type protein. The hydrogen bonding network involving the internal water molecules, intra-cavity protein residues and propionyl group of the heme is critical to the overall conformation of the protein[28] and the intensity of the propionyl bending modes appears to reflect directly its global stability, at least in the reduced state. Oxidation of the mutant cytochromes to the ferric state abolishes most of the differences in the low-wavenumber region. This may reflect the fact that in the oxidized state the protein is in a more open conformation which is less sensitive to the changes in the heme-protein interactions caused by the mutations. Although the exact triggering mechanism leading to the structural changes that accompany oxidation is not known[1], it is clear from physical and chemical behavior of

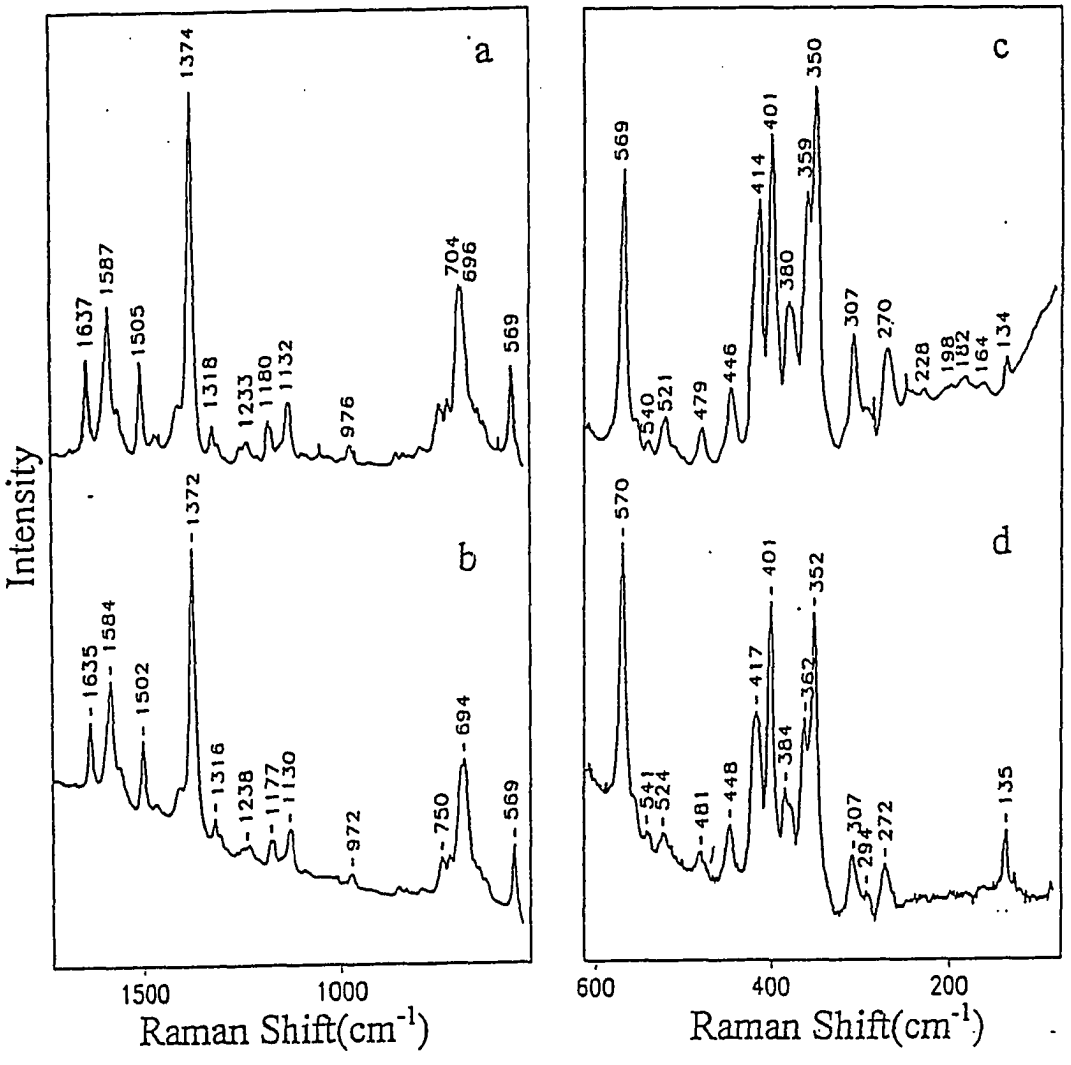

Figure 8. Resonance Raman spectra of 0.1 mM solution of oxidized cytochrome c: (a) and (c) wild type; (b) and (d) H26V mutant. Experimental conditions as in Fig. 3.

the two forms of the protein that the reduced form is more stable and in a more rigid conformation than the oxidized form[17,28]. Changes in the hydrogen bonding interactions within the cavity that accompany oxidation lead ultimately to a slight outward movement of the heme and more hydrophilic environment.

ACKNOWLEDGEMENT

The financial support of the National Institute of Health (GM35108) is gratefully acknowledged.

REFERENCES

1. G.R. Moore and G.W., Pettigrew, *Cytochromes*, Springer Verlag, New York (1990).
2. T. Takano and R.E. Dickerson, *J. Mol. Biol.* **153**, 79(1981).
3. E. Schechter and P. Saludjian, *Biopolymers* **5**, 790(1967).
4. Y.P. Meyer, *Methods Enzymol.* **54**, 1(1978).
5. T.G. Spiro and X.-Y. Li, in *Biological Applications of Raman Spectroscopy*, ed. T.G. Spiro, Vol 3, pp 217(1988).
6. (a) C.C. Moser, C.C. Page, R. Farid and P.L. Dutton, *J. Bioenerg. Biomembr.* **27**, 263(1995); (b) W.B. Curry, M.D. Grabe, I.V. Kurnikov, S.S. Skourtis, D.N. Beratan, J.J. Regan, A.J.A. Aquino, P. Beroza and J.N.J. Onuchic, *J. Bioenerg. Biomembr.* **27**, 285(1995).
7. (a) L. Ramdas, F. Sherman and B.T. Nall, *Biochemistry* **25**, 6952(1986); (b) L. Ramdas and B.T. Nall, *Biochemistry* **25**, 6959(1986).
8. H.-X. Zhou, *J. Am. Chem. Soc.* **16**, 10362(1994).

9. G.V. Louie, G.J. Pielak, M. Smith and G.D. Guillemette, C.M. Kay, M. Smith and A.G. Mauk, *Biochemistry* **27**, 7870(1988).

10. S.P. Rafferty, L.L. peace, P.D. Barker, J.G. Brayer, *Biochemistry* **29**, 9365(1990).

11. A.A. Raphael and H.B. Gray, *J. Am. Chem. Soc.* **13**, 1038(1991).

12. E. Margoliash, A. Schejter, T.I. Koshy, T.L. Luntz and E.A.E. Garber, in *Bioenergetics*, ed. C.H. Kim and T. Ozawa, pp 125, Plennum Press, New York(1990).

13. T.L. Luntz, A. Schejter, E.A.E. Garber and E. Margoliash, *Proc. Natl. Acad. Sci. USA* **86**, 3524(1989).

14. A. Schejter, T.L. Luntz, T.I. Koshy and E. Margoliash, *Biochemistry* **31**, 8336(1992).

15. A. Schejter, T.I. Koshy, T.L. Luntz, R. Sanishvili, I. Vig and E. Margoliash, *Biochem. J.* **302**, 95(1994).

16. A. Schejter and P. Geotge, *Biochemistry* **3**, 1045(1964).

17. E. Margoliash and A. Schejter, *Adv. Protin Chem.* **21**, 113(1966).

18. T.I. Koshy, T.L. Luntz, B. Plotkin, A. Schejter and E. Margoliash, *Biochim. J.* **299**, 347(1994).

19. W. Qin, R. Sanishvili, B. Plotkin, A. Schejter and E. Margoliash, *Biochim. Biophys. Acta* **1252**, 87(1995).

20. T.G. Spiro, in *Iron Porphyrins, Part II*, ed. A.B.P. Lever and H.B. Gray, pp 89, Addison Wesley, Reading, MA(1983).

21. P. Hildebrandt, G.J. Pielak and R.J.P. Williams, *Eur. J. Biochem.* **201**, 211(1991).

22. G. Smulevich, M.J. Bjerrum, H.B. Gray and T.G. Spiro, *Inorg. Chem.* **33**, 4629(1994).

23. W. Qin, Sanishvili, B. Plotkin, A. Schejter and E. Margoliash, *Biochim. Biophys. Acta* **1252**, 87(1995).

24. T. Koshy, T. Luntz, E.A.E. Garber and E. Margoliash, *Protein Express. Purif.* **3**, 441(1992).

25. S. Hu, I.K. Morris, J.P. Singh, K.M. Smith and T.G. Spiro, *J. Am. Chem. Soc.* **115**, 12446(1993).

26. X.-Y. Li, R.S. Czernuszewicz, J.R. Kincaid, P. Stein and T.G. Spiro, *J. Phys. Chem.* **94**, 47(1990).

27. A.M. Berghuis and G.D. Brayer, *J. Mol. Biol.* **223**, 959(1992).

28. A. Schejter, in *Cytochrome c, A Multidisciplinary Approach*, ed. R.E. Scott and A.G. Mauk, pp 335, University Science Press, Sausolito(1996)

CHAPTER 7

CIRCULAR DICHROISM AND RESONANCE RAMAN COMPARATIVE STUDIES OF WILD TYPE CYTOCHROME c AND F82H MUTANT

A paper accepted by to the *Biospectroscopy* in a special issue
in memory of Dr. Therese M. Cotton (#99-022)

Junwei Zheng, Shuyu Ye, Tianhong Lu, Therese M. Cotton, and George Chunanov

Abstract

The UV-visible, circular dichroism (CD) and resonance Raman (RR) spectra of the wild type yeast iso-1-cytochrome *c* (WT) and its mutant F82H in which Phe-82 was substituted with His were measured and compared for oxidized and reduced forms. The CD spectra in the Intrinsic and Soret spectral region as well as RR spectra in high, middle, and low frequencies regions are discussed. From the analysis of the spectra, it was determined that in the oxidized F82H the two axial ligands to the heme iron are His-18 and His-82 where as in the reduced form the sixth ligand switches from His-82 to Met-80 providing the coordination geometry similar to that of WT. Based on the spectroscopic data, it was also concluded that the porphyrin macrocycle is less distorted in the oxidized F82H as compared to the oxidized WT. Similar distortions are present in the reduced form of the proteins. Frequency shifts of Raman bands as well as the decrease of the α-helix content in the CD spectra indicate more open conformation of the protein around the heme.

Introduction

Mitochodrial cytochrome c is one of the most well characterized proteins because of its important physiological role as an electron carrier in various biological redox processes. Extensive studies of electron transfer properties were performed on naturally occurring and genetically engineered cytochrome c. The primary goal of these investigations was focused on the correlation of the protein structure with its function,[1,2] however, a complete understanding of the electron transfer mechanism is not yet available. The effect of different factors such as spin-state of the heme, axial ligands to the heme iron, protein environment surrounding heme on the electron transfer process remain under the question.[3,4]

Site-directed mutagenesis provides a powerful method for probing the effect of specific amino acid on the structure and function of proteins. Several c-type cytochrome mutants have been prepared. Yeast cytochrome c received a particular attention, because the structure of the wild type (WT) protein was determined in the crystal form and in the solution with high resolution by X-ray diffraction[5] and NMR.[6-9] This protein is also amenable to site-directed mutagenesis techniques. Phenylananine-82 (Phe-82), which is a phylogenetically conserved residue of mitochondrial cytochrome c and plays a critical role in the electron transfer process was the first residue changed using site-directed mutagenesis in c-type heme proteins.[10-13] Phenylalanine 82 was replaced with various amino acids, such as serine, tyrosine, leucine, isoleucine, alanine, glycine, etc..[10-15] One of the most interesting mutations in yeast cytochrome c is F82H - the substitution of Phe-82 by histidine (His). Using near-IR magnetic CD and NMR, it was demonstrated that in the oxidized mutant the histidine serves as the sixth coordination ligand to the iron instead of methoinine (Met) despite the fact that the latter amino acid is still present at the position 80.[16,17] This is unique example of the

change in the heme iron coordination structure achieved through site-directed mutagenesis, in which the original amino acid ligand is not removed.

Studies have shown that changes in axial ligation can largely influence electron transfer properties of cytochromes.[18-20] The replacement of Phe-82 by His in yeast cytochrome c provides unique opportunity for the study of these effects. In this paper, the UV/Vis, CD and RR spectra of WT and F82H in both oxidized and reduced forms are measured and compared in order to understand the effect of His on the structure and properties of the protein. Corresponding surface-enhanced Raman scattering and electrochemical studies will be published elsewhere.[21]

Experimental Section

Materials and Methods. WT and F82H were provided by Prof. Margoliash and were used as received. The preparation of the mutant was described previously.[22] Briefly, WT was firstly mutated by Ser codon to avoid disulfide dimerization of the mutant protein. This procedure did not change any optical and redox properties of WT.[17] F82H mutant was obtained by replacement of Phe-82 with His. All chemicals were reagent grade. The solutions for spectroscopic measurements contained 0.1 mM WT or F82H in the oxidized or reduced form in 0.025 M phosphate buffer (pH 7.0) and 0.5 mM KCl. Ferrocytochromes c were obtained by reduction with sodium dithionite.

Spectroscopic Measurements. The UV/Vis measurements were carried out using Perkin-Elmer UV/Vis spectrophotometer. The CD spectra between 200 and 500 nm were recorded at room temperature with Jasco 710 spectropolarimeter. Protein and Soret spectra were measured separately.

Raman measurements were performed using triple spectrometer (Spex Triplemate 1377) interfaced to a liquid nitrogen-cooled CCD detector (Princeton Instruments Model LN1152). Spectra were excited with 413.1 nm radiation from Kr^+ laser (Coherent, Innova 100). The power density did not exceed 100 mW/cm^2 at the samples. The scattered light was collected in a backscattering geometry. The total acquisition time was less than 2 min. All spectra were measured with ca. 2 cm^{-1} resolution at the excitation wavelength and calibrated relative to the Raman spectrum of indene.

Results and Discussion

UV/Vis and CD spectra. UV-visible spectra of the oxidized WT cytochrome c and F82H mutant in the wavelength region of 650-750 nm are shown in Figure 1. A band at 695 nm can be clearly observed in the spectrum of WT (curve a), while it completely disappeared in the spectrum of F82H (curve b). This band in oxidized heme proteins is due to the interaction of the heme ferric iron and the sixth coordination ligand, the thioether of Met-80. The band is assigned to the charge transfer from the Met-80 sulfur to the heme ferric iron and can be observed only when methionine sulfur is coordinated to the heme iron.[1,23] The disappearance of the 695 nm band in the spectrum of the oxidized F82H indicates the cleavage of the bond between Met-80 and heme iron in the mutant protein.

The intrinsic CD spectra of proteins (between 180 and 300 nm) can provide the information about the conformation of the backbone peptide chain. The intrinsic CD spectra of the oxidized WT and F82H proteins are almost identical (Figure 2). Two characteristic negative

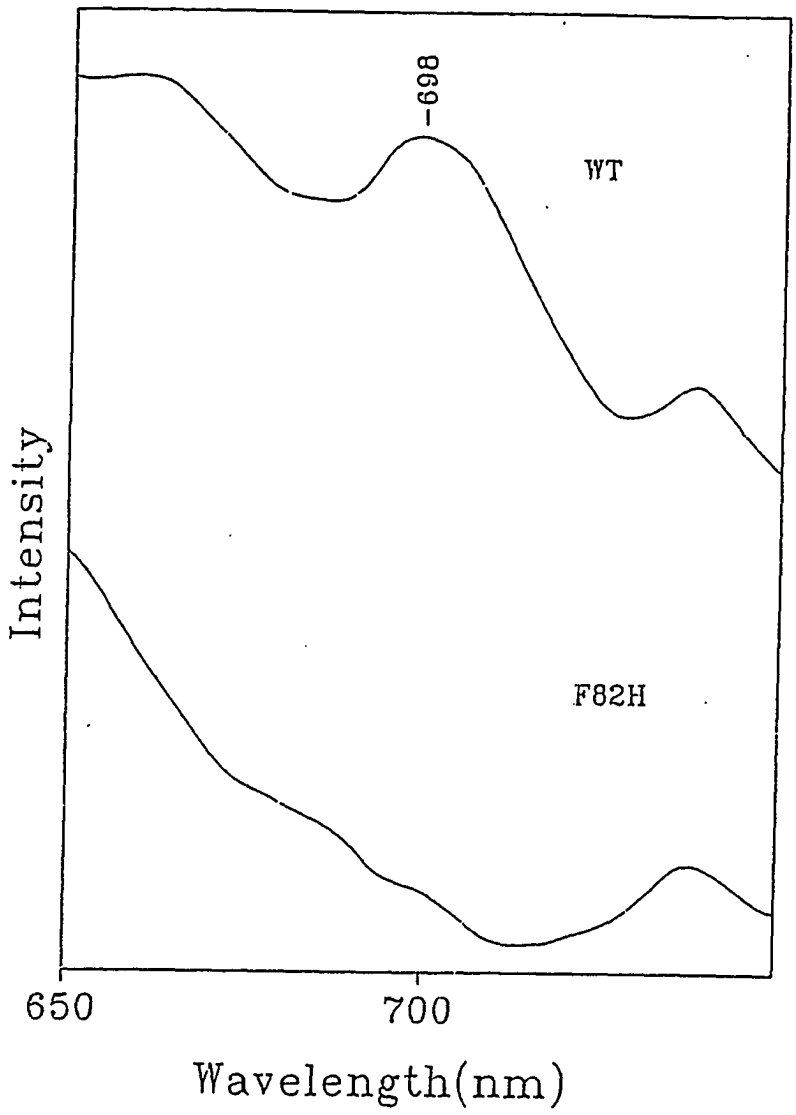

Figure 1. UV-visible absorption spectra of the oxidized (a) WT and (b) F82H. Concentrations of the proteins are 0.1mM.

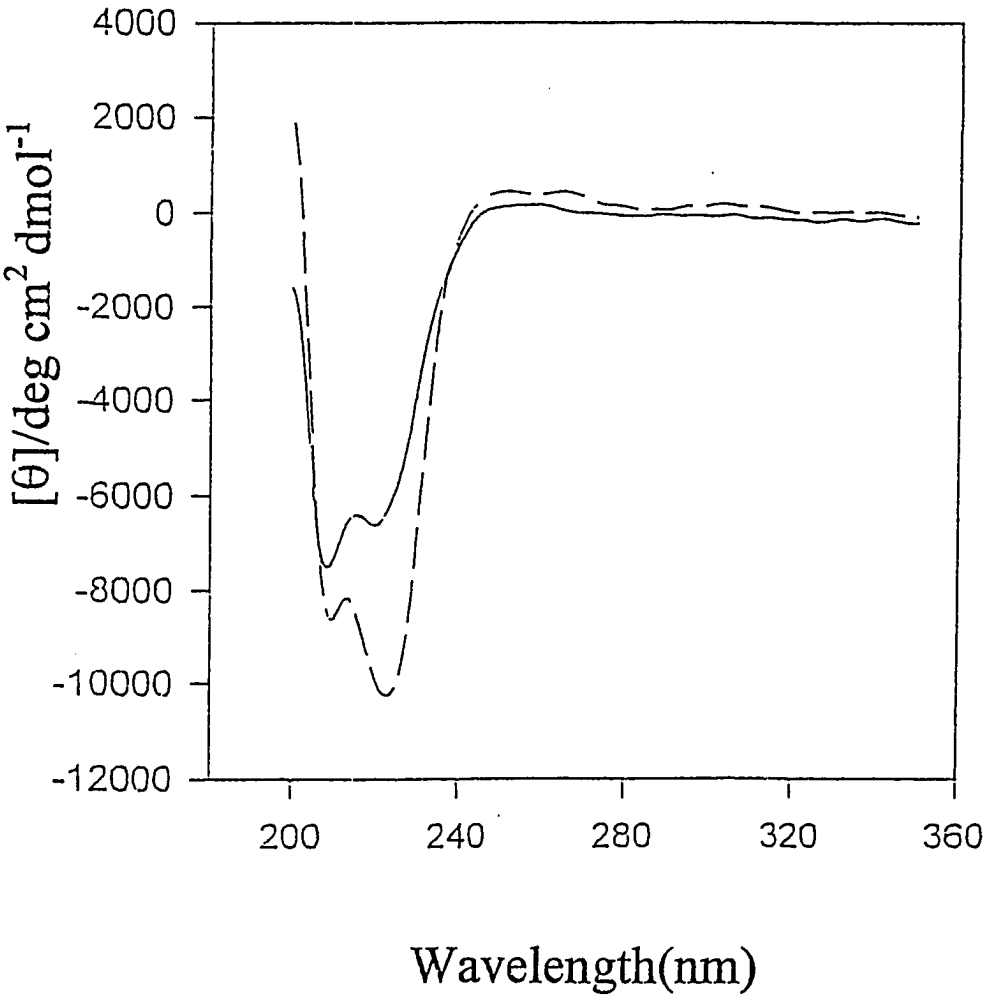

Figure 2. Intrinsic CD spectra of the oxidized (a) WT and (b) F82H.

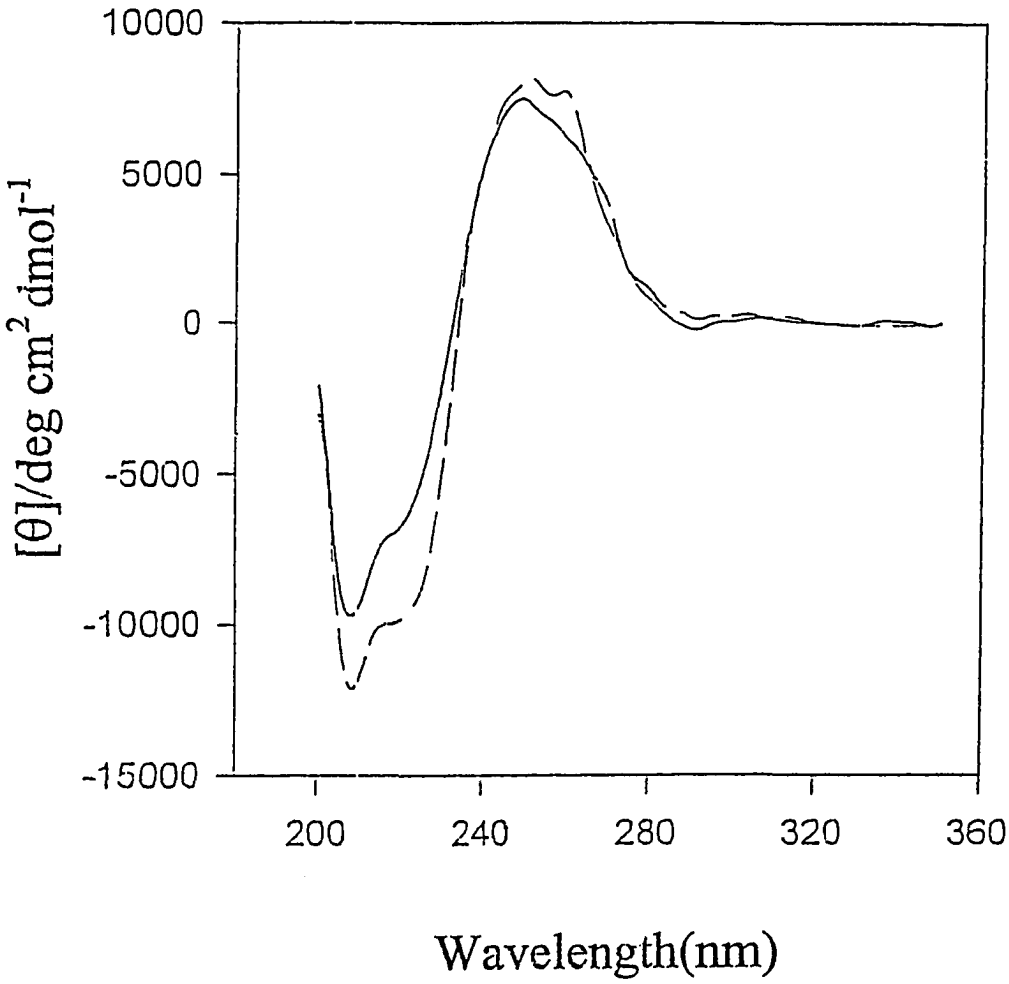

Figure 3. Intrinsic CD spectra of the reduced (a) WT and (b) F82H.

bands at 209 and 222 nm are associated with α-helical structure of the peptide backbone. [24] Differences between intrinsic CD spectra of WT cytochrome and F82H indicate that the replacement of Phe-82 with His slightly decrease the content of the α-helical structure in the mutant protein. Small change in the global structure of the protein upon the ligand substitution has also been confirmed by the fluorometric titration.[17]

The intrinsic CD spectra of the reduced WT and F82H are shown in Figure 3. With respect to 209 and 222 nm bands similar trend was observed in the reduced form. However, a new positive band at about 262 nm appeared in the spectra of the reduced WT and F82H (Figure 3) compared to the oxidized form of these proteins (Figure 2). This band resulted from the reduction of the heme group and was assigned to the reduced Met-80-S-Fe linkage in WT .[24] The band at 262 nm in CD spectrum of reduced F82H suggests the presence of the same linkage to the heme iron in this protein. This result is consistent with that obtained using NMR[17] and magnetically induced CD[16] techniques. It is difficult to ascertain in detail differences in the heme environment in WT cytochrome c and F82H mutant in both reduced and oxidized forms from the intrinsic CD spectra.

CD spectra measured in the Soret spectral region of the oxidized WT and F82H are shown in Figure 4. Both spectra have a positive band at 405 nm with well resolved shoulder at 365 nm. However, the spectrum of oxidized WT features a strong negative band at 417 nm (curve b) that is completely absent in that of F82H. Generally, the Soret CD spectra result from the interaction of the heme group with the protein environment. Hsu and Woody[25] suggested that the origin of the Soret Cotton effects in myoglobin and hemoglobin is a coupled oscillator interaction between the heme Soret transition and transitions in nearby aromatic amino acid residues. Pielak and his coworkers[11, 15] further suggested that the source of the negative Cotton

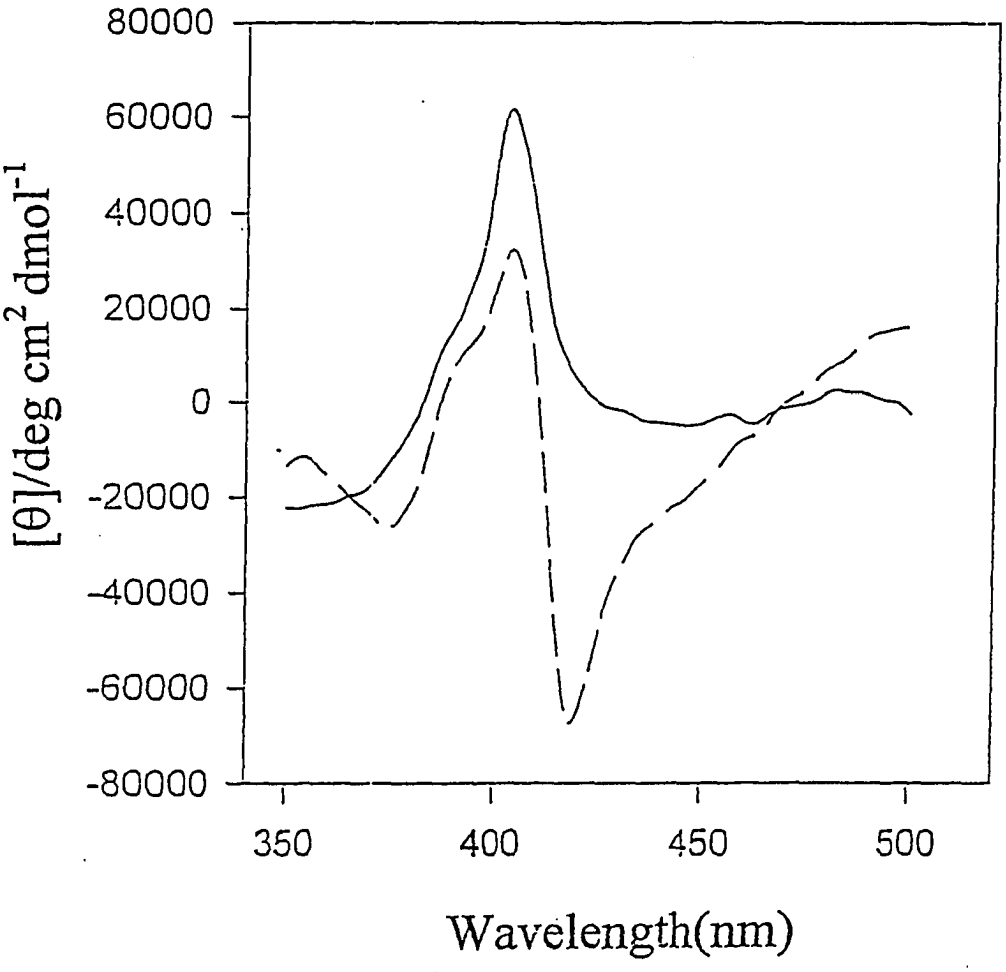

Figure 4. Soret CD spectra of the oxidized (a) WT and (b) F82H.

effect observed in the oxidized cytochrome c is the direct interaction of the π-π^* transition of the aromatic ring of Phe-82 with the π-π^* transition of the heme group. It appears that the presence of an aromatic residue at position 82 is essential for intense negative Cotton effect in Soret spectral region of the oxidized c-type cytochromes. When Phe-82 in S. cerevisiae iso-1-cytochrome c was replaced with aromatic tyrosine, the intense, negative Cotton effect was still observed in the Soret CD spectrum of the mutant.[11] On the other hand, the substitution of Phe-82 with serine and glycine in the same protein completely eliminated the negative feature in the CD spectrum.[15] In the current study, the replacement of Phe-82 with His resulted in total disappearance of the negative band in the Soret CD spectrum of the oxidized protein despite the fact that His is an aromatic residue. Explanation for this, at the first glance contradicting result, invokes unfavorable orientation of the aromatic residue and the porphyrin ring. For an efficient interaction and negative Cotton effect, π-π^* transitions in both systems should be parallel to each other. Disappearance of the negative band in the oxidized form of F82H indicates that the plane of His-82 was no longer parallel to the porphyrin plane. That, in turn, suggests that the histidine residue act as a sixth coordination ligand to the iron thereby adopting an orientation perpendicular to the porphyrin plane.

Contrary to the oxidized form, the Soret CD spectra of the reduced WT and F82H exhibit only minor differences indicating the similarity in the protein environment near the heme group (Figure 5). This similarity implies that in the reduced form both WT and mutant have the same coordination ligands. In particular, the sixth coordination ligand to the heme is Met-80 in these proteins. The analysis of the CD spectra in Soret spectral region clearly revealed the ligand switching process between the reduced and oxidized forms in F82H mutant.

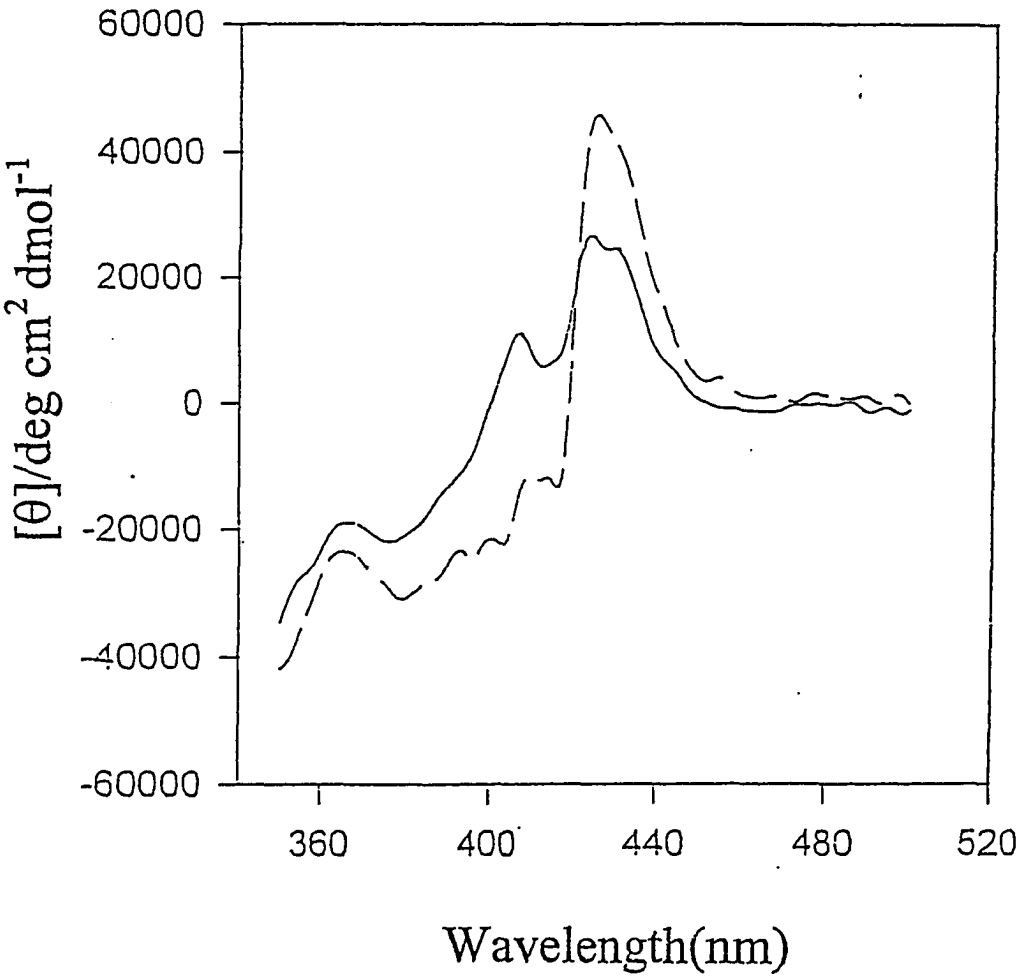

Figure 5. Soret CD spectra of the reduced (a) WT and (b) F82H.

RR spectra. Resonance Raman spectra of oxidized WT and F82H in high frequency region is shown in Figure 6. All band frequencies in the spectrum of WT (Figure 6, a) are in good agreement with those previously reported.[26] The oxidation state marker band, ν_4, is located at 1372 cm^{-1} and the coordination and spin state sensitive band, ν_3, appears at 1502 cm^{-1}, thereby assuring that the heme group in the oxidized WT is in the six-coordination, low-spin, oxidized state.[27] The RR spectrum of the oxidized F82H (Figure 6, b) is similar to that of the oxidized WT. Noted differences include, for example, high frequency shifts for ν_{10}, ν_2 (1584 cm^{-1} in WT), ν_4 and ν_3 of about 5, 5, 4, and 3 cm^{-1}, respectively, for F82H relative to WT. These bands correspond to the inner and outer ring stretching vibrations and are sensitive to oxidation and spin states of heme iron as well as to distortion of the macrocyclic ring.[28,29] Because the observed high frequency shifts are smaller than those expected from the change in oxidation and spin states, the former should be attributed to a decrease in the ring distortion. Indeed, ν_{10} band, which is particularly sensitive to the ring distortion, is shifted from 1635 cm^{-1} for WT to 1640 cm^{-1} for F82H, implying less distorted configuration in the mutant. The distortion of the porphyrin ring in WT results, among others, from the asymmetry of the axial ligands to the heme iron. It is reasonable to assume that the decrease in the distortion in the mutant is associated with His-82 being a sixth ligand that together with His-18 provide more symmetric ligation to the heme iron. These data are consistent with the results of the UV-visible and CD spectra demonstrating that the fifth and sixth ligands in the oxidized F82H are His-18 and His-82, while the oxidized WT has His-18 and Met-80 axial ligands. A similar phenomenon was also observed by Debois et al.[30] in their RR study of microperoxidase-8 complex with imidazole. The shift to high frequencies of the corresponding bands for $(Im)_2$-MP-8 was also attributed to the diminishing of the less

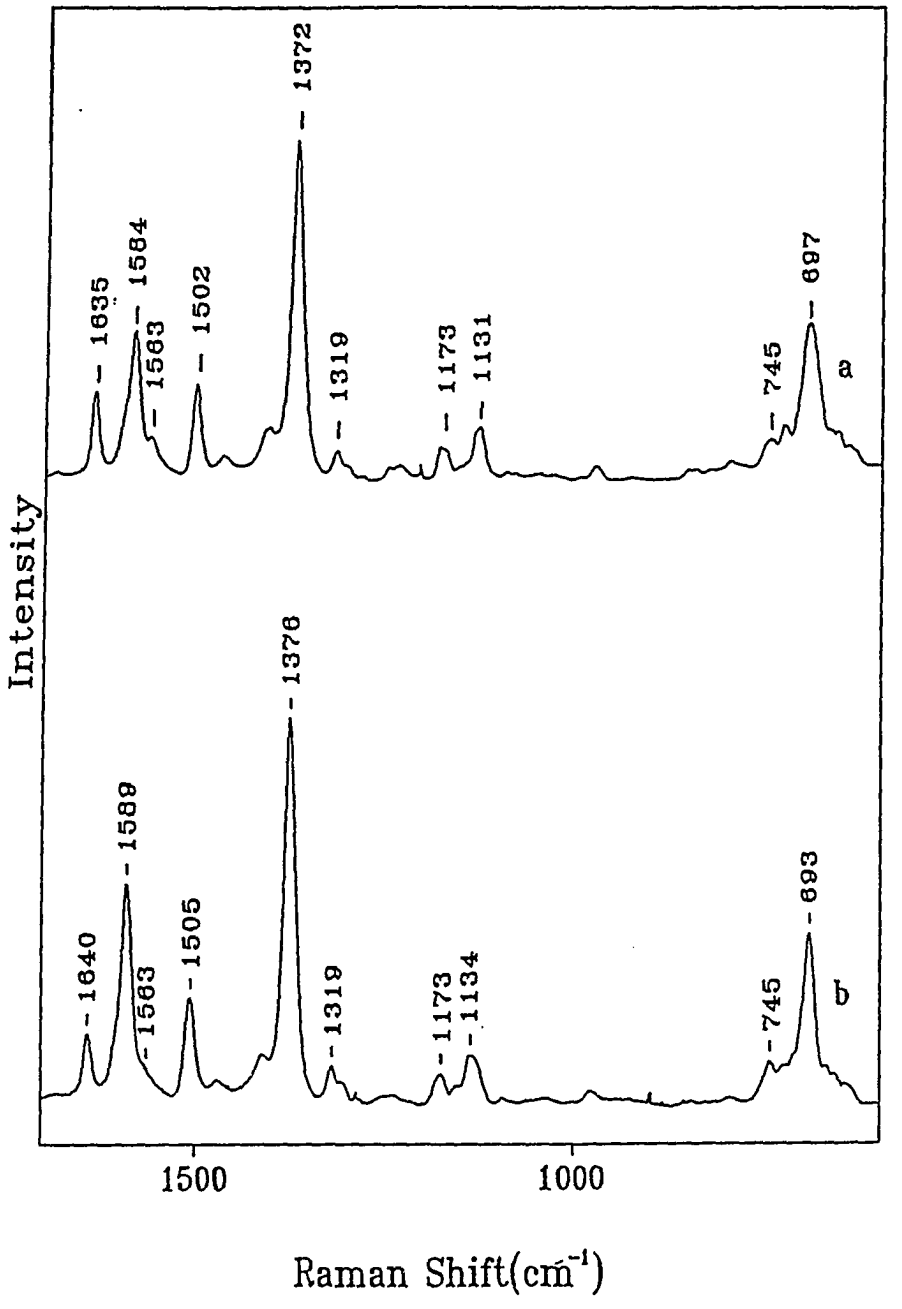

Figure 6. Resonance Raman spectra of the oxidized (a) WT and (b) F82H in the high frequency region.

distortion of the porphyrin ring due to the identical axial ligands.

The most prominent difference in middle spectral region includes the downshift of the $\nu(C_a\text{-}S)$ band from 697 cm^{-1} in the spectrum of the oxidized WT to 693 cm^{-1} in the spectrum of the oxidized F82H. It is known that the frequency of C-S stretch is sensitive to the conformation of $C_\beta\text{-}C_\alpha$ bond.[31] However, a shift of 4 cm^{-1} observed in the spectra is much smaller than that expected for trans/gauche transition thereby indicating only minor conformational difference around (C_a-S) band in WT and mutant.

Raman spectra of the oxidized WT and F82H in low frequency region contain many well-pronounced features (Figure 7). The bands are mainly due to out-of-plane vibrations of the porphyrin ring substituents that are particularly enhanced when heme macrocycle is distorted from its planner configuration. Bands due to the iron-axial ligand stretching are not expected, because these modes do not gain sufficient enhancement [26]. Indeed, the same bands (although of different intensities) are present in the spectra of two proteins; no appearance of new bands or disappearance of existing bands can be reliably associated with the ligand switching process resulted from the mutation. However, several bands underwent frequency shifts after the mutation. For example, $\delta(C_\beta C_c C_d)$ of the propionate and $\delta(C_\beta C_a S)$ of the thioether upshifted from 382 to 385 cm^{-1} and from 397 to 404 cm^{-1}, respectively. At the same time, ν_8 and ν_9 bands that represent the combinations of the Fe-N(pyrrole) stretching and pyrrole substituent bending downshifted from 351 to 347 cm^{-1} and from 279 to 273 cm^{-1}, respectively.

Because the propionates and thioethers are directly involved in the binding of the heme to the protein, their frequency differences in RR spectra of two proteins most likely

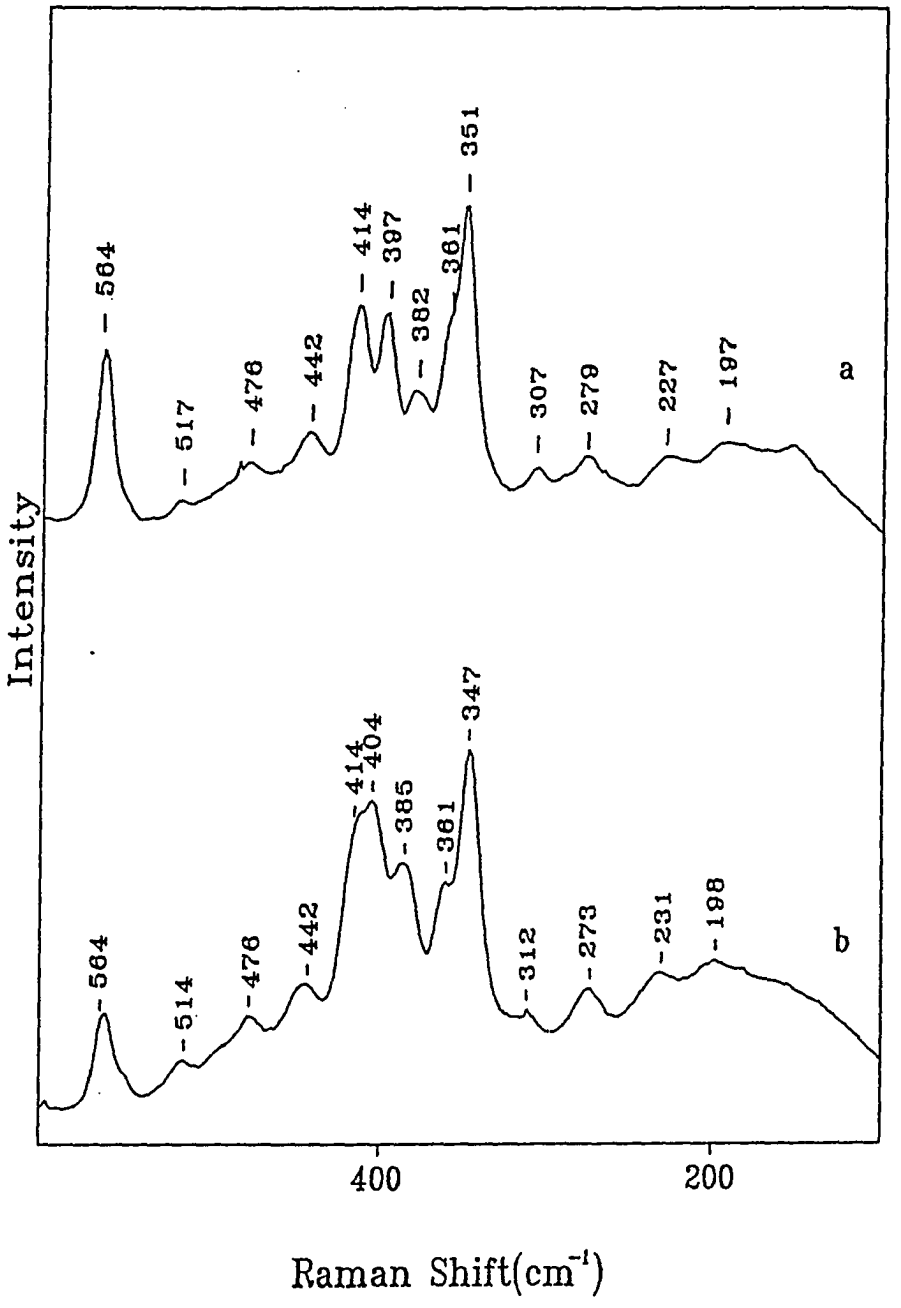

Figure 7. Resonance Raman spectra of the oxidized (a) WT and (b) F82H in the low frequency region.

reflect changes in the protein environment around the heme. For propionates, the corresponding Raman frequency is also affected by the polarity of the heme pocket or by the exposure of the heme to the solvent. It is known that the protein structure of WT in the oxidized form is more opened than that in the reduced form. Consequently, $\delta(C_\beta C_c C_d)$ is upshifted for the oxidized form. Using the same argument, one can assume that the protein structure of F82H in the oxidized form is more opened than that of WT, because $\delta(C_\beta C_c C_d)$ frequency appeared upshifted after the mutation. Indeed, Phe-82 in WT controls the exposure of the heme to solvent via small changes in its local conformation. The replacement of this residue with His that coordinates to the heme iron in the F82H removes the control mechanism making the heme pocket more opened to solvent and affecting the hydrogen bonding of the propionic group to the protein. Another argument for more open structure of F82H in the oxidized form can be retrieved from the following observation. Splitting of the bands in the low frequency Raman spectrum of F82H appeared less pronounced than that in the spectrum of WT due to the overlap of bands that are broader in the mutant as compared to WT. This trend can be observed for both oxidized and reduced forms of the proteins. From RR studies of cytochrome *c*, it was concluded that broader bands in the oxidized form reflect more open structure of the heme pocket[32]. Likewise, broader bands observed in the RR spectrum of F82H also suggest more opened structure of the heme pocket in this protein. Frequency shifts of ν_8 and ν_9 in the RR spectrum of F82H most likely reflect a change in the Fe-N(pyrrole) bond and/or a conformation change of pyrrole substituents due to the different axial coordination strength to Fe(III) resulted from the mutation.

Resonance Raman frequencies for oxidized forms of WT and F82H are summarized in Table 1. For comparison, literature data for WT[26] and data for the complex of microperoxidase-8 with imidazole (MP-8-ImH)[30] are also provided. Band assignments are given according to the literature.[26]

Resonance Raman spectra of WT and F82H in the reduced form are shown Figure 8 and Figure 9 for the different frequency regions. It is evident that the RR spectra of F82H and WT are almost identical in the high frequency region (Figure 8). Frequency shifts for ν_{10}, ν_2, ν_4 and ν_3 are much smaller than those for the oxidized form and are well within calibration uncertainty. This result is expected because the high frequency region in RR spectra represents vibrations of the heme itself, conformation of which is very similar in reduced WT and F82H due to the identity of axial heme ligands in both proteins. Some minor differences between the RR spectra of F82H and WT can be observed in the middle and low frequency regions. These include small shifts from 690 to 688 cm^{-1} for $\nu(C_a\text{-}S)$ (Figure 10), from 399 to 401 cm^{-1} and from 380 to 382 cm^{-1} for $\delta(C_\beta C_a S)$ and $\delta(C_\beta C_c C_d)$, respectively (Figure 9). These frequency differences reflect changes in the protein environment of heme group. Even though two ligands for the heme iron are the same in both WT and F82H proteins, the mutation still affects the interaction of the heme substituents with the protein, as discussed above. Resonance Raman frequencies and band assignments for the reduced WT and F82H and data for MP-8-ImH[30] and cytochrome c[26] are summarized in Table 2.

Table I. A Comparison of RR Modes (cm^{-1}) of Oxidized WT, F82H, MP-8-ImH Complex and Cyt c

Modes[a]	WT	F82H	MP-8-ImH[b]	Cyt c[a]
ν_{10}	1635	1640	1637	1635
ν_2	1584	1589	1588	1586
ν_{11}	1563	1563	1569	1561
ν_3	1502	1505	1503	1501
ν_{29}	1408	1409	1407	1407
ν_4	1372	1376	1375	1371
ν_{21}	1319	1319	1316	1316
$\nu(C_a\text{-}S)$	697	693	----	701
γ_{22}	442	442	445	442
$\delta(C_\beta C_a S)$	397	404	404	397
$\delta(C_\beta C_c C_d)$	382	385	385	380
ν_{50}	361	361	362	359
ν_8	351	347	347	349
ν_{51}	307	312	318	304
ν_9	279	273	271	272
γ_{24}	227	231	225	226

[a]From Ref. 26. [b]From Ref. 30.

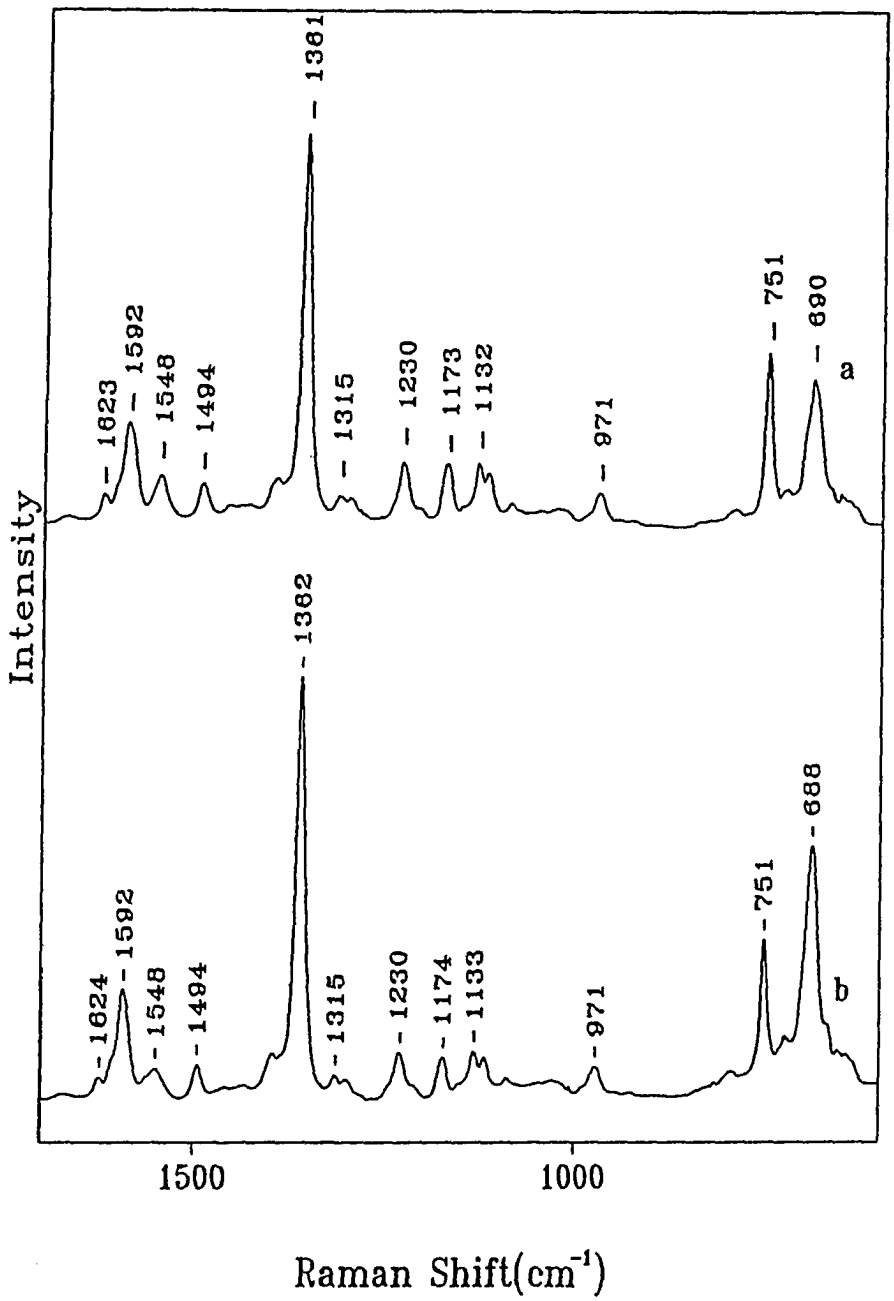

Figure 8. Resonance Raman spectra of the reduced (a) WT and (b) F82H in the high frequency region.

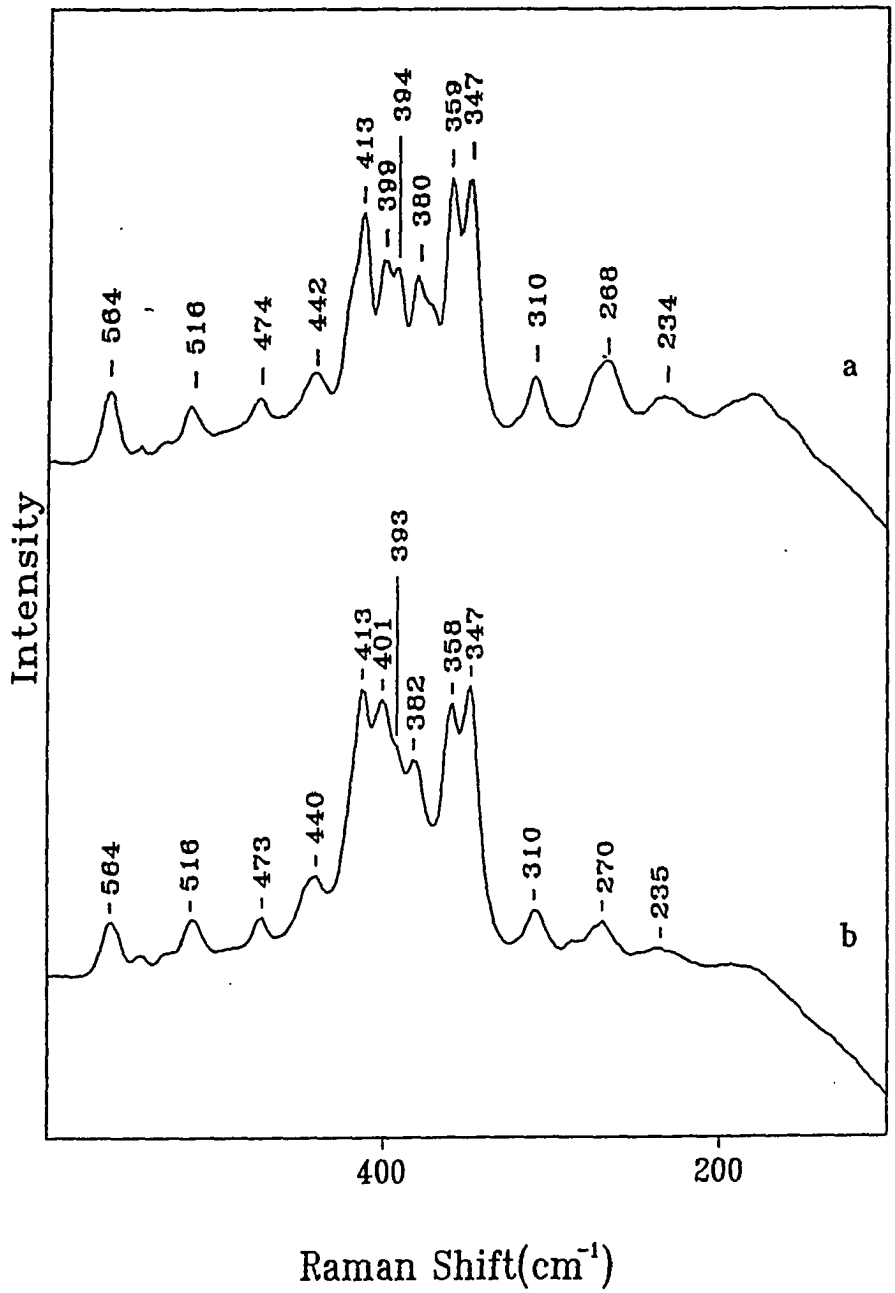

Figure 9. Resonance Raman spectra of the reduced (a) WT and (b) F82H in the low frequency region.

Table II. A Comparison of RR Modes (cm^{-1}) of Reduced WT, F82H, MP-8-ImH Complex and Cyt c

Modes[a]	WT	F82H	MP-8-ImH[b]	Cyt c[a]
ν_{10}	1623	1624	1617	1626
ν_2	1592	1592	1592	1596
ν_{11}	1548	1548	1539	1551
ν_3	1494	1494	1494	1496
ν_{29}	1397	1398	1396	1403
ν_4	1361	1362	1358	1364
ν_{21}	1315	1315	1313	1314
$\nu(C_a\text{-}S)$	690	688	----	692
γ_{22}	442	440	446	442
$\delta(C_\beta C_a S)$	399	401	404	401
$\delta(C_\beta C_c C_d)$	380	382	381	382
ν_{50}	359	358	362	359
ν_8	347	347	345	347
ν_{51}	310	310	314	309
ν_9	268	270	267	271

[a]From Ref. 26. [b]From Ref. 30.

Conclusions

Comparative studies using UV/Vis, CD and RR spectroscopies of wild type yeast iso-1-cytochrome *c* and its mutant F82H in which Phe-82 is replaced with His revealed the ligand switching process between the reduced and oxidized forms of the mutant protein. In the oxidized F82H two ligands are His-18 and His-82, where as in the reduced form the sixth ligand switches to the Met-80 producing the coordination geometry similar to that of WT. Both CD and RR data suggest more open structure of the mutant compared to that of the wild type in oxidized and reduced forms. Analysis of Raman spectra reveal less distorted porphyrin macrocycle in the oxidized F82H due to the larger symmetry of the axial ligands to the heme iron.

Acknowledgement

The work was supported by National Institutes of Health (GM35108). The authors thank Dr. Kostic for the assistance in CD measurements.

References

1. G. R.Moore, G. W. Pettigrew, Ed. *Cytochrome c, Evolutionary Structural and phylological Aspects*, Springer-Verlay, Berlin, 1990.
2. J. R. Winkler, H. B Gray, "Electron transfer in ruthenium-modified proteins," *Chem. Rev.* **1992**, 92, 369-379.
3. F. S. Mathews, "The structure, function and evolution of cytochrome c," *Prog. Biophys. Mol. Biol.* 45, 1-56(1985).

4. S.K. Chapman, S. Daff, and A.W. Munro, "Heme: the most versatile redox center in biology," *Structure Bonding* **88**, 40-72(1997).

5. A. M.Berghuis, G. D. Brager, "Oxidation-state dependent conformational changes in cytochrome *c*," *J. Mol. Biol.* **223**, 959-976(1992).

6. G. J. Pielak, R. A. Atkinson, J. Boyd, R. J. P. Williams, "Two-dimensional NMR as a probe of structural similarity applied to mutants of cytochrome *c*," *Eur. J. Biochem.* **177**, 179-185(1988).

7. G. J. Pielak, J. Boyd, G. R. Moore, R. J. P. Williams, "Proton-NMR studies show that the Thr-102 mutant of yeast iso-1-cytochrome c is a member of the eukaryotic cytochrome c family," *Eur. J. Biochem.* **177**, 167-177(1988).

8. Y. Gao, J. Boyd, R. J. P. Williams, G. J. Pielak, "Assignment of proton resonances identification of secondary structural elements, and analysis of backbone chemical shifts for the C102T variant of yeast iso-1-cytochrmome *c* and horse cytochrome *c*," *Biochemistry* **29**, 6994-7003(1990).

9. Y. Gao, J. Boyd, G. J. Pielak, R. J. P. Williams, Comparison of reduced and oxidized yeast iso-1-cytochrome c using proton paramagentic shifts," *Biochemistry* **30**, 1928-1934(1991).

10. N. Liang, A. G. Mauk, G. J. Pielak, J. A. Johson, M. Smith, B. M. Hoffman, "Regulation of interprotein electron transfer by residue 82 of yeast cytochrome *c*," *Sciences* **240**, 311-313(1988).

11. S. P. Rafferty, L. L. Pearce, P. D. Barker, J. G. Guillemette, C. M. Kay, M. Smith, A. G. Mauk, "Electrochemical, kinetic, and circular dichroic consequences of mutations at position 82 of yeast iso-1-cytochrome *c*," *Biochemistry* **29**, 9365-9369(1990).

12. N. Liang, G. J. Pielak, A. G. Mauk, M. Smith, B. M. Hoffman, "Yeast cytochrome c with phenylalanine or tyrosine at position 87 transfers electrons to zinc cytochrome c peroxidase at a rate ten thousand times that of the serine-87 or glycine-87 variants," *Proc. Natl. Acad. Sci., U.S.A.* **84**, 1249-1252(1987).

13. G. J. Pielak, A. G. Mauk, and M. Smith, "Site-directed mutagenesis of cytochrome c shows that an invariant Phe is not essential for function," *Nature* **313**, 152-154(1985).

14. G. V. Louie, G. J. Pielak, M. Smith, and G. D. Brayer, "Role of phenylalanine-82 in yeast iso-1-cytochrome c and remote conformational changes induced by a serine residue at this position," *Biochemistry* **27**, 7870-7876(1988).

15. G. J. Pielak, K. Oikawa, A. G. Mauk, M. Smith, and C. M. Kay, "Elimination of the negative Soret Cotton effect of cytochrome *c* by replacement of the invariant phenylalanine using site-directed mutagenesis," *J. Am. Chem. Soc.* **108**, 2724-2727(1986).

16. B. K. Hawkins, S. Hilgen-Willis, G. J. Pielak, and J. H. Dawson, "Novel axial ligand interchange in cytochrome c: incorporation of a histidine at position 82 leads to displacement of the wild-type methionine-80 ligand," *J. Am. Chem. Soc.* **116**, 3111-3112(1994).

17. A. Schejter, G. Taler, G. Navon, X. Liu, and E. Margoliash, "Oxidation state-induced change of iron ligand in the phenylalanine-82 to histidine mutant of yeast iso-1-cytochrome *c*," *J. Am. Chem. Soc.* **118**, 477-478(1996).

18. A. G. Mauk, "Electron transfer in genetically engineered proteins. The cytochrome *c* paradigm," *Structure Bonding* **75**, 132-157(1991).

19. A. L. Raphael, and H. B. Gray, "Semisynthesis of axial-ligand (position 80) mutants of cytochrome c," *J. Am. Chem. Soc.* **113**, 1038-1040(1991).

20. G. Liu, W. Shao, S. Zhu, and W. Tang, "Effects of axial ligand replacement on the redox potential of cytochrome *c*," *J. Inorg. Biochem.* **60**, 123-131(1995).

21. J. Zheng, T. Lu, G. Chunanov, E. Margoliash, T. M. Cotton, "Study of the stability and redox properties of yeast cytochrome c mutant F82H using Surface-enhanced resonance Raman scattering and electrochemical techniques," to be submitted to *Bioelectrochem. Bioenerg.*

22. T.I. Koshy, T.L. Luntz, E.A.E. Garber, E. Margoliash, *Protein Express. Purif.* **1992**, 38, 441.

23. A. Schejter, B. Plotkin, "The binding characteristics of the cytochrome *c* iron," *Biochem. J.* **1988**, 255, 353-356.

24. Y. P. Myer, A. Pande, "Circular dichroism studies of hemoproteins and heme models," in *he Porphyrins, Vol III, Physical Chemistry, Part A.*, ed. by D. Dolphin, Academic Press, New York, 1978, pp. 271-322.

25. M. C. Hsu, R. W. Woody, "The origin of the heme Cotton effects in myoglobin and hemoglobin," *J. Am. Chem. Soc.* **93**, 3515-3525(1971).

26. S. Hu, I. K. Morris, J. P. Singh, K. M. Smith, and T. G. Spiro, "Complete assignment of cytochrome c resonance Raman spectra via enzymatic reconstitution with isotopically labeled hemes," *J. Am. Chem. Soc.* **115**, 12446-12458(1993).

27. H. D. Bist, Ed. *Raman Spectroscopy: Sixty Years on Vibrational Spectra and Structure*, Elsevier Science, Netherlands, 1989.

28. B. Carttling, "cytochrome *c*," in *Biological Applications of Raman Spectroscopy*, ed. by T. G. Spiro, John Wiley & Sons, Inc., New York, 1988, pp.217-248.

29. C. Zhou, J. Zheng, A. Schejter, W. Qin, E. Margoliash, and T.M. Cotton, "Resonance Raman study of cytochrome *c* water mutants," *J. Raman Spectrosc.* **29**, 955-962(1998).

30. S. Othman, A. Le Lirzin, and A. Desbois, "Resonance Raman investigation of imidazole and imidazolate complexes of microperoxidase: characterization of the bis(histidine) axial ligation in c-type cytochromes," *Biochemistry* **33**, 15437-15448(1994).

31. Ohsaku, M., "Molecular vibrations and force fields of alkyl sulfides. XI. C-S stretching vibrations of some simple aliphetic sulfides," *Bull. Chem. Soc. Jpn.* **48**, 707-708(1975).

32. P. Hildebrandt, T. Heimberg, D. Marsh, and G. L. Powell, "Conformational changes in cytochrome c and cytochrome oxidase upon complex formation: a resonance Raman study," *Biochemistry* **29**, 1661(1990).

CHAPTER 8

STUDY ON THE STABILITY AND REDOX PROPERTIES OF YEAST ISO-1-CYTOCHROME c MUTANT F82H BY ELECTROCHEMICAL AND SURFACE-ENHANCED RRESONANCE RAMAN SCATTERING TECHNIQUES

A paper submitted to the *Bioelectrochemistry and Bioenergies*

Junwei Zheng, Tianhong Lu, Therese M. Cotton and George Chumanov

Abstract

The electrochemistry and surface enhanced resonance Raman scattering (SERRS) spectra of the yeast iso-1-cytochrome c (WT) mutant with histidine (His) substituting for phenylananine-82 (Phe-82) was studied at the 11-mercaptoundecanoic acid (MUA) modified electrodes. The results indicate that the redox reactions of the mutant shifted to much more negative potentials than that of WT. The mutant adsorbed on the MUA modified roughened silver electrode surface shows higher stability respect to the photoinduced reduction of the proteins. It is demonstrated that His-82 replacing methionine-80 (Met-80) as the sixth ligand stabilized the oxidized form of the mutant, resulting in the negative shift of the reduction potential. The oxidation of the protein also occurred at more negative potential than that of WT, even though Met-80 recoordinated to heme iron in the reduced form. A mechanism was proposed for the ligand switching process in the redox reactions.

Introduction

Homogeneous and heterogeneous electron transfer processes associated with the c-type cytochromes have been widely studied because such studies can yield important information not only about thermodynamic, kinetic and structural properties of the proteins, but also provide novel insights into the electron transfer mechanism of the proteins in vivo[1-3]. The electron transfer processes of the proteins are affected by various factors, such as the charges on the protein, the spin-state of the heme iron and the distance between the prosthetic groups, the axial ligation of the heme group[4-7]. Many efforts have been devoted to understand the electron transfer mechanism of c-type cytochromes, especially cytochrome c[8-11].

The emergency of molecular genetic techniques provided an opportunity to study a variety of spectroscopic properties on the structure basis and the correlation between the electron transfer and structure of the protein in such a designed way that the structure of the proteins can be specifically modified. The first attempt to clone and sequence structural genes for metalloproteins was reported by Hall and Smith[12,13]. With the development of oligodeoxyribonucleotide-directed site specific mutagenesis[14,15], three mutants of yeast iso-1-cytochrome c with tyrosine, serine and glycine substituting for Phe-82 were first prepared and expressed by Pielak et al.[16]. Thereafter, yeast iso-1- cytochrome c has become a paradigm for exploring the factors that affect the electron transfer properties of this protein. The replacement of phenylananine-82 with other amino acids is of particular interesting, due to the critical role of this amino acid residue on regulation of the electron transfer properties of cytochrome c[17-20]. It has been substituted by various amino acids, such as serine, tyrosine, leucine, isoleucine, alanine, glycine and histidine etc.[16-24]. The relationship between the

electron transfer property and the substituting residues has been studied by several groups. For example, Liang et al.[17] demonstrated that when iso-1-cytochrome c has been mutated with amino acids to replace Phe-82, the interprotein electron transfer rate of the mutants with aliphatic residues was found to be ~10^4 slower than that of the mutants with aromatic residues. Mauk et al.[18] reported that the replacement of Phe-82 with other amino acids, such as tyrosine, leucine, isoleucine, alanine, serine and glutamate, lowered the reduction potential less than 43 mV, which depends on the size of the replacing residues. On other hand, Zhou[25] applied a continuum model to calculate the effect of point mutations and complex formation on the reduction potentials of yeast iso-1-cytochrome c and yeast cytochrome c peroxidase. In the calculation the effects of the charge and polarity of a surface residue, the polarity of an interior residue, and the size of a residue that controls the exposure of heme to the solvent, were considered.

Although little attention has been directed at purbation of the heme iron ligands in cytochrome c through site directed mutagenesis, the importance of the mutations that directly affect the coordination environment of the central metal has also been recognized. Such mutants offer an opportunity for perturbing the ligand binding properties of the active site in a controlled manner and directly modifying the kinetics and thermodynamics of the electron transfer properties of the protein. Sorrell et al.[26] studied the effect of the replacement of His-18 with Arg residue in yeast iso-2-cytochrome c on the cyclic voltammetric behavior. A less reactive of the mutant on electrode surface demonstrated higher reorganization energy and lower electron transfer rate for the mutant in which the coordination of Arg-18 to the heme is limited. Raphael and Gray[27] used chemical semisynthesis method to substitute Met-80 with

cysteine in cytochrome c and found that the reduction potential of the mutant was 600 mV more negative than that of native protein.

Recently, Morgoliash et al. reported one of the most interesting mutations, in which Phe-82 is substituted by His. The interesting feature of the mutant is that in oxidized protein, His-82 can replace Met-80 as the sixth coordination ligand of the heme group even though Met is still at the position 80[23,24,28]. It is a unique example of a change in the heme iron coordination structure achieved through site-directed mutagenesis, in which the original amino acid ligand coexists. In our previous paper, the UV-visible, circular dichroism and resonance Raman spectra of yeast iso-1-cytochrome c (WT) and its mutant with His substituting for Phe-82 (F82H) were studied in order to elucidate the effect of the replacement of Phe-82 with His on the change in the structure of the oxidized and reduced protein[28]. In this paper, the attention was mainly focused on the effect of this mutation on the stability and redox properties of the protein using surface-enhanced resonance Raman scattering and electrochemical techniques.

Experimental

Materials. WT and F82H were obtained from Dr. Margoliash's group. WT was firstly mutated by Serine Instead of cysteine-102 to avoid disulfide dimerization of the mutant protein. This procedure did not change any optical and redox properties of WT.[24] Then, F82H was obtained by replacement of Phe-82 with His. The preparation procedures were described previously.[29] All other chemicals were reagent grade.

Apparatus and methods. A BAS 100 electrochemical analyzer and a conventional three-electrode electrochemical cell were used for the electrochemical measurements. A Pt wire

was used as the auxiliary electrode. A saturated calomel electrode (SCE) served as the reference electrode and all the potentials reported here were respected to the SCE. In order to prevent cytochrome c from denature in the case of direct contact with metal electrode surface, the working electrode used in this work is the MUA-modified gold electrode for the electrochemical measurements or the MUA-modified roughened silver electrode for the spectroscopic measurements.

The working electrode was constructed from a silver or gold rod, which was sealed into glass tubing with Torr Seal (Varian). The electrode was sequentially polished with 5, 0.3 and 0.05 um alumina/water slurries until a shiny, mirrorlike finish was obtained. It was then sonicated in milipore water twice and washed thoroughly with milipore water. The roughened silver electrode was prepared as follows. The polished silver electrode was roughened in 0.1 M Na_2SO_4 solution by an oxidation reduction cycle (ORC). This consisted of a double potential step from -0.5 to 0.6 V, where 250 uC charge was allowed to pass. Then, the electrode potential was stepped back to -0.5 V to reduce the silver ions. In order to prepare the MUA-modified electrode, the polished gold electrode or the roughened silver electrode was dipped in the 1.0 mM MUA methanol solution for at least 10 h, followed by rinsing with methanol and water.

After the MUA-modified gold or roughened silver electrode was prepared, the protein adsorption process was carried out by dipping the electrode in the 0.1 mM F82H + 0.025 M phosphate buffer (pH 7.0) + 0.05 M KCl solution for 1 h. Then, the electrode was placed in electrochemical cell with 0.025 M phosphate buffer (pH 7.0) + 0.05 M Na_2SO_4 solution for the electrochemical or spectroscopic measurements. The solutions were purged with nitrogen for 30 min prior the measurements to remove the oxygen in the solution.

The Raman instrument included a spectrograph (Spex Triplemate 1377) interfaced to a liquid nitrogen-cooled CCD detector (Princeton Instruments Model LN1152) and an Innova 100-k3 krypton ion laser as an excitation source. The SERRS spectra were obtained by excitation with 413 nm radiation. The laser power used was about 1 mW at the samples. The total acquisition time was less than 2 min. The resolution of the Raman instrument was ca. 2 cm^{-1} at the excitation wavelength used here. The scattered light was collected in a backscattering geometry. The Raman spectra were calibrated with indene.

Results

Cyclic voltammogram (CV) of F82H adsorbed at the MUA-modified gold electrode is shown in Figure 1. A well-defined pair of redox peaks was observed in the potential range between -0.1 and -0.7 V. The peaks are due to the reduction and oxidation of F82H adsorbed on the electrode surface. The cathodic peak current is almost equal to the anodic peak current. The cathodic and anodic peaks are located at -0.51 and -0.39 V, respectively. These potentials are much more negative than that for WT reported under the similar conditions by Bowden et al..[30,31]

The CVs of F82H adsorbed on the surface of the MUA-modified roughened silver electrode at different scan rates are shown in Figure 2. The reduction peak potential shifted to the negative direction and the oxidation peak potential shifted to positive direction as the scan rate increased from 20 to 500 mV/s. The cathodic peak current is almost equal to the anodic peak current for the different scan rates. However, a linear correlation between the peak currents and scan rates as expected for the surface defined species was not obtained in the scan rate range used here.

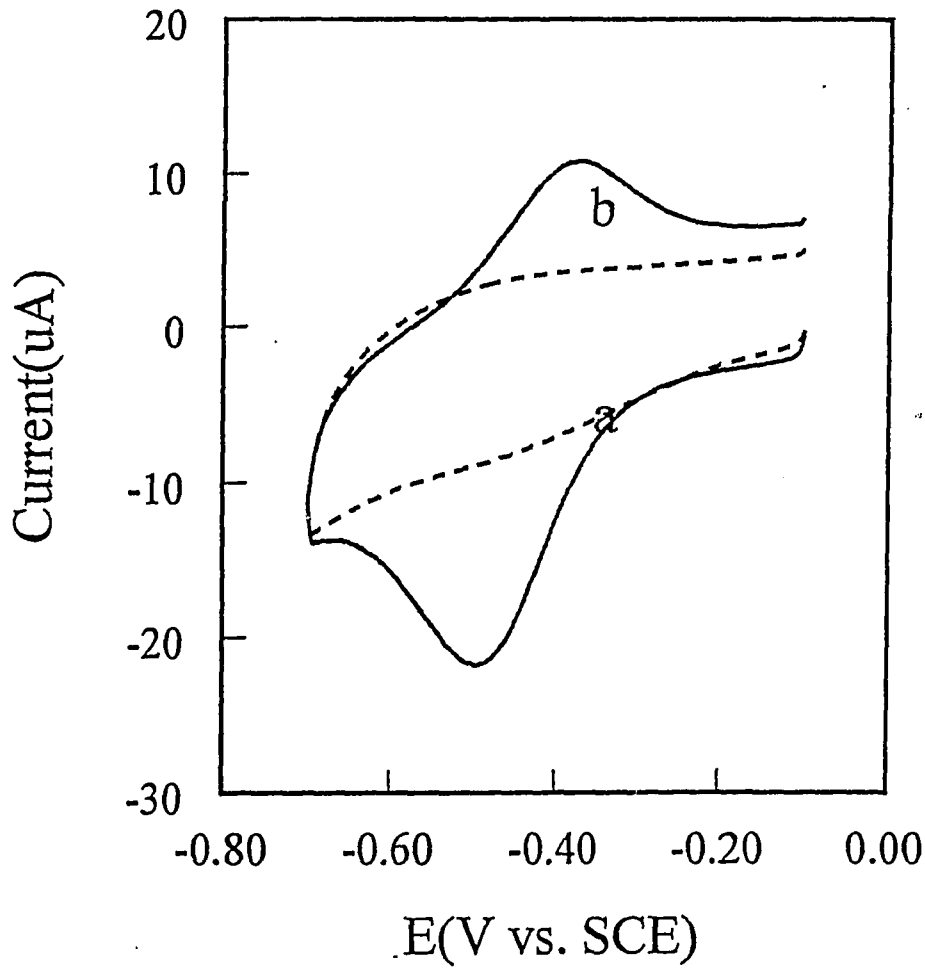

Figure 1. Cyclic voltammogram of F82H adsorbed on the MUA-modified gold electrode. The scan rate: 100 mV s^{-1}.

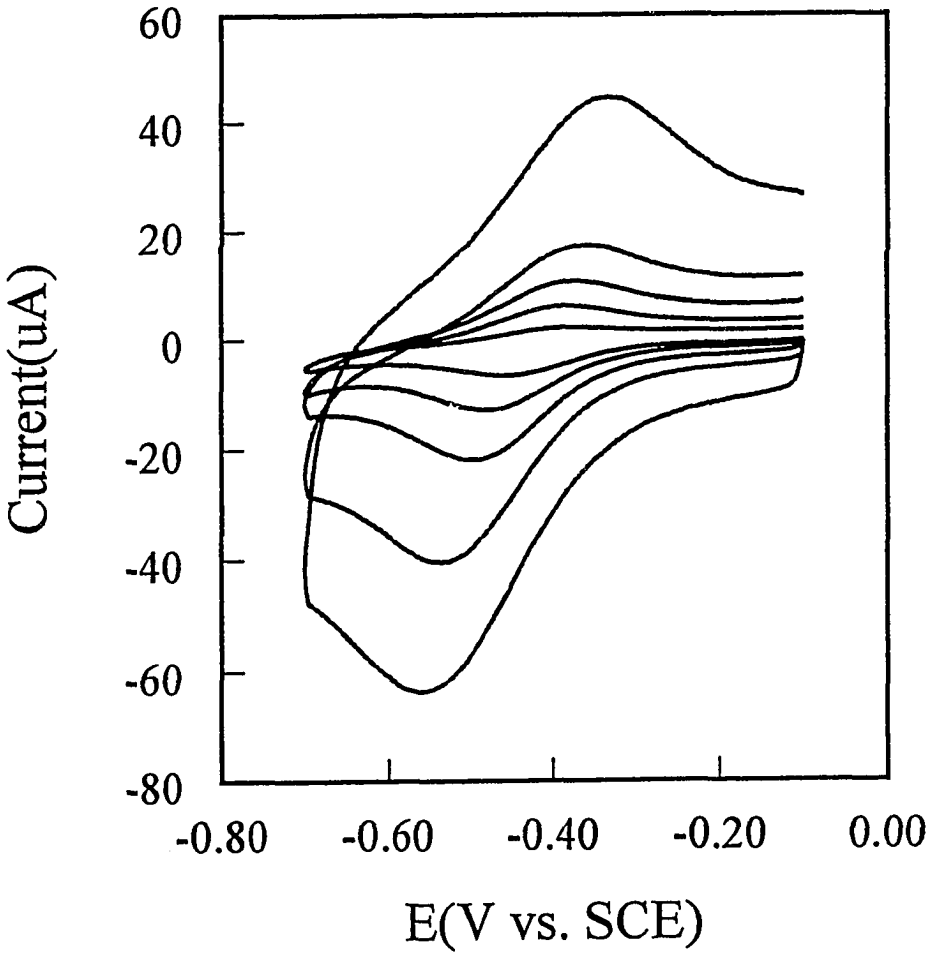

Figure 2. Cyclic voltamograms of F82H adsorbed on the MUA-modified gold electrode at the different scan rates. (a) 20, (b) 50, (c) 100, (d) 300, (e) 500 mV s^{-1}.

Surface-enhanced Resonance Raman Scattering (SERRS) was further used to determine the conformations and redox properties of WT and F82H adsorbed on bare and MUA modified Ag electrode surfaces. In order to gain sufficient resonance and surface enhancement, an excitation of 413 nm were used for the measurements of SERRS.

The SERRS of WT and F82H on bare roughened silver electrodes are shown in Figure 3 and 4, which were obtained with the electrode potential at 0.20 and –0.50 V, respectively. In addition to the six-coordinate, low-spin state sensitive band at 1504 and 1496 cm-1, the appearance of the band at 1496 and 1469 cm^{-1}, corresponding to five-coordinate state of heme iron, indicates that WT was denatured under experiment conditions (Fig. 3a and Fig. 4a). However, the spectrum of F82H is mainly characteristic of six-coordinate, low-spin state of heme, implying that F82H is less denatured under the same conditions. These results suggest that F82H with His-82 replacing Phe-82 is more stable than WT.

It should be pointed out that F82H mutant might also be denatured as it was adsorbed on the electrode surface and irradiated for a long period of time. In order to prevent the proteins from being denatured, SERRS measurements were performed on MUA modified roughened silver electrodes. The SERRS spectrum of the oxidized WT adsorbed on the surface of the MUA-modified roughened silver electrode under the open circuit condition is shown in Figure 5(a). Comparing to the RR spectra of the oxidized and reduced WT,[28] it was found that except for the oxidation state marker band at 1373 cm^{-1} and the spin and coordination sensitive band at 1503 cm^{-1}, other two bands at 1362 and 1494 cm^{-1} were also observed. The 1373 and 1503 cm^{-1} bands are the characteristic for WT with oxidized, low-spin and six coordination state. While the other two bands at 1362 and 1494 cm^{-1} are

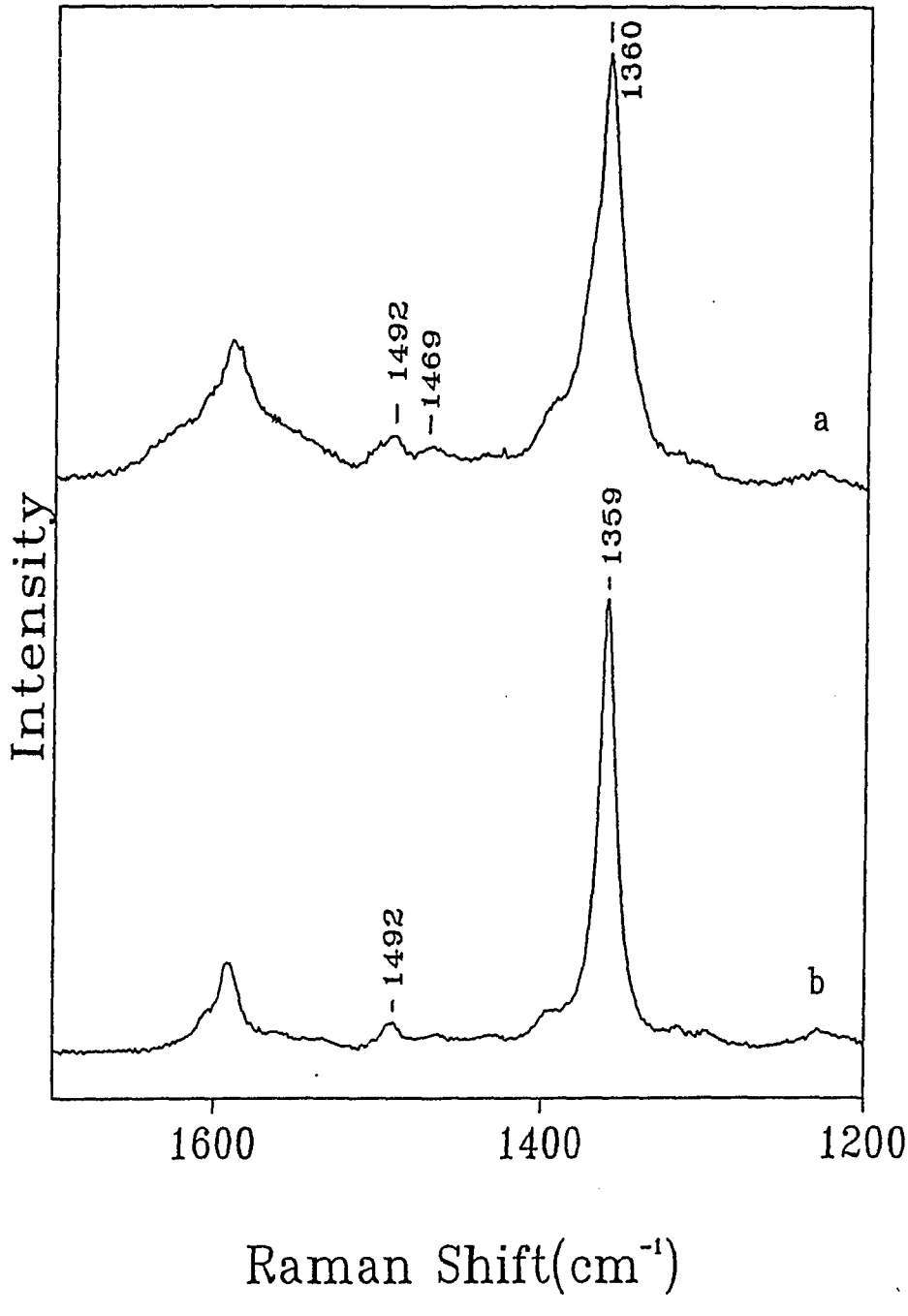

Figure 3. SERRS spectra of WT(a) and F82H(b) adsorbed on the bare surfaces of roughened silver electrodes at 0.20 V.

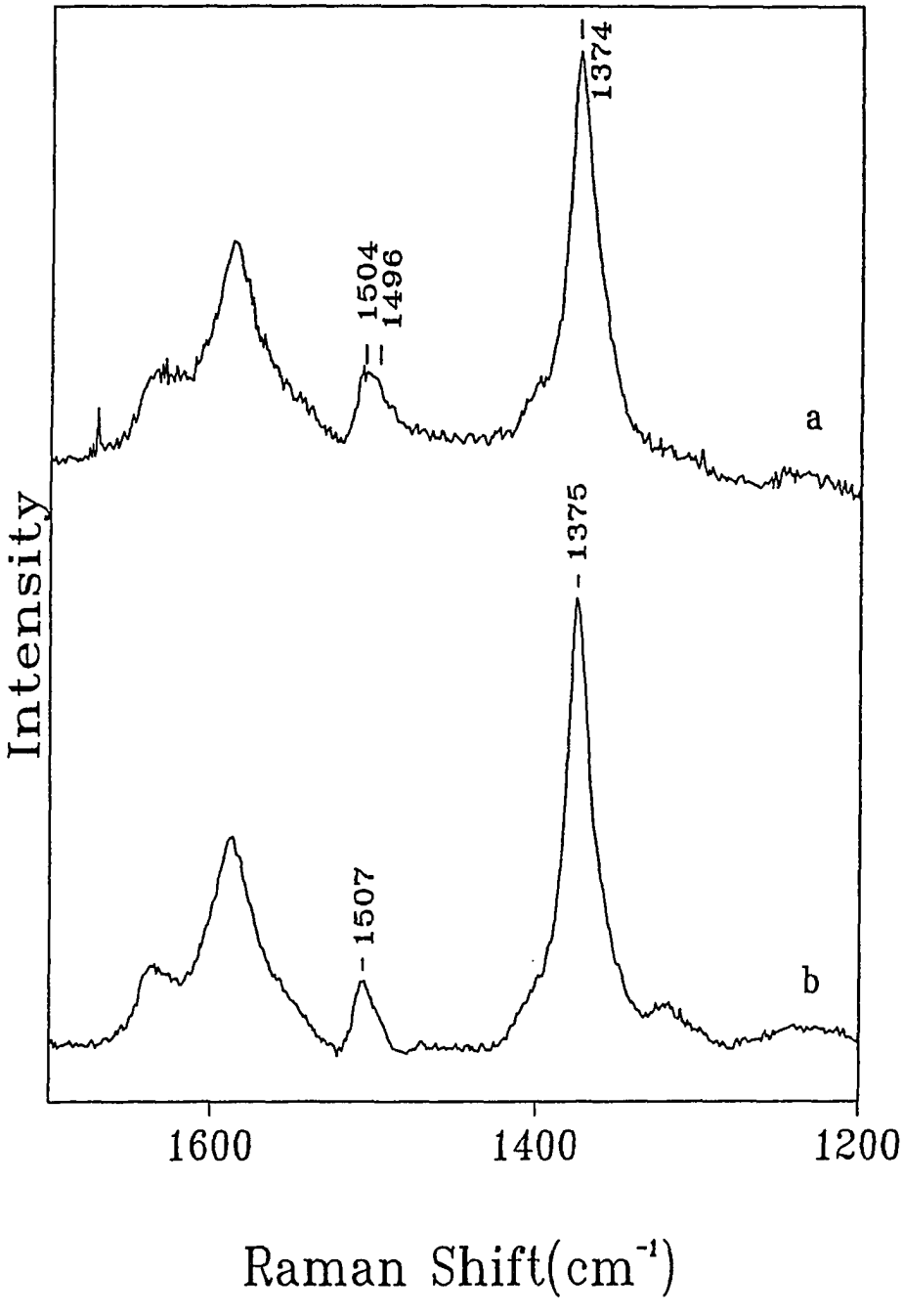

Figure 4. SERRS spectra of WT(a) and F82H(b) adsorbed on the bare surfaces of roughened silver electrodes at -0.50 V.

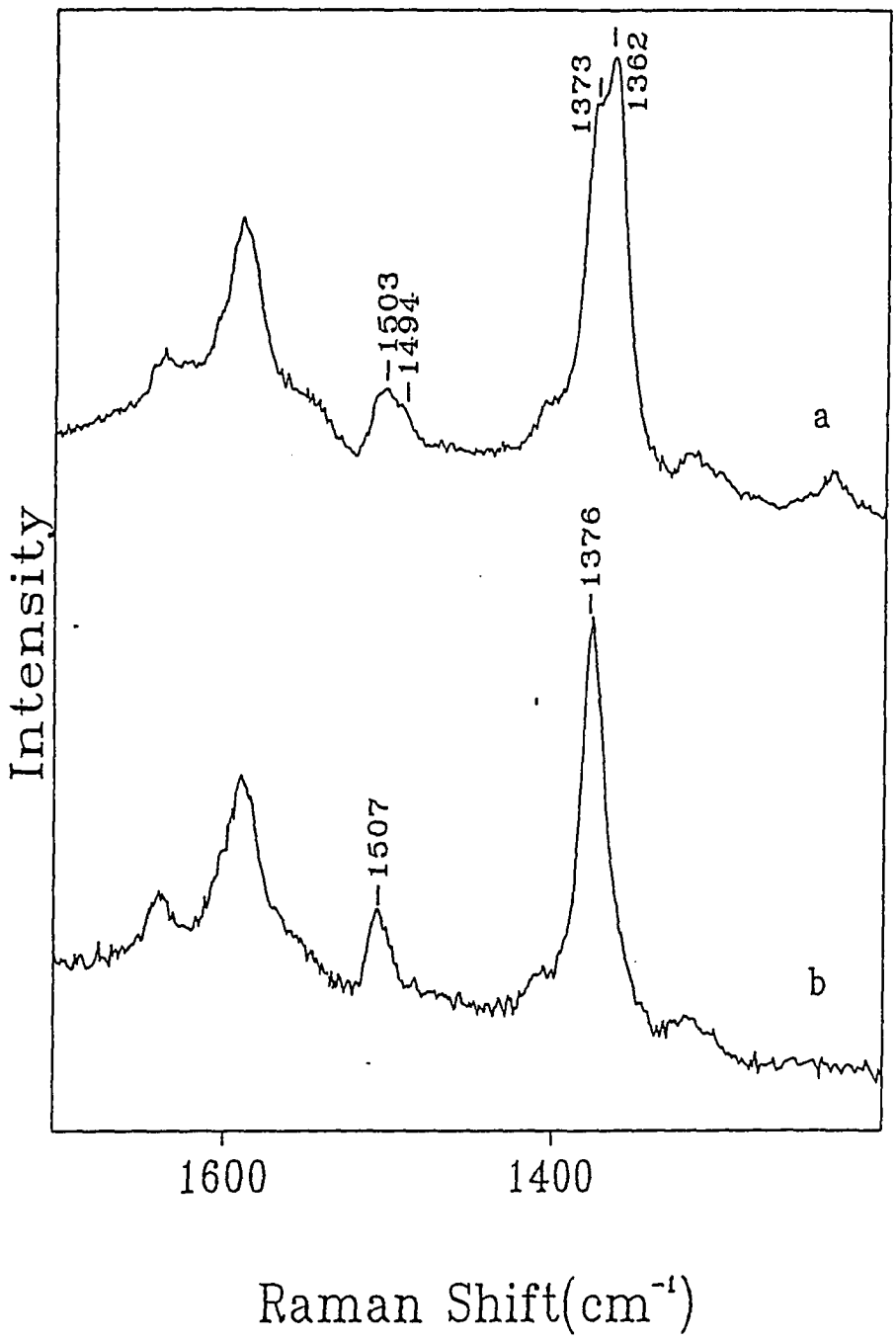

Figure 5. SERRS spectra of WT (a) and F82H (b) adsorbed on the surface of the MUA-modified roughened silver electrode under the open circuit condition.

indicative of the reduced, low spin and six coordination state for WT.[28, 32] Therefore, the adsorbed WT at the MUA-modified roughened silver electrode surface was partially reduced under the open circuit and illumination conditions. A similar photo-induced reduction phenomenon was also observed in the previous SERRS investigation of horse heart cytochrome c adsorbed on the iodide-modified roughened silver electrode.[33] This phenomenon was attributed to the photoinduced electron transfer between the nanoscale silver particles at the surface and the adsorbed species.

The SERRS spectrum of F82H adsorbed on the surface of the MUA-modified roughened silver electrode (Figure 5, b) obtained under the open circuit conditions is comparable to the RR spectrum of F82H reported in the previous paper.[28] Only the oxidation state marker band at 1376 cm^{-1} and the spin state and coordination marker band at 1507 cm^{-1} were observed in the spectrum. These bands indicate that F82H exits in an oxidized, low-spin, six-coordination state under experimental conditions.[28, 32] Thus, the native conformation of F82H was well preserved upon adsorption on the surface of the MUA-modified roughened silver electrode. The fact that no reduced state band was observed in the spectrum further demonstrates that the oxidized state of F82H is much more stable than that of WT and the photo-induced reduction can not occur under the experiment conditions.

Figure 6 shows the potential dependence of the SERRS spectra of WT adsorbed on the surface of the MUA-modified roughened silver electrode. A band at 1373 cm^{-1} with a small shoulder at 1362 cm^{-1} was observed when the electrode potential is at 0.15 V. The appearance of 1362 cm^{-1} band indicates that WT started to be reduced at about 0.15 V. As the potential shifts to the negative direction, the intensity of the 1373 cm^{-1} band gradually decreased and the intensity of the 1362 cm^{-1} band accordingly increased. When the potential

is at -0.2 V, the 1373 cm^{-1} band almost completely disappeared and only the 1362 cm^{-1} band was observed, indicating that WT is nearly fully reduced at this potential.

Figure 7 shows the potential dependence of the SERRS spectra of F82H adsorbed on the surface of the MUA-modified roughened silver electrode. It can be seen that only a band at 1376 cm-1corresponding the oxidized state of F82H was observed even the electrode potential was as negative as -0.25 V. A small shoulder at 1362 cm^{-1} started to appear when the electrode potential was at -0.30 V, along with the band at 1376 cm^{-1}, indicating that F82H started to be reduced at about -0.30 V. When the potential was stepped to negative direction, the intensity of the 1376 cm^{-1} band gradually decreased and the intensity of the 1362 cm^{-1} band accordingly increased. A fully reduced form of F82H can be obtained at -0.5V as indicated by the complete disappearance of 1376 cm^{-1} band.

The relative intensities of oxidation marker bands for WT and F82H were plotted as a function of applied potential (Figure 8). The midpoint potentials estimated from the curves were 0.025 V for WT and –0.432 V for F82H.

Discussion

The electrochemistry of mitochondrial cytochrome c has been extensively studies on various electrodes.[34-36] The reduction potential of mitochondrial cytochrome c is usual about 0 V. However, the cathodic peak of F82H adsorbed on the MUA-modified gold electrode is located at -0.51 V (Figure 1). The potential dependence of the SERRS spectra of WT and F82H adsorbed on the surface of the MUA-modified roughened silver electrode also demonstrated that the reduction of F82H occurs at the potential much more negative than that for WT. In addition, the SEERS spectra of WT and F82H at open circuit conditions

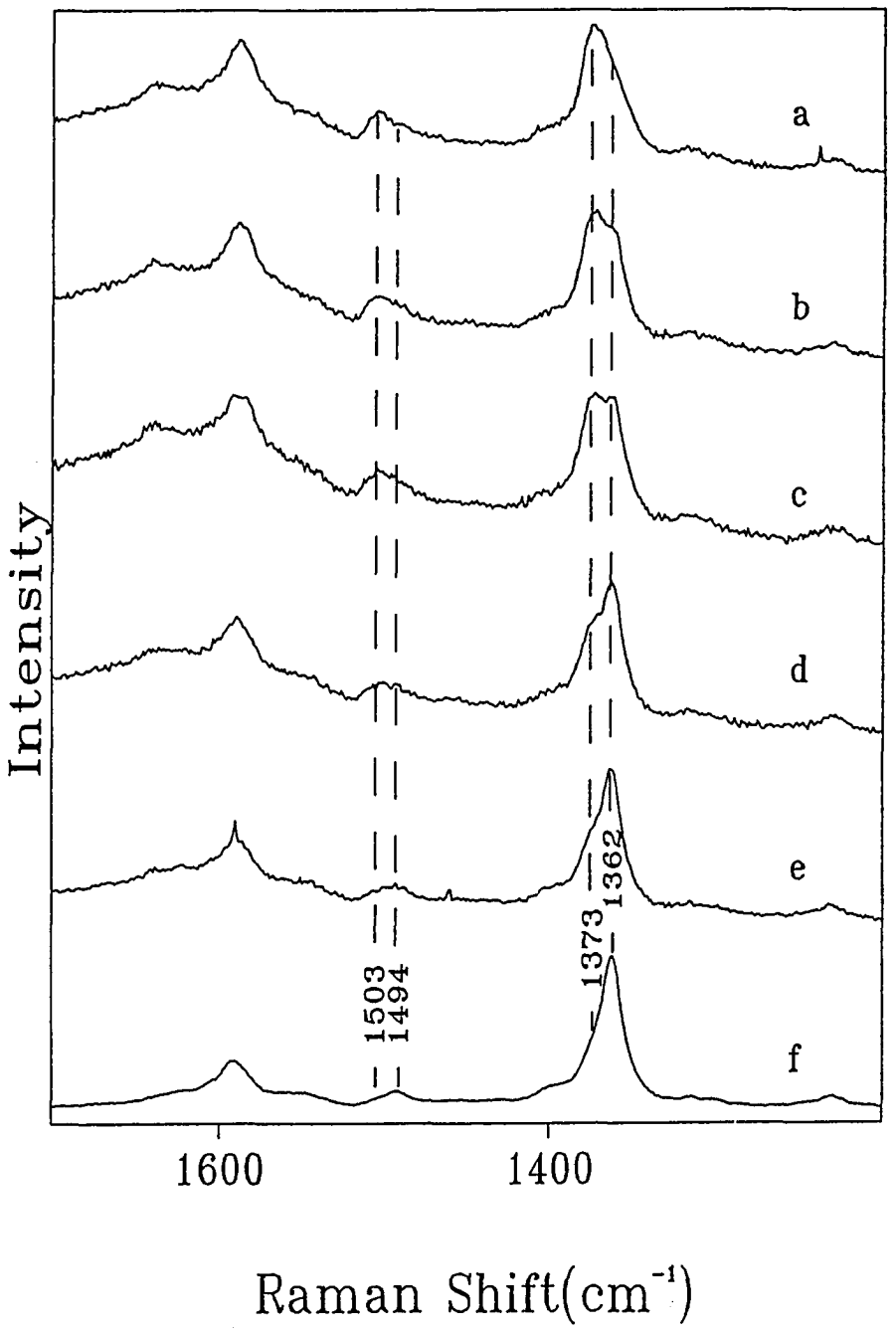

Figure 6. SERRS spectra of WT adsorbed on the surface of the MUA-modified roughened silver electrode at (a) 0.15, (b) 0.05, (c) 0.00, (d) -0.05, (e) -0.10, (f) -0.20 V.

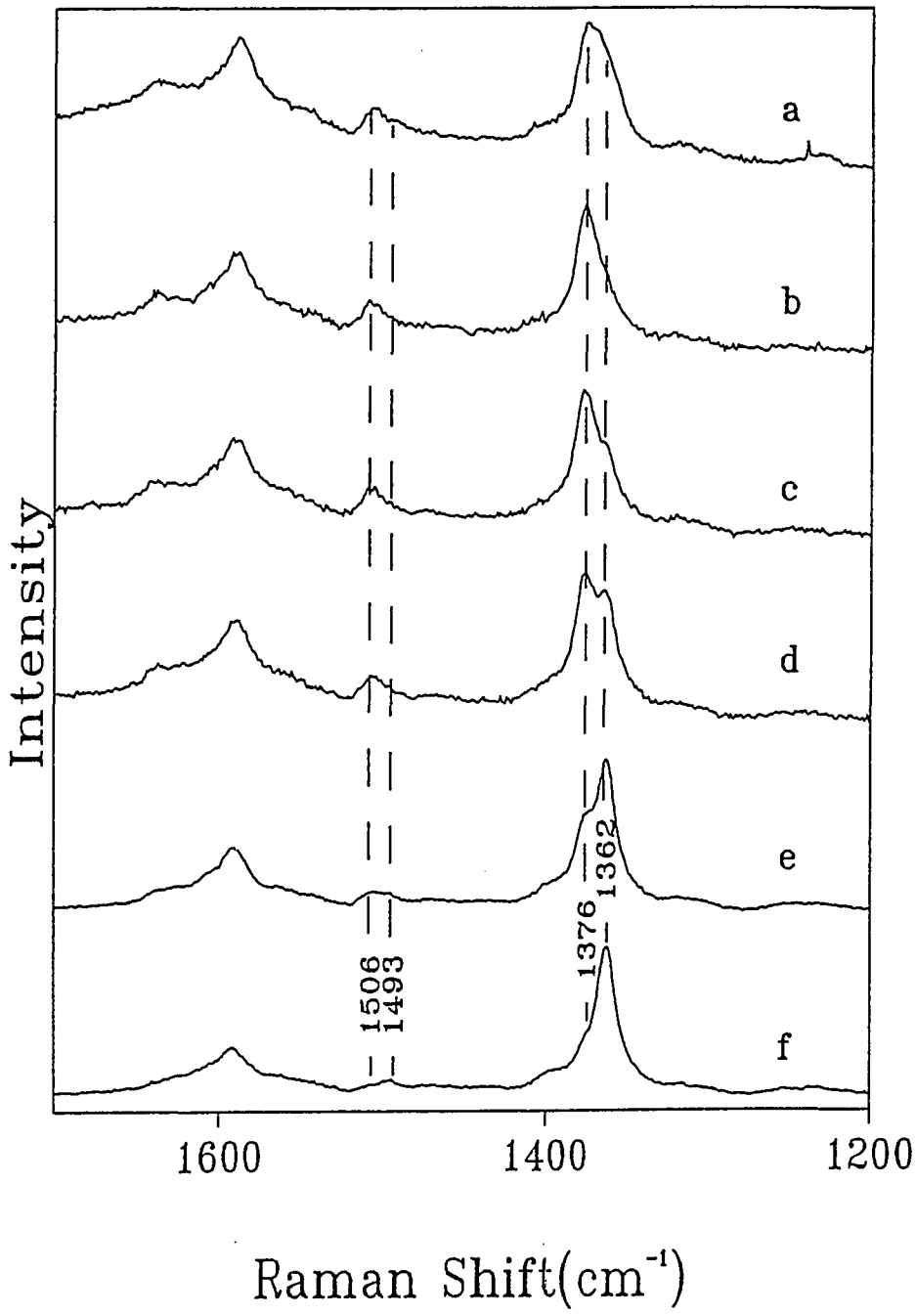

Figure 7. SERRS spectra of F82H adsorbed on the surface of the MUA-modified roughened silver electrode at (a) -0.20, (b) -0.30, (c) -0.35, (d) -0.40, (e) -0.45, (f) -0.50 V.

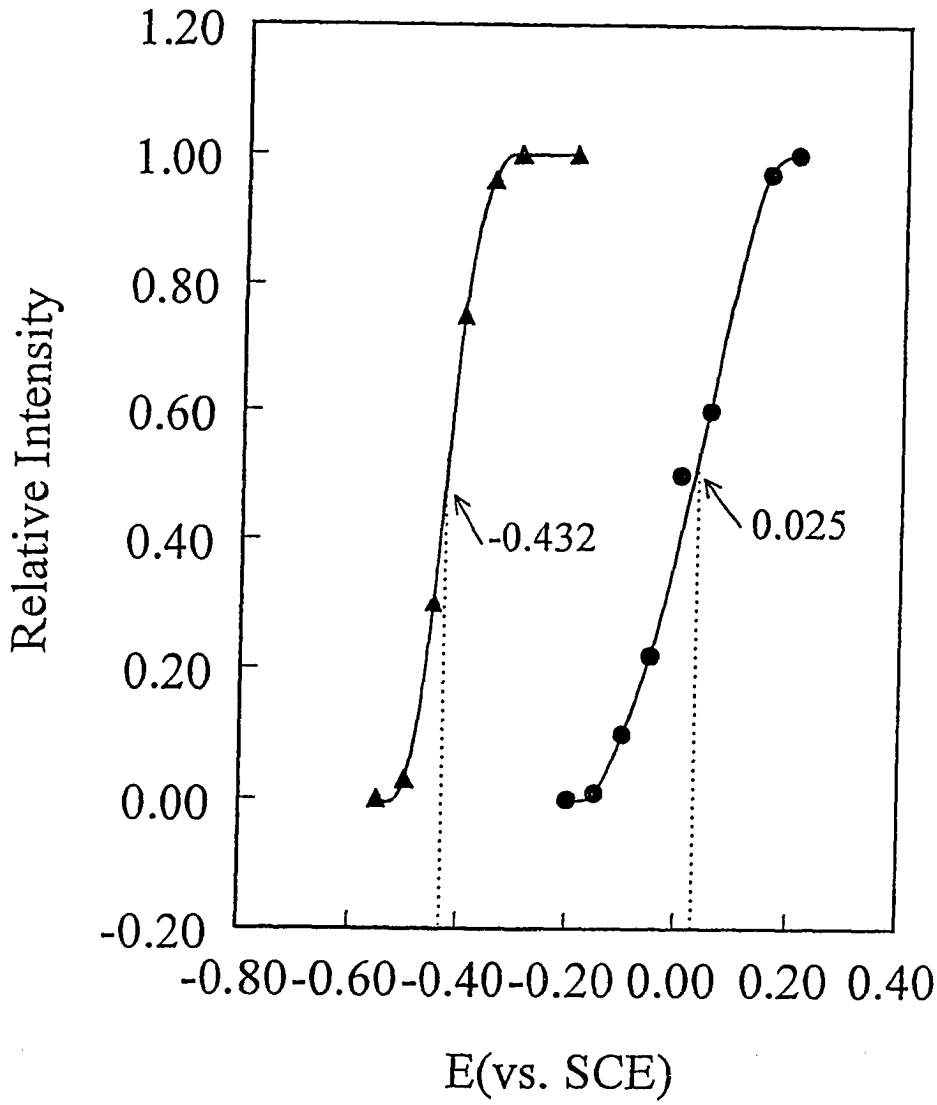

Figure 8. Plot of the intensities of oxidation marker bands of WT(a) and F82H(b) as a function of applied potentials.

(Figure 2) shows that similar to horse heart cytochrome c;[33] WT can undergo the photo-induced reduction at the MUA-modified roughened silver electrode. In contrast, the photo-induced reduction of F82H was not observed. All those results demonstrated that F82H is more

stable in oxidized state and difficult to be reduced as Phe-82 was replaced by His-82 in the protein structure.

The largely negative shift of the reduction potential of F82H relative to that of WT is unlikely due to any conformational changes in F82H as it was adsorbed on the electrode surface. The similarity between the RR[28] and SERRS spectra (Figure 5) of WT and F82H confirms that the proteins were in the native state when they were adsorbed on the surface of the MUA-modified roughened silver electrode. Bowden et al.[30] reported that the formal redox potential of WT adsorbed on the surface of the MUA-modified electrode is about 25 mV. A comparable value can also be estimated from potential dependence of the SERRS spectra (Fig. 8). This indicate that the adsorption of the protein on the surface of the MUA-modified electrode does not change the formal redox potential.

The negative shift of formal redox potential was also reported by Mauk et al.[18] for the mutants in which Phe-82 was replaced with other amino acids, such as tyrosine, leucine, isoleucine, alanine, serine and glutamate. However, the largest shift in those cases was only ca. 43 mV, which was attributed to the slight alternation of heme group environment by the mutations. The changes in the surrounding environment of heme group resulting from replacement of Phe-82 with other amino acid residues, obviously only caused a very small change in the formal redox potential of the protein. The large shift of the redox potential for F82H thereby could not be explained only by the change in the surrounding environment of

heme group.

The effect of ligand switching of heme iron is therefore considered next. It is well known that in the mitochondrial cytochrome c, the heme iron is ligated by the imidazol of His-18 and the sulfur of Met-80 at the fifth and sixth coordination positions, respectively[37]. When Phe-82 is substituted with amino acids, such as tyrosine, leucine, isoleucine, alanine, serine and glutamate, the coordination of the heme iron remains unchanged. In the case of F82H, however, imidazole group of His-82 residue is coordinated with the heme iron instead of Met-80 sulfur in the oxidized state as demonstrated in our previous study and the studies from other researchers.[23,24,28] The replacement of Phe-82 with His-82 not only results in a possible change in the surrounding environment of heme group, but also the change of the coordination of the heme iron. Our previous RR study revealed that the change in the sixth ligand of the heme iron by the replacement of Phe-82 with His leads to a less distorted porphyrin macrocycle and the changes in the interactions of the substituents on the porphyrin ring with surrounding protein. The less distortion of porphyrin macrocycle can also be seen from the comparison of the SERRS spectra of the oxidized WT and F82H. For example, the sensitive band, ν_{10}, shift from 1635 cm^{-1} for WT to 1640 cm^{-1} for F82H (Figure 5). The high frequency shifts of this band as well as the other core size sensitive bands such as ν_2 (from 1584 to 1589 cm^{-1}), ν_3 (from 1502 to 1505 cm^{-1}) and ν_4 (from 1372 to 1376 cm^{-1}), also indicate that the core size of the porphyrin ring in oxidized F82H is smaller than that in WT.[28] The less distortion and smaller core size of porphyrin macrocycle in oxidized F82H mutant were attributed to the identical axial ligands of heme iron due to the replacement of Met-80 with His-82. Therefore, it can be concluded that the significant negative shift in the reduction potential of the mutant mainly results from the change of the sixth ligand of the

heme iron.

Nevertheless, in reduced state the coordination of the heme iron in F82H is the same as that in WT because of the recoordination of Met-80 upon reduction.[23, 24,28] However, the oxidation peak in the CV of adsorbed F82H (Figure 1) appears at -0.39 V, which is also much more negative than that for the adsorbed WT. The possible explanation is that the oxidation reaction is followed by a ligand switching process, where the His-82 replaces Met-80 at the sixth coordination position. The oxidation is a typical electrochemical process via EC mechanism. Because the higher affinity of His-82 to Fe(III) relative to Met-80, the oxidized state of F82H could be more stable than that of WT. This essentially makes the oxidation of F82H much easier than that of WT. In other word, the oxidation of F82H takes place at more negative potential.

The analysis of the results demonstrates that the axial liagnds in the heme proteins play an important role in the electron transfer process. The relative coordination strength of the axial ligands determines the redox potential of the proteins.

Based on the above consideration, the electrochemical reactions of F82H could be expressed as followings:

For the reduction process,

$$\text{His(82)-Fe(III)} + e \leftrightarrows \text{His(82)-Fe(II)} \qquad (1)$$

$$\text{His(82)-Fe(II)} + \text{Met(80)} \rightarrow \text{Met(80)-Fe(II)} + \text{His(82)} \qquad (2)$$

For the oxidation process,

$$\text{Met(80)-Fe(II)} - e \leftrightarrows \text{Met(80)-Fe(III)} \qquad (3)$$

$$\text{Met(80)-Fe(III)} + \text{His(82)} \rightarrow \text{His(82)-Fe(III)} + \text{Met(80)} \qquad (4)$$

where His(82)-Fe(III) etc. represent the sixth ligand and the oxidation states of F82H. The

above reaction mechanism is typical for an electrochemical reaction followed by a chemical reaction.

Bowden et al.[30] reported that the electrochemical reaction of WT at the MUA-modified electrode is slow. The fact that the reduction or oxidation peak potential shifted to negative or positive direction with increasing the scan rate (Figure 2) also indicates the slow electrochemical reactions of the mutant at MUA-modified gold electrode. The sixth ligand switching in F82H due to the oxidation and reduction of F82H may be much faster than the electrochemical oxidation and reduction of F82H. For example, if the ligand switch rate is comparable to the rate of the electrochemical reduction of F82H, there should be two oxidation peaks in the CV of F82H. One is for Met(80)-Fe(II) - e ⇆ Met(80)-Fe(III). Another is for His(80)-Fe(II) - e ⇆ His(80)-Fe(III). Actually, only one oxidation peak was observed even the scan rate was as high as 500 mVs^{-1}. This illustrates that the ligand switch rate is relatively faster than the rate of the electrochemical reaction.

Conclusions

Cyclic voltammetry and SERRS were used to study the stability and electrochemical behaviors of yeast iso-1-cytochrome c mutant F82H. The substitution of His for Phe-82 in the mutant resulted in a more stable conformation compared to that of the wild type protein. The reduction and oxidation potentials of F82H shifted to the negative direction for about 400 mV relative to that for WT. The redox potential shifts were attributed to the ligand switching of heme group between His-82 and Met-80 during the oxidation and reduction of F82H. The results demonstrate that the axial ligands of the heme iron play an important role in the electron transfer rate of heme proteins. The possible mechanism of the

electrochemical reaction of F82H was proposed.

Acknowledgement

The Financial support of the National Institutes of Health (GM35108) is gratefully acknowledged.

References

1. G. R. Moore and G. W. Pettigrew, Cytochome c, Evolutionary Structural and Phylological Aspects, Springer-Verlay, Berlin, 1990.
2. J. R. Winkler and H. B. Gray, Chem. Rev. 92 (1992) 369.
3. F. A. Armstrong, H. A. O. Hill and N. J. Walton, Acc. Chem. Rev. 21 (1988) 407.
4. S. Wherland, H. B. Gray, in A. W. Addison, W. R. Cullen, D. Dolphin, B. R. James (Eds.), Biological Aspects of Inorganic Chemistry, Wiley-Interscinece, New York, 1977, p. 289.
5. R. A. Macus and N. Sutin, Biochim. Biophys. Acta, 811 (1985) 265.
6. G. Mclendon and J. R. Miller, J. Am. Chem. Soc. 107 (1985) 7811.
7. F. Salemme, J. Mol. Biol. 102 (1985) 563.
8. J. C. Marchon, T. Mashiko and C. A. Reed, in C. Ho (Ed.), Electron Transport and Oxygen Utilization, Elsevier North Holland, New York, 1982, P. 67.
9. H. Senn and K. Q. Wuthrich, Rev. Biophys. 18 (1985) 111.
10. R. E. Dickson and R. Timkovich, in P. Boyer (Ed.), The Enzymes, Vol. XI, Academic Press, New York, 1975, p. 297.

11. B. Hagihara, N. Sato and T. Yamanaka, in P. Boyer (Ed.), The Enzymes, Vol. XI, Academic Press, New York, 1975, p. 549.

12. M. Smith, D. W. Leung, S. Gillam, C. R. Astell, D. L. Montgomery and B. D. Hall, Cell, 16 (1979) 753.

13. D. L. Montgomery, D. W. Leung, M. Smith, P. Shalit, G. Fay and B. D. Hall, Proc. Natl. Acad. Sci. U. S. A. 77 (1980) 541.

14. C. A. III, Hutchison, S. Phillips, M. H. Edgell, S. Gillam, P. Jahnke and M. Smith, J. Biol. Chem. 253 (1978) 6551.

15. A. Razin, T. hirose, K. Itakura and A. D. Riggs, Proc. Natl. Acad. Sci. U. S. A. 75 (1978) 4268.

16. G. J. Pielak, A. G. Mauk and M. Smith, Nature, 313 (1985) 152.

17. N. Liang, A. G. Mauk, G. J. Pielak, J. A. Johson, M. Smith and B. M. Hoffman, Sciences, 240 (1988) 311.

18. S. P. Rafferty, L. L. Pearce, P. D. Barker, J. G. Guillemette, C. M. Kay, M. Smith and A. G. Mauk, Biochem. 29 (1990) 9365.

19. N. Liang, G. J. Pielak, A. G. Mauk, M. Smith and B. M. Hoffman, Proc. Natl. Acad. Sci. U. S. A. 84 (1987) 1249.

20. T.L. Poulos and J. Kraut, J. Biomol. Chem. 255 (1990) 10322.

21. G. V. Louie, G. J. Pielak, M. Smith and G. D. Brayer, Biochem. 27 (1988) 7870.

22. G. J. Pielak, K. Oikawa, A. G. Mauk, M. Smith and C. M. Kay, J. Am. Chem. Soc. 108 (1986) 2724.

23. B. K. Hawkins, S. Hilgen-Willis, G. J. Pielak and J. H. Dawson, J. Am. Chem. Soc. 116 (1994) 3111.

24. A. Schejter, G. Taler, G. Navon, X. Liu and E. Margoliash, J. Am. Chem. Soc. 118 (1996) 477.

25. H.-X. Zhou, J. Am. Chem. Soc. 116 (1994) 10362.

26. T.N. Sorrell, P.K. Martin, E.F. Bowden, J. Am. Chem. Soc. 111 (1989) 766.

27. A.L. Raphael and H.B. Gray, J. Am. Chem. Soc. 113 (1991) 1038.

28. J. Zheng, S. Ye, T. Lu, T. M. Cotton, and G. Chunanov, submitted to Biospectrosc.

29. T. I. Koshy, T. L. Luntz, E. A. E. Garber and E. Margoliash, Protein Expression Purif. 38 (1992) 441.

30. A. E. Kasmi, J. M. Wallace, E. F. Bowden, S. M. Binet and R. J. Linderman, J. Am. Chem. Soc. 120 (1998) 225.

31. M. J. Tarlov and E. T. Bowden, J. Am. Chem. Soc. 113 (1991) 1847.

32. P. Hildebrandt and M. Stockburger, in H. D. Bist (Ed.), Raman Spectroscopy: Sixty Years on vibrational Spectra and Structure, Elsevier Science, Nertherland, 1989, vol. 17A, p. 443.

33. M. S. Sibbald, G. Chumanov, T. M. Cotton, J. Phys. Chem. 100 (1996) 4672.

34. R. W. Henderson and W. R. Rawlinson, Biochem. 62 (1956) 21.

35. X. Qu, T. Lu, S. Dong, C. Zhou and T. M. Cotton, Bioelectrochem. Bioenerg. 34 (1994) 153.

36. T. Lu, X. Yu, S. Dong, C. Zhou, S. Ye and T. M. Cotton, J. Electroanal. Chem. 369 (1994) 79.

37. T. Takano and R. E. Dickerson, J. Mol. Biol. 153 (1980) 74.

CHAPTER 9

GENERAL CONCLUSIONS

Surface plasmon resonance has been successfully applied in the enhancement of photoinduced electron transfer at silver/solution interfaces. The study of photoinduced electrochemical reduction of nitrite at roughened silver electrode demonstrates that the roughness feature or the presence of nanostructured silver particles on the electrode surface is essential for the enhancement of the reduction of nitrite. The action spectrum of photocurrent response for the nitrite reduction confirmed the contribution of surface plasmon. Nevertheless, the photocurrent still obeys the classic model of photoemission for metal/solution interface. In the case of CO_2 reduction, however, the large photoinduced reduction current can only be obtained in the presence of adsorbed methylviolegen. These adsorbed methylviolegen molecules serves as mediator for the electron transfer between silver electrode and CO_2 in the solution, allowing the excited electron in silver metal to be directly tunneled to CO_2. A photoinduced reduction of heme protein model complex, microperoxidase-11, adsorbed on roughened silver electrode was also observed. EPR method has been employed in the study of photoinduced electron transfer between nanostructured silver particles and adsorbed electron acceptors (methylviolegen and nitrophenol) and electron donor (methanol). The formation of the radical is associated with the contribution of surface plasmon resonance.

Resonance Raman scattering spectroscopy has been applied to correlate the structural modification to the global and local stability of cytochrome c. The resonance Raman spectra of three water mutants, Y67F, N52I and H26V of rat cytochrome c, have been investigated.

The bands in resonance Raman spectra of the proteins in low frequency region were found extremely sensitive to the alternation of the protein conformation immediately next to heme group, particularly those bands associated with the thioether and propionic acid side chains. The oxidized form of the protein, on the other hand, possesses more open conformation.

The structural and conformational changes of yeast iso-1-cytochrome c mutant, F82H, were studied by using UV/Vis, CD, resonance Raman and surface-enhanced resonance Raman spectroscopic techniques. With His substitutes for Phe-82, the heme structure and the protein conformation surrounding heme group are largely changed, compared to that of wild type protein. In the oxidized form of the mutant, His-82 instead of Met-80 functions as the sixth coordination ligand to heme iron, whereas Met-80 switches back to coordinate with heme iron in the reduced form. Large perturbation of the conformation of protein was determined in the resonance Raman spectrum of the mutant in low frequency region. The effect of the sixth ligand on heme porphyrin macrocycle was demonstrated in the resonance Raman spectrum of mutant in high frequency region. The mutant possesses a more open structure both in oxidized and reduced forms, compared to the wild type protein. Porphyrin macrocycle in the oxidized F82H is less distorted due to the identity of the axial ligands to the heme iron. A comparison of surface-enhanced resonance Raman spectra of the wild type and mutant indicates that the replacement of Phe-82 with His stabilizes the global structure of the protein; the mutant adsorbed on the bare silver electrode is less denatured. Both electrochemical and surface-enhanced resonance Raman measurements of the proteins showed that the reduction potential of the cytochrome c is largely affect by the axial ligand of the heme iron. An approximate 500 mV negative shifts in the reduction and oxidation potentials of mutant was observed, with regard to that of the

wild type protein. The relatively low reduction potential of the mutant is attributed to the sixth ligand switching process as well as the change in the polarity of heme environment.

AKNOWLEDGEMENTS

I particularly would like to express my appreciation and respect to Professor Therese M. Cotton for her valuable guidance, support, and encouragement during the time as my major professor. Her patience, understanding, and friendship are always appreciated.

My sincere thanks are especially given to Professor Edward S. Yeung, my major professor, for his encouragement and support for the completion of my study in Iowa State University.

I am also grateful to the other members of my dissertation committee: Dr. Dennis C. Johnson, Dr. Marc D. Porter, Dr. Nadad M. Kostic and Dr. Donald J. Graves for their helpful suggestions regarding this work.

Special thanks are due to Dr. George Chumanov, a collaborator and friend, for his important friendship, encouragement, and hard work throughout my time as a graduate student in Cotton group.

I would also like to thank past and present members in this group who assisted me at different stages of my research work. I wish to express my appreciation particularly to the following people: Chengli Zhou, Albert Avila, Richard Walsh, Sa Lin, John Gering, Juan Xie, for providing me with a source of support and friendship.

Finally, I appreciate the financial supports for the works in the dissertation from National Institutes of Health and U.S. Department of Energy.